博 士 論 文

Study on Integration Technology of Flow Cytometry Chip

（フローサイトメトリーチップ集積化技術に関する研究）

佐 藤　友 美

広島大学大学院先端物質科学研究科

2018 年 3 月

目次

１．主論文

Study on Integration Technology of Flow Cytometry Chip

Tomomi Sato

２．公表論文

(1) Sheath flow forming by using twisted micro-channel

T. Sato and R. Miyake

Transaction of the JSME, **80**(813), (2014). DOI:10.1299/transjsme.2014 mn0132 (in Japanese) (11 頁)

(2) Cell Measurement by Flow Cytometry Chip with Twisted Micro Sheath Flow Channel

T. Sato and R. Miyake

Analytical Methods, **9**, pp. 3992-3997, (2017). DOI:10.1039/C7AY00886D

３．参考論文

(1) Sheath-flow forming by using twisted micro-channel

T. Sato and R. Miyake

The 26th IEEE International Conference on Micro Electro Mechanical Systems, pp. 1175-1178, (2013). DOI:10.1109/MEMSYS.2013.6474461

(2) Particle measurement by using twisted micro sheath flow cell

T. Sato and R. Miyake

The 19th International Conference on Miniaturized Systems for Chemistry and Life Sciences, pp. 458-460, (2015).

(3) Compact and Low-cost Flow Cytometry Unit for Monitoring Particles in Water

T. Sato and R. Miyake

The 7th International Multidisciplinary Conference on Optofluidics 2017, (2017). DOI:10.3390/optofluidics2017-04233

主論文

Contents

Chapter 1 Introduction

In chapter 1, the background and the objectives of this research are introduced.

1.1 Background

Flow cytometry is a technique for quickly analyzing the characteristics of individual microscopic particles or cells arranged in a line [1]-[3]. With this technique, it is possible to count the number of particles per unit volume and even detect rare kinds of biological cells. Flow cytometers have been used in a wide range of fields, from medical treatment to biological science, for not only capturing images of blood but also for detecting cancer cells and evaluating cultured cells. For instance, analysis of leukocytes using a flow cytometer can aid in the diagnosis of certain diseases. In recent years, cancer stem cells that may be responsible for tumor recurrence have been identified and characterized using a flow cytometer [4]. Flow cytometers are so widely used now that they are considered basic scientific tools. However, while the performance of current flow cytometers is excellent, their size and cost are prohibitive. To expand the availability of this technique, it is necessary to integrate the components, thereby providing a more compact, low-cost system that includes a pre-treatment system for the particle staining reaction [5].

The most important function of flow cytometry is the formation of sheath flow to analyze particles accurately. As shown in Figure 1-1, the conventional sheath flow cell has a double tube structure, with a total length of a few centimeters. A tiny nozzle is made in the center of the cylindrical glass tube. Sheath fluid flows in the cylindrical tube around the center nozzle and sample fluid is dispensed from the nozzle. The tube is connected to a thin capillary. The sample fluid is wrapped in the sheath fluid and gathers in the narrower area in the center of the capillary cross section. The fluid is thus compressed within in the capillary. With this structure, it is possible to generate stable flow in sample fluid having a diameter (φ) of 10 μm and a flow rate of a few meters per second. Moreover, the particles flow in a line at high speed. A conventional conical tube is typically used to form smooth, constricted, three-dimensional (3D) sheath flow. However, fabricating such a complex glass structure on a small scale is extremely difficult.

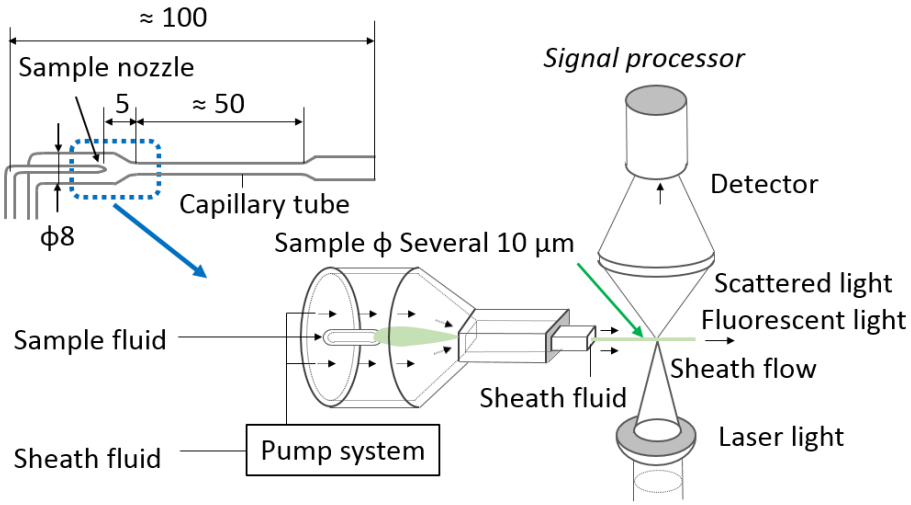

Figure 1-1 Principle of sheath flow formation

To reduce the size and cost of the entire system, it is ideal to fabricate an integrated pre-treatment part and sheath flow cell using a microfabrication technique, such as lithography in a single step. In general, silicon, glass or resin is used as a material for microfabrication, and the structure is planar, whereas the sheath flow cell with a 3D structure is made of glass. Currently, it is impossible to fabricate the sheath flow cell with a complex 3D structure using a single microfabrication step.

Many methods for forming sheath flow using microfluidics have been reported [6]-[14].

Miyake et al. succeeded in gathering particles in the center of a channel made of stainless steel. The channels were made using wet etching on three thin stainless-steel sheets, and then the sheets were stacked and bonded. However, with this method, it is necessary to precisely position the channel of each layer, and fabrication remains difficult. Furthermore, since the pre-treatment part connected upstream of the sheath flow cell has a two-dimensional (2D) channel, such as a mixer and a branch, it is extremely difficult to fabricate it simultaneously with the 3D sheath flow cell. On the other hand, Mao et al. reported forming sheath flow using Dean flow [15]. Dean flow is generated in the cross section of a 2D curved flow channel due to the centrifugal force, making it possible to flow particles in the horizontal direction at the center of the channel cross section. The sheath fluids flow in the sample channel from both sides and the particles gather in the center of the channel cross section. However, since the magnitude of the centrifugal force depends on the flow velocity, there is only a limited range of suitable flow velocities to keep the particles at the center of the channel cross section. In contrast, Lee et al. developed sheath flow using a local bending flow [16]. By repeated stepwise expansion and contraction in one side of the channel, a local bending flow is generated. The particles are gathered in the channel cross section using induced

swirling flow. However, the positions of the particles vary depending on the flow velocity, again limiting the range of suitable flow velocities.

Therefore, the following attributes are desired for a micro channel to form sheath flow:

(1) Simple and easy fabrication process

(2) Easy fluid control

(3) No external forces

(4) Compact and low-cost

I proposed a novel micro channel structure to form sheath flow that does not depend on the flow velocity using a planar channel fabrication process, and studied a method for determining the specifications of a flow cell created using the simple fabrication method. Furthermore, I aimed to create an integrated flow cytometry chip with a pre-treatment part and a sheath flow cell. Conventionally, after cells were pre-treated, the sample fluid with the stained cells were introduced into a flow cytometer. For instance, cells or particles are manually stained. There are limits to how much the volume of the sample fluid and the reagent can be reduced in manual steps, and there is also some loss of sample fluid. I surmised that both volumes by manual steps and reagent loss could be reduced by integrating the microfabricated pre-treatment part and sheath flow cell. Although sufficient time for the staining reaction is required, using a micro channel shortens the mixing reaction of the sample fluid and the reagent fluid. Furthermore, integrating the pre-treatment part and the sheath flow cell eliminates the need for a dispensing operation, shortens the operation time.

The design specifications of the flow cytometry chip must, however, simultaneously satisfy the function of the pre-treatment part, such as cell staining,

and the function of the sheath flow cell with its 3D structure. Furthermore, to create a compact, low-cost flow cytometer, it is necessary to design not only the flow cytometry chip but also the entire system including the measurement system. Therefore, I studied design technology for aligning and integrating a pre-treatment part and a flow cell. The potential of ultra-compact and low-cost flow cytometer was discussed.

In this thesis, I report on a study on the integration technology of a flow cytometry chip.

The specific target is to apply the ultra-compact and low-cost flow cytometer to the on-site measurement of bacteria in water, and the following steps are required for it.

(1) Counting of particles

(2) Counting of bacteria

(3) Detection of the cell viability

(4) Cell type discrimination

In this study, I aimed (1) counting of particles by using the ultra-compact and low-cost flow cytometer.

The next section shows the objectives of this thesis.

1.2 Objectives of this thesis

To create an ultra-compact, low-cost flow cytometry chip, I focused our research on:

(1) Survey of reported techniques related to microfluidic devices for forming sheath flow and associated problems.

(2) Investigation of a method to form 3D micro channel network and proposal of a simple method for fabrication of the network using polydimethylsiloxane (PDMS).

(3) Study of a method for determining the specifications of a flow cell fabricated using simple fabrication method.

(4) Research of a design technology for aligning and integrating a pre-treatment part and a sheath flow-forming part.

(5) Fabrication and performance evaluation of the flow cytometry chip.

(6) Discussion on versatility and potential of the method for fabrication of the 3D micro channel network.

Chapter 2　Three-dimensional structure to form sheath flow

In chapter 2, the mechanism of sheath flow formation is introduced. Studies related to microfluidic devices that form sheath flow (hereafter, sheath flow cells) are also reviewed, and their methods for forming sheath flow and the requirements to form stable sheath flow are presented. A 3D flow channel structure and a method for fabricating a 3D micro channel network are investigated, and a novel method (a simple method for fabrication of the 3D micro flow channel network) is proposed. The advantages and drawbacks of the proposed method are compared with those of the conventional methods.

2.1　Mechanism of forming sheath flow

Flow cytometry technology is well known as a method for detecting biological cells, and is a method for analyzing individual cells using flow [17], [18]. Figure 2-1 shows a typical flow cytometer (Gallios; Beckman Coulter).

Generally, biological cells are labeled with a marker by an immunoreaction, a unique reaction for specific cells, and the suspensions are dispensed into the flow cytometer. The labeled cells are excited by laser light and emit fluorescence. The fluorescence is detected using a photo multiplier tube (PMT) detector, and then the cells are classified. The configuration of the flow cytometer is based on the laser and the PMT. Sometimes, the flow cytometer includes a function to charge cells and sort them. Thus, it is possible to identify target cells at high speed, exceeding 1,000 cells per second. Figure 2-2 shows the typical configuration of a flow cytometer.

The formation of sheath flow is one of the most important aspects of flow cytometry. Essentially, a sample fluid is wrapped in a sheath fluid, and the cells or particles in the sample fluid are arranged linearly. Figure 2-3 shows the formation of sheath flow in the flow cytometer. As shown in Figure 2-3, it is important that the cells or particles pass through the position where the laser light is in focus.

Figure 2-1 Example of a flow cytometer

(Gallios; Beckman Coulter).

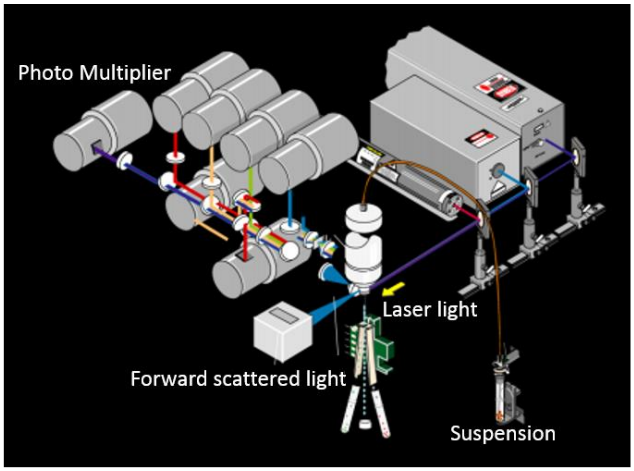

BECKMAN COULTER ; Introduction to FCM for beginner
https://www.bc-cytometry.com/FCM/beginner/beginner01.html#pretop

Figure 2-2 Typical configuration of a flow cytometer

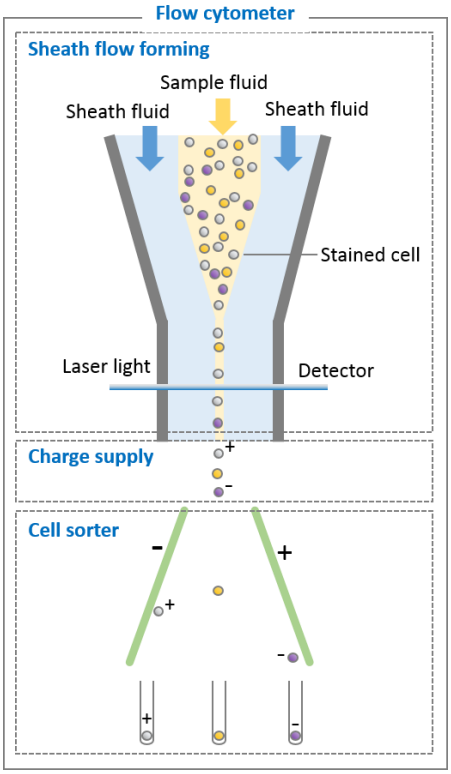

Figure 2-3 Formation of sheath flow and cell sorting

Flow cytometers are used especially for life science research and drug discovery. They can even be used to detect rare cells with high accuracy. Recently, flow cytometers have been used for the detection of circulating tumor cells (CTCs). CTCs are released from primary tumor tissue or metastatic tumor tissue and infiltrate into the blood, and detection of these cells can indicate the presence of cancer. Generally, there are several to several tens of CTCs in 10 ml of blood. By forming sheath flow, the flow cytometer can detect even a few CTCs accurately and reproducibly [19].

Conventionally, a cylindrical double glass tube, as shown in Figure 1-1, is needed to form sheath flow. A sample fluid is wrapped with a sheath fluid and flows into a conical tube. The fluids are compressed and form a stable flow, with a diameter of approximately 10 μm and a flow velocity of a few meters per second in the center of the tube. The cells in the fluid flow in a row at a high velocity. Although a flow cytometer can measure many cells at high speed and with high accuracy, fabricating a structure like the double glass tube is difficult, and the equipment and its running costs are very expensive. Therefore, use of the conventional flow cytometer has been limited.

For wider application of this technology, it is necessary to reduce the costs and miniaturize the equipment. To create a compact, low-cost flow cytometer, firstly, I studied a method to form sheath flow, the most important aspect of flow cytometry, using a microfluidic device.

I surveyed the reports on forming sheath flow using microfluidic devices. These reports are introduced in the next section.

2.2　Forming sheath flow in microfluidic devices and related issues

Methods for forming sheath flow using a microfluidic device include using a 3D micro channel structure that reproduces a conventional cylindrical double glass tube structure [10]-[14], [20]-[27], using flow controlled by surface acoustic waves (SAWs) [28]-[31], using dielectrophoresis [32], using a secondary flow [33]-[36], and several others [37]-[41]. Representative methods concerning the formation of sheath flow using microfluidic device are described below, and their features and issues are clarified.

2.2.1　Three-dimensional micro channel structure that reproduces a conventional cylindrical double glass tube structure

Sundararajan et al. achieved sheath flow using a 3D micro channel structure that reproduces a conventional cylindrical double glass tube structure [12].

Figure 2-4 shows one of their ideas. This method forms 3D sheath flow via a 3D planer flow channel. Although it is easy to make each flow channel in a plane, it is necessary to bond the properly aligned PDMS sheets of the channel. The assembly process is very complex.

The patterns of the individual channels of this structure are simple, but multiple exposures and alignments are necessary to fabricate the mold. Any shift in alignment affects the formation of the sheath flow, so each channel sheet has to be precisely aligned during assembly. The complex process to fabricate this structure affects the costs and limits its applicability.

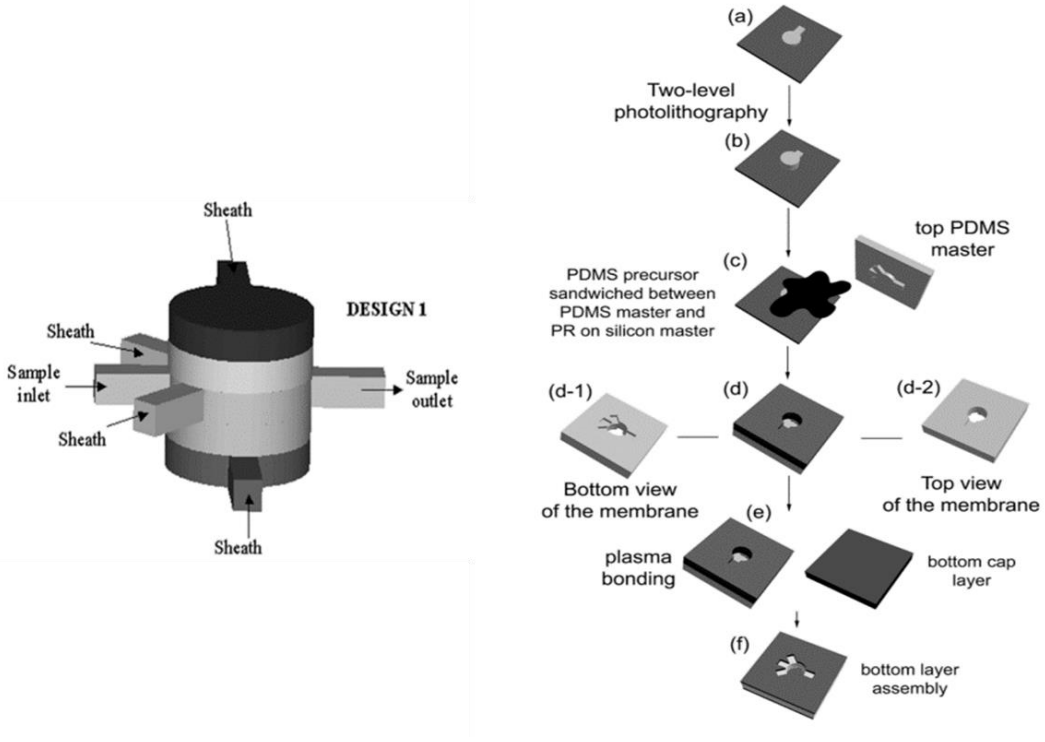

Figure 2-4 Three-dimensional structure and process for fabricating a 3D micro channel

2.2.2 Flow controlled by surface acoustic waves

Shi et al. achieved sheath flow with SAWs using interdigital transducers (IDTs) on both sides of the channel [28]. Figure 2-5 shows the formation of sheath flow using SAWs. Once an Radio Frequency (RF) signal is applied to both IDTs, two series of SAWs propagate in opposite directions toward the particle suspension solution inside the micro channel. The constructive interference of the two SAWs results in the formation of a standing surface acoustic wave (SSAW), as well as the periodic distribution of the pressure nodes (minimum pressure amplitude) and antinodes (maximum pressure amplitude) on the substrate. When the SSAW encounters the fluid medium inside the channel, leakage waves in the longitudinal mode are

generated, causing pressure fluctuations in the medium. These pressure fluctuations result in acoustic radiation forces that act laterally (X direction in Figure 2-5) on the particles. As a result, the suspended particles inside the channel are forced toward either the pressure nodes or antinodes, depending on the density and compressibility of the particles and the medium. When the channel width covers only one pressure node (or antinode), the particles will be trapped in that node. Consequently, particles are gathered at the node position where the pressure is low due to the standing wave.

A piezoelectric material for generating SAWs and an RF signal generator are necessary, which increases the overall size of the system. Moreover, since the line width of the IDT affects the acoustic frequency characteristic, a highly accurate fabrication process is required. This, in turn, makes the system expensive.

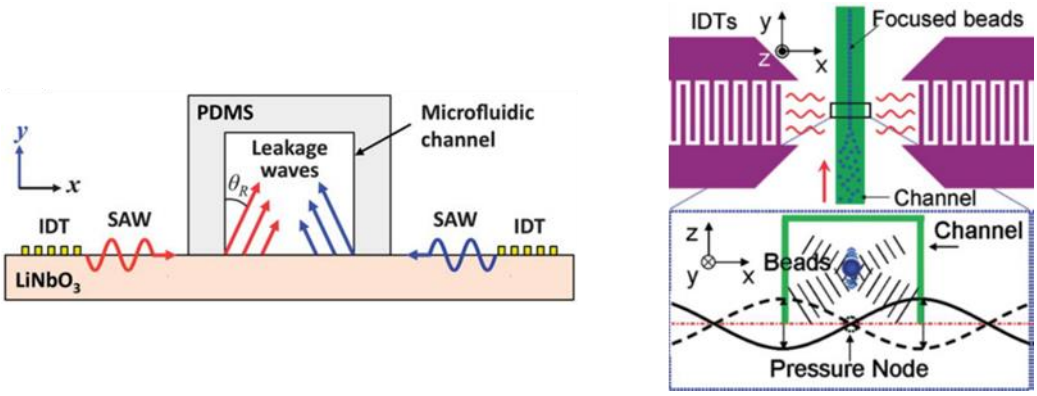

Figure 2-5 Formation of sheath flow using surface acoustic waves

2.2.3 Flow controlled by dielectrophoresis

Holmes et al. achieved sheath flow using dielectrophoresis [32]. The sample fluid is sandwiched by the sheath fluid in the horizontal direction, and forms 2D sheath flow. Downstream of the junction, an alternating current (AC) is applied to the four

electrodes, and particles are collected at the center of the flow path by dielectrophoresis. The 3D focusing flow can be formed by changing the AC voltage applied to the electrode according to the volume of the sample. It is necessary to fabricate the electrodes in the channel, and the fabrication process is complex. A voltage variable AC power supply is also required, which makes the entire system large and expensive.

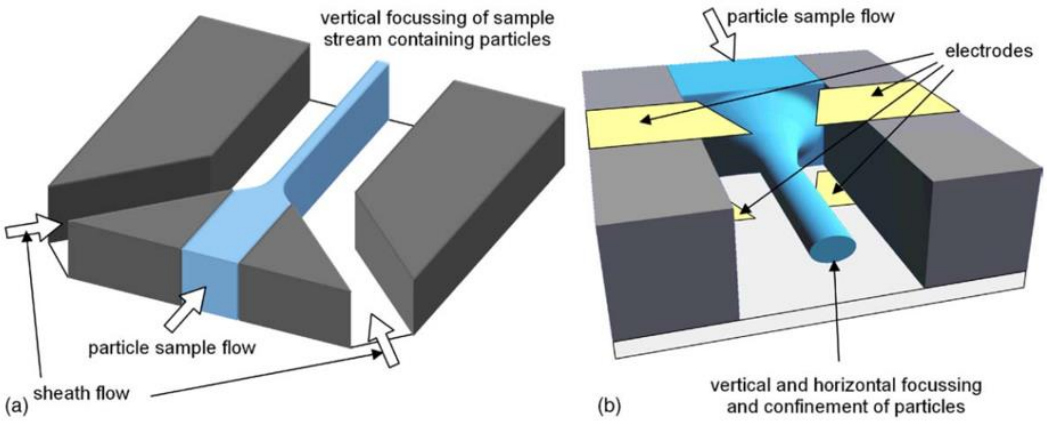

Figure 2-6 Formation of sheath flow using 2D sheath flow and dielectrophoresis

2.2.4 Secondary flow

Mao et al. achieved sheath flow using Dean flow generated by a curved channel [15]. Figure 2-7 shows the micro channel structure to form sheath flow and its principle. The micro channel structure has two inlets, the sample fluid including particles is introduced from inlet A and the sheath fluid is introduced from inlet B. After the introduced fluids are combined, the fluids flow through the curved micro channel. Dean vortices as the secondary flow occur due to the curved channel. A pair of counter-rotating vortices (Dean vortices) occur in the upper and lower parts of the channel cross section, and generate transverse flow. After the particles in the sample

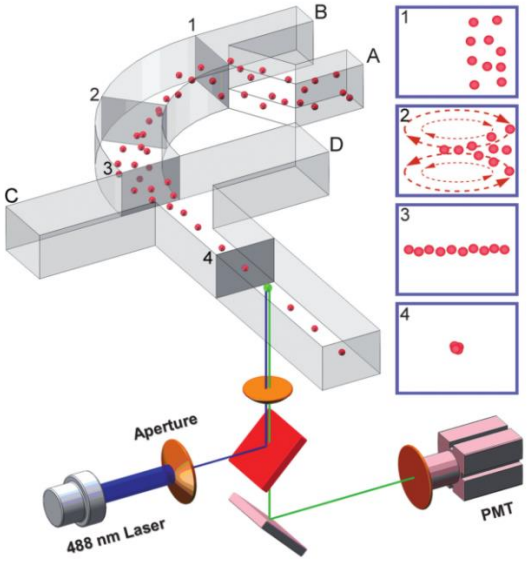

Figure 2-7 Formation of sheath flow using Dean flow

fluid are introduced, they are lined up along the wall by the sheath fluid. While the particles flow through the curved channel, they drift transversely to the opposite side of the channel. They are arranged vertically at the center of the micro channel height, as shown in Figure 2-7, inset 3.

The vertically focused sample flow is compressed horizontally with two horizontal sheath flows (water, insets 3 and 4) from both sides C and D.

As a result, the particles are gathered at the center of the channel. This micro channel is only a planar structure, and the fabrication process is simple. However, it is necessary to design, and the flow must be strictly controlled. Since the sheath fluid must be introduced at the position where the particles are vertically aligned by Dean flow, the fluid properties and the flow conditions must be taken into consideration when designing the micro channel. Since the Dean flow differs according to the flow velocity, the tolerance range of the flow velocity is narrow and it is difficult to control the flow rate of each fluid.

In summary, the following points are important.

1) easy fabrication process

2) easy control of fluids

3) no high-power supply and no RF power

4) low cost

Complex fabrication processes and methods for controlling fluid increase the size and cost of the system. To solve these problems, I proposed a novel structure.

The concept and design of the proposed structure are described and shown in the next section.

2.3 Concept of the twisted micro channel

A 3D micro channel structure is required to form sheath flow without applying an extra force. As a simple, low-cost fabrication process, microfabrication technology is suitable for making a planar micro channel. However, making a 3D structure using this technology is difficult. I propose a completely novel structure made of polydimethylsiloxane (PDMS) as a material [42]. Soft lithography with PDMS is a powerful fabrication technique and suitable for making complex microfluidic structures for an integrated fluidic chip [43]. However, the process has a weak point - it cannot be used to make 3D channel structures. Consequently, I propose a new structure to form sheath flow by taking advantage of the unique material property of PDMS, its elasticity. In other words, I twist a 2D micro channel to introduce the sheath fluid before and after the twist. The sample micro channel has two junctions to introduce the sheath fluids and is twisted by 90° between the two junctions. I thought that sheath flow could be formed by the addition of the sheath fluids from the horizontal direction at the first junction and from the vertical direction at the

second junction, thereby constricting the sample fluid in the center of the channel. The concept of the twisted micro channel is shown in Figure 2-8. I came up with the idea of "twisting" the micro channel from processing the flexible PDMS with a technique called soft lithography[44], [45].

The sample fluid is introduced into the central micro channel, and the sheath fluids are introduced from the left and right at the first junction. The sample fluid is sandwiched between the sheath fluids and takes on a vertically elongated rectangular shape. The central micro channel is twisted by 90° to the second junction, and the sample fluid flows while retaining is vertically elongated rectangular shape. At the second junction, the sheath fluids are introduced from the vertical direction. As a result, the sample fluid is compressed from the top, bottom, left and right, and gathered in the center of the channel cross section.

In the case of the channel with a circular cross section, even if the channel is twisted, the cross-sectional shape of the sample fluid does not change (Figure 2-8). Therefore, the sample fluid is expected to gather in the center of the channel cross section downstream of the second junction. However, since the cross-sectional shape of the fabricated channel is rectangular, a swirling flow generated due to the corners may affect the shape of the cross-sectional flow.

Prediction of sheath flow formation using numerical flow analysis and discussion regarding the influence of the rectangular channel are provided in the next section.

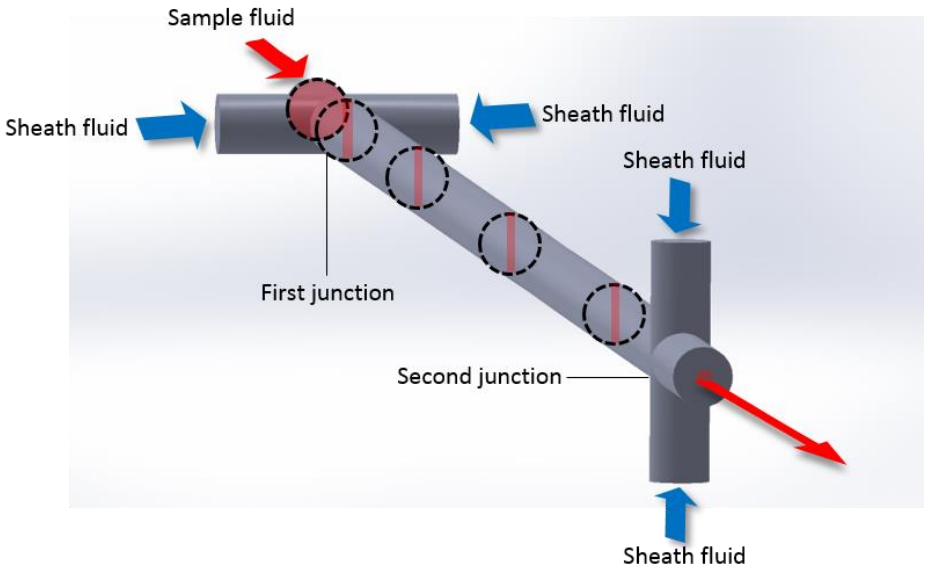

Figure 2-8 Concept of sheath flow formation using a twisted channel

2.4　Prediction of sheath flow formation using numerical flow analysis

First, I assessed the feasibility of our proposed idea using the finite element method (FEM). For the purpose of visualizing the flow in the micro channel, the flow was analyzed using numerical simulation. The flow in the channel is calculated from the Navier–Stokes equation and the convection-diffusion equation.

Figure 2-9 (a) shows an image of the sheath flow cell. A channel for sheath fluid connected with an inlet port is divided into two channels. Each channel is divided into two channels again toward the first junction and the second junction. The sheath fluids sandwich the sample fluid at each junction. Figure 2-9 (b) shows the twisted sheath flow cell. The simple model was used in a numerical simulation similar to what is shown in Figure 2-10.

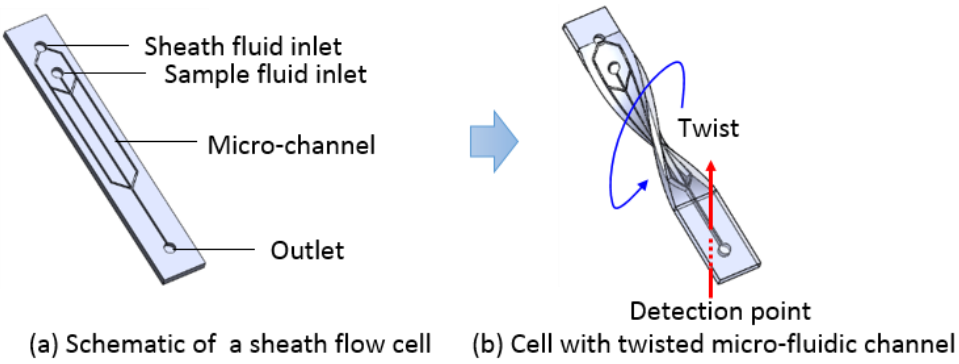

Figure 2-9 Image of the sheath flow cell

As shown in Figure 2-10, the model has two junctions where 2D channels merge. The central channel is twisted by 90° between the two junctions. Figure 2-10 (a) shows the model of a non-twisted channel and (b) shows the model of a twisted channel. The cross-sectional area of each channel is 0.04 mm^2, and the length of the central channel is 2 mm. The position of each junction is set at 0.2 mm and 1.8 mm from inlet of the central channel. The average flow velocity at the sample inlet is set to 0.01 m/s, the sample concentration is set to 100 mol/m^3, and the diffusion coefficient is 1×10^{-10} m^2/s. The sample fluid flows into the central micro channel with two junctions. At each junction, the sheath fluids sandwich the sample fluid. The concentration of the sample fluid is set to 100% (100 mol/m^3) and that of the sheath fluids is set to 0%.

The flow of the sample fluid in the channel was visualized using the numerical simulation to the concentration distribution. The channel is divided into 20 cross sections in the flow direction, and the concentration distribution at each cross section is displayed in color. At the first junction, the sample fluid is sandwiched as a rectangular shape in the channel cross section by the horizontal (Y direction) sheath fluids. Then, the sample fluid is moving downward through the twisted micro channel in the same direction, while retaining its shape. At the second junction, the sample fluid is sandwiched again by vertical (Z direction) sheath fluids. As a result,

the sample fluid is gathered into the center of the channel cross section.

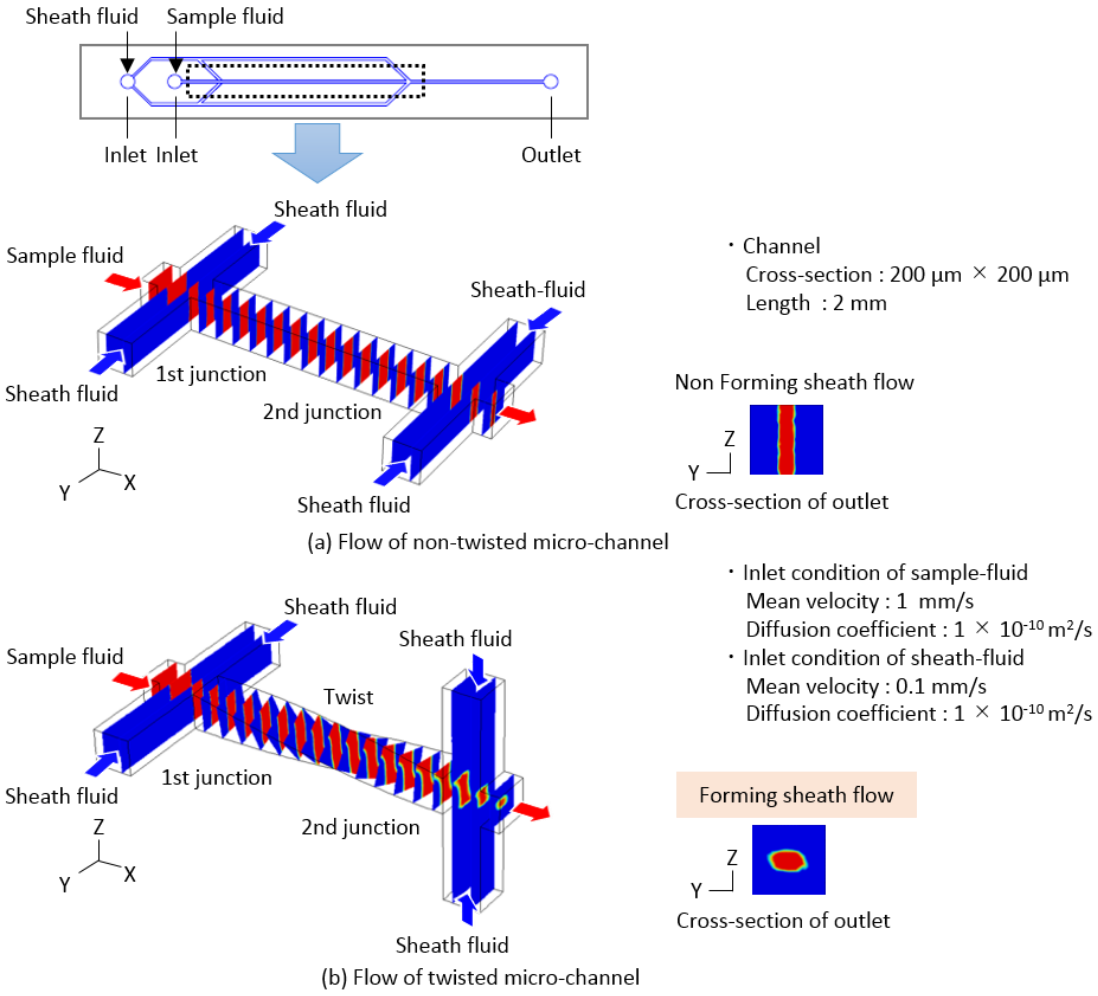

Figure 2-10 Model of a sheath flow cell with a twisted channel

There was concern that the swirling flow affected the sample flow. Therefore, the sample flow was analyzed in detail using water containing particles as the sample fluid.

The model is the same as the one shown in Figure 2-10. The dynamic viscosity (0.893×10^{-6} m²/s) and the density (997 kg/m ³) of water at 25 °C were set as the physical properties of the water for the numerical simulation. To analyze the shape

of the sample flow in the channel cross section, particles were introduced into the sample fluid and the distribution of the flow was analyzed. The particles were set at a density equal to that of water to neglect the influence of mass and diffusion. The average flow velocity of the sample fluid was 0.1 mm/s at the inlet, and the average flow velocity of the sheath fluid was 10 mm/s at the inlet.

Figure 2-11 (a) and (b) show the particle trajectory in red [46]. The channel is divided into 10 cross sections in the flow direction. In the case of Figure 2-11 (a), the sheath fluids are introduced from the horizontal directions (Y direction in the figure) at the first and second junctions, and the sample fluid is sandwiched between the sheath fluids. The particles are gathered in a vertically elongated rectangular shape and the sheath flow is not formed. The sample fluid is gathered in two dimensions and the shape of the sample fluid is rectangular. On the other hand, in the case of (b), the sheath fluids are introduced from the horizontal direction at the first junction, and then the channel is twisted by 90°. Some particles move along the wall surface near the channel wall in front of the second junction, but the shape of the entire particle distribution remains a vertically elongated rectangle. Even if the channel cross section is rectangular, it hardly affects the flow. The sheath fluids are introduced from the vertical direction (Z direction in the figure) at the second junction, and the particles are gathered in the center of the channel cross section. Comparing the particle distribution at the exit in (a) and (b), I see that in the case of (a), the particles are gathered in a vertically elongated rectangular shape, and in the case of (b), the particles are gathered in the center of the channel cross section.

Although there was concern that the swirling flow affected the sample flow, these results show that the sample fluid near the wall follows the curvature of the twisted channel, but hardly affects the overall flow of the sample.

Thus, I surmised that sheath flow could be formed using the proposed twisted micro channel, and fabricated the sheath flow cell with the twisted micro channel and evaluated the flow in the channel.

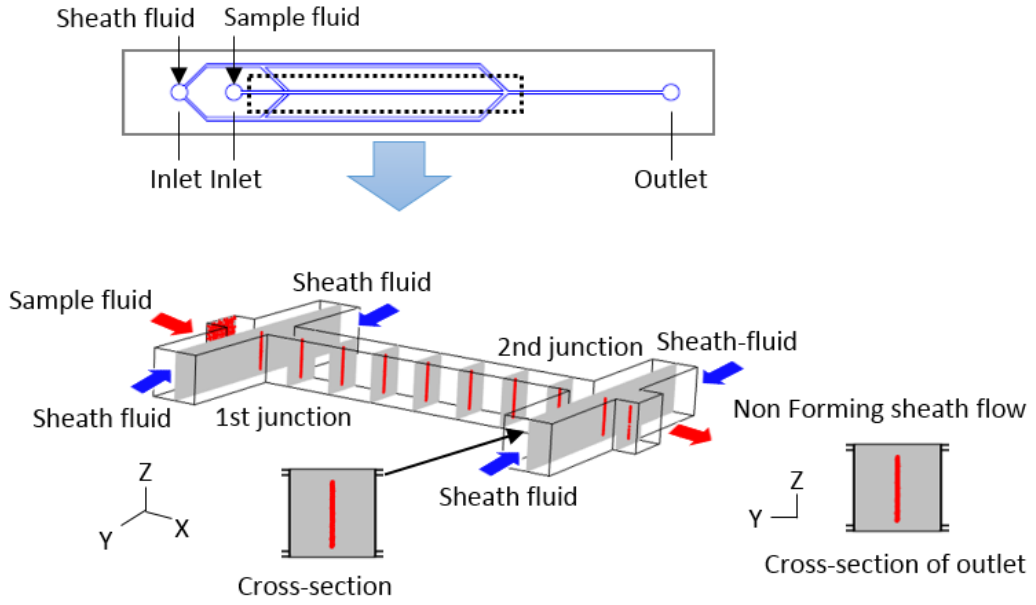

(a) Flow of non-twisted micro-channel

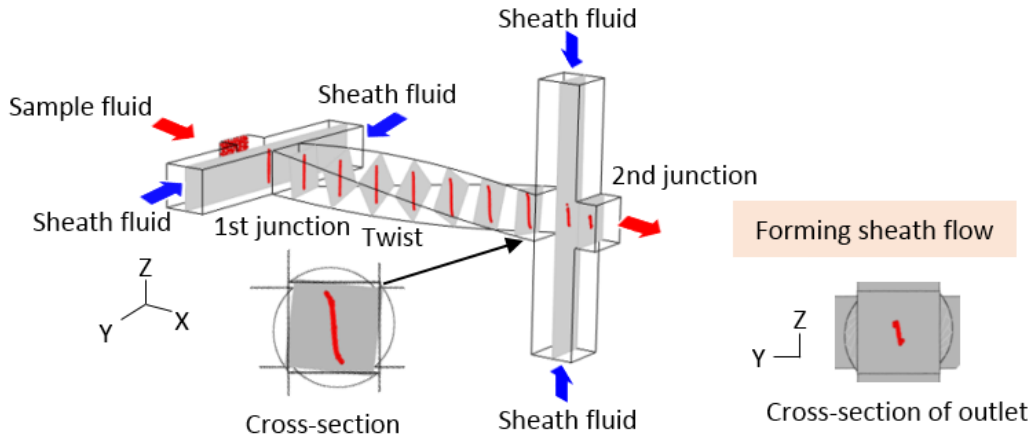

(b) Flow of twisted micro-channel

- Channel
  Cross-section : 200 μm × 200 μm
  Length : 2 mm
- Inlet condition of the sample-fluid
  Mean velocity : 0.1 mm/s
  Fluid : water with particles
- Inlet condition of sheath-fluid
  Mean velocity : 10 mm/s
  Fluid : water

Figure 2-11 Assessment of particle trajectory in twisted and non-twisted micro channels using numerical simulation

Chapter 3　Sheath flow cell with twisted micro channel

The method for optimizing the specifications of the proposed sheath flow cell structure and a simple fabrication method are described in this chapter. Specifically, using the dimensions of each micro channel as a parameter, the design of the sheath flow cell was optimized so an isotropic sheath flow is formed downstream of the second junction. An isotropic sheath flow means the sample fluid is focused at the center of the channel cross section. Based on the design specifications, a sheath flow cell was fabricated, and the flow in the micro channel is observed to verify whether sheath flow was formed [46].

3.1　Design of the twisted micro channel

The length from the sheath fluid inlet to the outlet was set to be approximately 70 mm, which is almost the same as the length of a glass slide. This made observation using a microscope easy. The entire sheath flow cell is relatively long and thin. As shown in Figure 2-9 (b), the sheath flow cell can be twisted easily between the two junctions.

To gather the particles at the center of the channel cross section, the flow rates in

the sheath fluids introduced at both junctions must be equal. The flow rate of each sheath fluid was estimated using numerical simulation.

The flow rate Q is calculated using equation (1) [47]-[49].

$$Q = \frac{\pi D^4}{8\mu} \frac{\Delta p}{l} \quad (1)$$

Q: Flow rate

D: Hydraulic diameter

μ: Viscosity

$\triangle p$: Pressure fluctuation

l: Length

Here, the pressure fluctuation is calculated using the Darcy–Weisbach equation (2).

$$h = \frac{\Delta p}{\rho g} = \lambda \frac{L}{d} \frac{v^2}{2g}$$

$$\Delta p = \rho g \lambda \frac{L}{d} \frac{v^2}{2g} \qquad (2)$$

h: Head loss

Δp: Pressure fluctuation

ρ: Density of the fluid

d: Hydraulic diameter

v: Mean flow velocity

λ: Friction coefficient

According to equation (1), the flow rate in the micro channel at each junction is proportional to the fourth power of the hydraulic diameter of the micro channel and inversely proportional to the length of the micro channel. The flow rate of the sheath fluids can be equalized by adjusting the hydraulic diameter and the length of the micro channel.

Figure 3-1 shows a flow diagram of the proposed model, which is similar to the sheath flow cell shown in Figure 2-9. A channel for a sheath fluid connected to the inlet is divided into two channels. Each channel is divided again into two channels toward the first junction and the second junction. The sheath fluids sandwich the sample fluid in each junction. Here, to form an isotropic focusing flow, the length and the width of each micro channel were calculated so the pressure fluctuation of

each channel was equal. As shown in Figure 3-1, parameters were the widths (W_1 and W_2) and the lengths (L_1 and L_2). All heights were assumed to be 150 μm. The flow rate of the sheath fluid toward the first junction is Q_1 and that toward the second junction is Q_2.

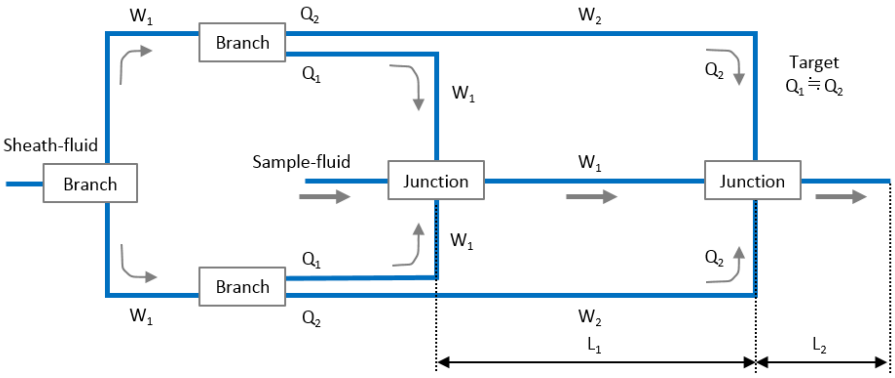

Figure 3-1 Flow diagram of the twisted micro channel

The length of the downstream portion of the channel after the first junction was assumed to be 50 mm to make the channel easier to twist. The flow rate ratio of the sample fluid and the sheath fluid was assumed to be 1:100. The mathematical model was constructed as shown in Figure 3-2, and the parameters L_1, L_2, W_1 and W_2 were optimized using numerical simulation. The model-based analysis method developed by Miyake et al. was used to obtain the flow distribution between the complex channel networks that repeatedly branch and merge [2]. Figure 3-2 shows a schematic diagram of the mathematical model of the sheath flow cell.

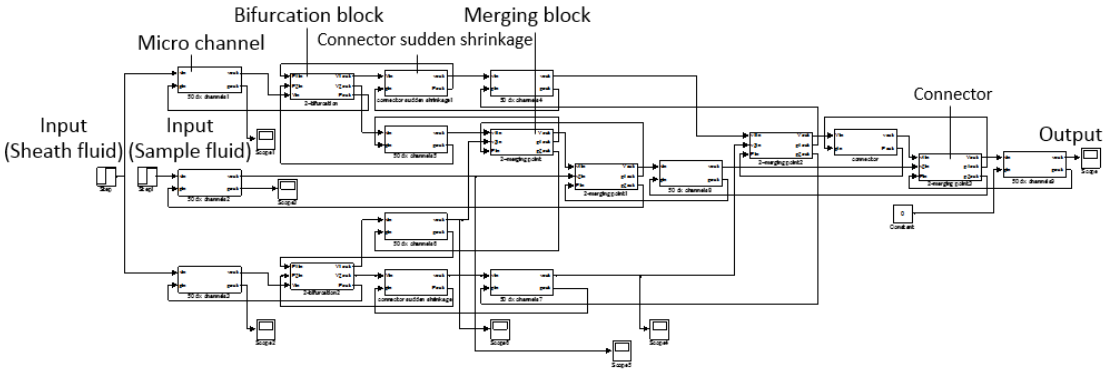

Figure 3-2　Channel block model of the sheath flow cell

The parameters were the width W2 and length L1 (L2 = 50 – L1) of the sheath fluid micro channel, the width of the sample fluid micro channel W_1 was fixed at 150 μm. Since the cross section of the micro channel is rectangular, the hydraulic diameter D shown in equation (3) was calculated and input in the model.

$$D = \frac{4\,(W_2 \times \text{Channel depth})}{2\,(W_2 + \text{Channel depth})} = \frac{4\,(W_2 \times 150)}{2\,(W_2 + 150)} \qquad (3)$$

W_2: Channel width (cf.　Figure 3-1 W_2)

Channel depth: 150 μm

The fluid was assumed to be water at 25 °C. Figure 3-3 shows the calculation results. As shown in Figure 3-3 (a), the flow rate ratio Q_1/Q_2 depends on the length L_1. The vertical axis represents the flow rate ratio Q_1/Q_2, and the horizontal axis represents the length of the micro channel L_1. If the length of the sample fluid micro

channel is 20 mm or more, the flow rate ratio is almost constant and does not change. This is because when the length is increased, the channel lengths of the sample fluid and the sheath fluid can be regarded as equal. The ratio of the pressure fluctuation becomes constant, so the flow ratio also remains constant. The micro channel may be extended in the longitudinal direction when the micro channel is twisted. Because the flow rate ratio was almost constant at lengths greater than 20 mm, L_1 was set to 23 mm.

Next, the flow rate ratio Q_1/Q_2 was calculated for different widths of the micro channel W_2. The results are shown in Figure 3-3 (b). The vertical axis shows the flow rate ratio Q_1/Q_2, and the horizontal axis shows the channel width W_2. W_2 and the flow rate ratio Q_1/Q_2 are inversely proportional to each other. Thus, a W_2 of 110 μm, where $Q_1/Q_2 = 1$, was selected. According to the parameter analysis, the size of the sheath flow cell was set as shown in Figure 3-4.

Next, based on the design specifications, the sheath flow cell was fabricated, and the flow in the channel was observed with a fluorescent fluid to assess the formation of sheath flow. The next section describes the fabrication process of the sheath flow cell.

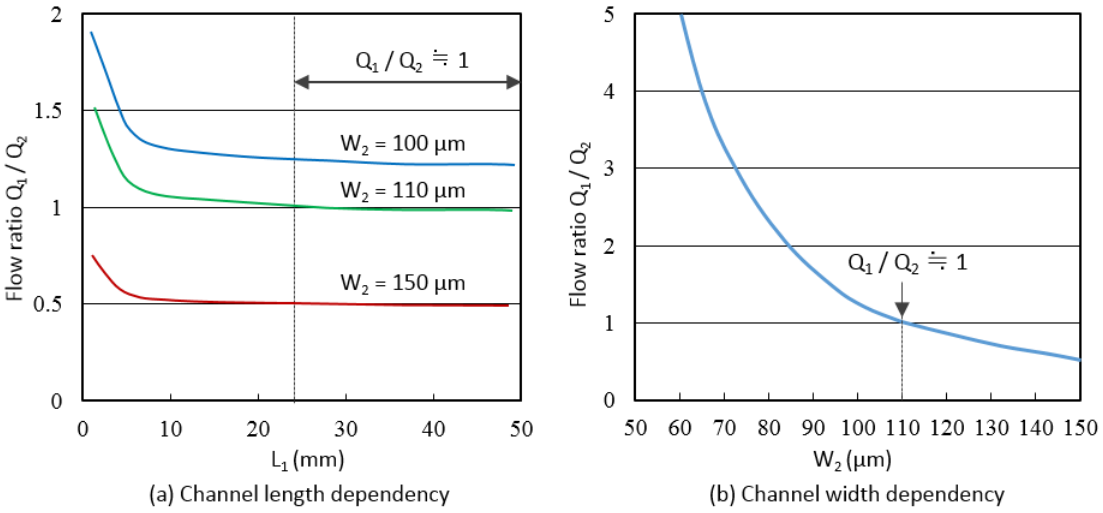

Figure 3-3 Effect of (a) channel length and (b) channel width on the flow ratio

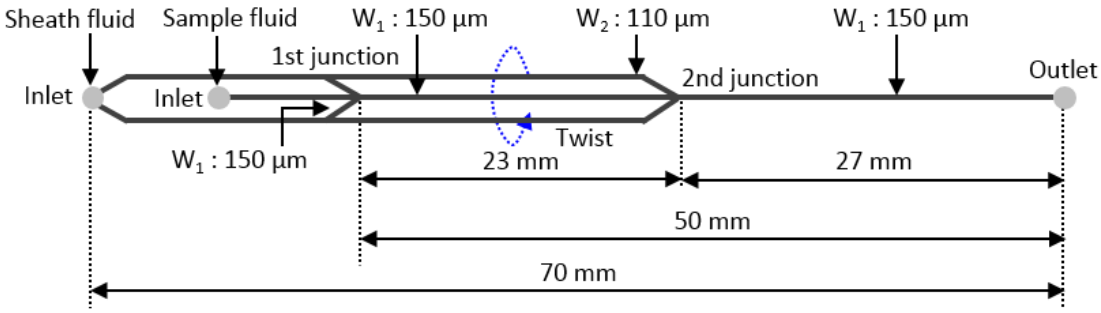

Figure 3-4 Geometry of the sheath flow cell

3.2　Micro channel fabrication

The micro channel of the sheath flow cell was fabricated by molding. Silicon (Si) and photoresist are available materials for making molds via microfabrication, and the material is typically selected according to the processing shape, durability, cost and so on. For a simple method, SU-8 3050 (Nippon Kayaku Co., Ltd.) photoresist was used in this experiment. SU-8 3050 is a negative photoresist for coating a thick

film and can be coated to a thickness of approximately 50 μm by spin coating at 3000 rpm.

First, SU-8 3050 was coated on a silicon wafer and then exposed to the ultraviolet (UV) light. The mold with the channel pattern was completed using photolithography, and then the channel pattern was transferred to a PDMS sheet. The PDMS sheet with the transferred channel pattern was bonded with another plain PDMS sheet after surface treatment with soft plasma. Each PDMS sheet was 1 mm thick. Finally, the PDMS sheet was cut into a long, narrow piece, measuring 8 mm × 80 mm, so it could be twisted easily.

The fabrication process is described in detail in the following section.

3.2.1 Fabrication process

The procedures to fabricate the PDMS micro channel are:

・Creation of channel pattern mold

・Transfer to PDMS

・Assembly

Figure 3-5 shows the fabrication process flow. The micro channel is fabricated using soft lithography.

As described in section 2.2, the previously reported fabrication processes are complex, whereas this fabrication process is very easy. Because photolithography is required only once during the fabrication process, alignment of multiple sheets is not necessary.

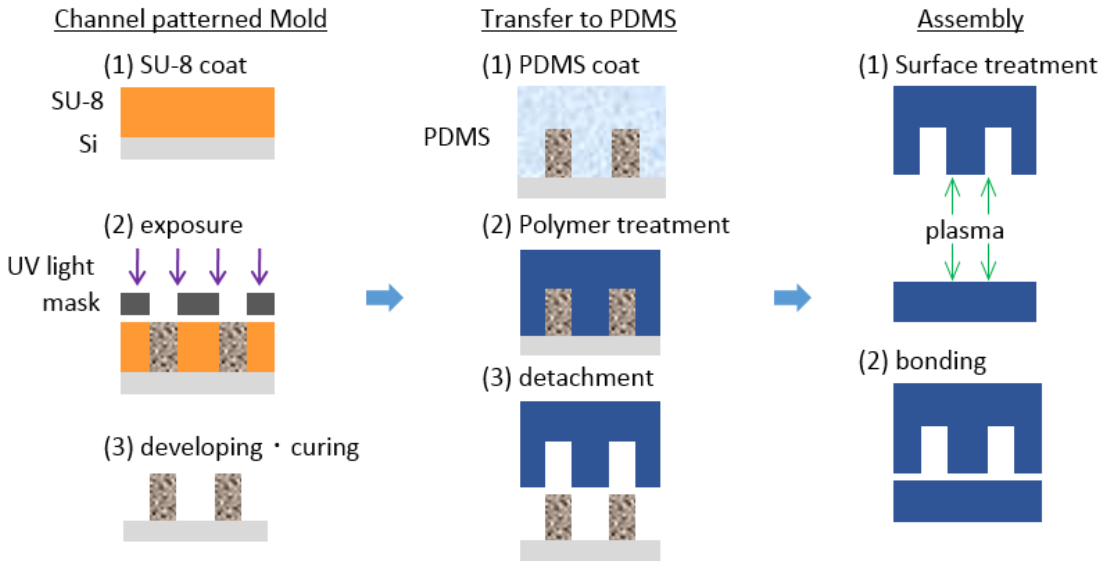

Figure 3-3 Process flow for fabrication of the PMDS micro channel

First, an SU-8 mold is fabricated [50], [51]. SU-8 is a negative photoresist and chemically amplify type resist. Hydrogen as a catalyst is generated from the resist by exposure to the UV light, and a crosslink reaction proceeds by baking. The thickness of the SU-8 becomes the height of the micro channel. It should be noted that a uniform thickness is important for the fabrication of the micro channel. It is difficult to coat SU-8 on a Si wafer with high uniformity using the spin coating method, which is a common method in semiconductor manufacturing, because SU-8 has high viscosity. Therefore, I examined SU-8 coating methods that could be used to control the thickness with high uniformity. The experiments on the coating methods and the results are explained in the next section.

Since PDMS has high transfer ability, a submicron structure can be transferred to PDMS [52], [53]. Moreover, PDMS has excellent characteristics; it is colorless, transparent, exhibits negligible absorption in the visible light region, and has almost no auto-fluorescence. Fabrication processes utilizing PDMS are generally very easy and inexpensive. Therefore, PDMS is used in many applications in both chemistry

and biology, such as chemical analysis and synthesis, and protein analysis.

The following sections describe the steps to fabricate the PMDS micro channel.

[Creation of channel pattern mold]

The SU-8 3050 was coated at a thickness of approximately 50 μm on the Si wafer by spin coating at 3000 rpm. After baking and drying (i.e., soft baking) for 45 min, the SU-8 3050 was recoated on the Si wafer. These operations were repeated three times to achieve a thickness of 150 μm. The SU-8 was then exposed and baked (post exposure bake). The micro channel pattern was exposed using a DL-1000 (Digital micromirror device-based maskless photolithography system, NanoSystem Solutions Inc.) or an MA6+ (Mask Aligner, SUSS MicroTec Company). It took approximately 10 h for the exposure using the DL-1000 because of direct drawing, whereas it took only tens of seconds using the MA6+ for the exposure. However, it was necessary to prepare the photomask drawn from the micro channel pattern in advance. In developing process, the non-exposed SU-8 was removed and the exposed SU-8 remained as a mold. Subsequently, the SU-8 mold was cured by baking.

[Transfer to PDMS]

The PDMS used in this study is a liquid bi-component silicone (Sylgard 184, Dow Corning). The main material is mixed with a crosslinking material. The mixed PDMS material (viscosity = 3,500 cP) was coated on the Si wafer with the mold. If the PDMS is too thin, the shape cannot be maintained; however, if the PDMS is too thick, the PDMS with the channel pattern cannot be twisted easily. Therefore, the thickness of the PDMS used to form the sheath flow cell was set at 1 mm. When 8 g of the mixed PDMS is coated on a φ100 mm Si wafer, the thickness of the PDMS is

approximately 1 mm. Air bubbles in the PDMS were removed using a vacuum, and the PDMS was cured at 80 °C for 1 h in an oven. After the PDMS was peeled off from the mold, holes for inlets and an outlet were made in the PDMS. Similarly, a plane PDMS sheet with a thickness of 1 mm was also fabricated.

[Assembly]

The bonding surfaces of the channel-patterned PDMS and the plane PDMS sheet were treated by plasma ashing at 10 W for 45 s using an SEDE-P soft plasma generator (Meiwafosis Co., Ltd.). The sheets were then adhered and cured at 80 °C for 1 h in an oven. Finally, the PDMS was cut into the suitable shape, thereby completing the fabrication of the sheath flow cell with micro channel.

One of the important factors to consider during fabrication of the micro channel is controlling the thickness of the SU-8 as the mold. The next section describes my trial-and-error methods for coating SU-8 with high uniformity on Si.

3.2.2 SU-8 coating methods

The resist used for the experiment was SU-8 3050, and its kinematic viscosity is 12000 cSt (1 cSt = 1 mm^2/s, reference values: water 1 cSt, salad oil 70 cSt). In a general coating method, for example OFPR 800 LB 23 cP (= 23 cSt at a density of 1 g/ml, Kinematic viscosity (cSt) = Viscosity (cP) / Density (g/cm^3)) (Tokyo Ohka Kogyo), approximately 4 ml of resist is placed in the center of a φ100 mm Si wafer and then spin-coated. The resist spreads toward the periphery of the wafer as it spins. In the case of OFPR 800 LB 23 cP, when the resist is spin-coated at 3000 rpm, the thickness uniformity of the resist is ±3%, excluding 5 mm of the wafer periphery.

First, SU-8 3050 was coated on a Si wafer by the same general method, and the distribution of the resist thickness was measured using DekTak (Bruker) after exposure. Table 3-1shows the SU-8 coating protocol and each condition. In the specifications provided by the manufacturer, when the wafer is rotated at 3000 rpm to coat SU-8 3050, According to the manufacturer, the thickness of spin-coated SU-8 3050 on a Si wafer rotated at 3000 rpm is 50 μm. The conditions recommended by the manufacturer were applied in this protocol.

As the test pattern, rectangles measuring 798 μm × 1 mm were arrayed with a pitch of 1.024 mm on the diameter line (see Figure 3-6).

Table 3-1 Coating protocol of SU-8

Process	Condition
Wafer	φ100mm New wafer
Wafer bake	180℃ 3 min Heating by hot plate
Hexamethyldisilazane	4 ml HMDS
(HMDS) coat	500 rpm 10 sec (slope 5 sec)
	3000 rpm 30 sec (slope 8.5 sec)
Wafer bake	130℃ 2 min Heating by hot plate
SU-8 coat	6 ml SU-8
	500 rpm 10 sec (slope 5 sec)
	3000 rpm 30 sec (slope 8.5 sec)
Soft bake	95℃ 15 min Heating by hot plate
Exposure	100 J/cm^2 by mask-less lithography system
Post exposure bake	95℃ 5 min Heating by hot plate
Developing	Dipping the wafer in developer until development is completed
Cleaning	Wash the water using developer
Hard bake	95℃ 5 min Heating by hot plate

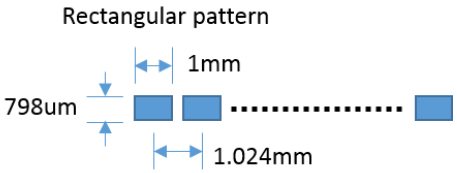

Figure 3-4 Rectangular test pattern for evaluation of SU-8 thickness

The heights of the patterns were measured from the center of the wafer toward the periphery. Figure 3-7 shows photographs of the measurement results. The SU-8 thickness was estimated from these photographs.

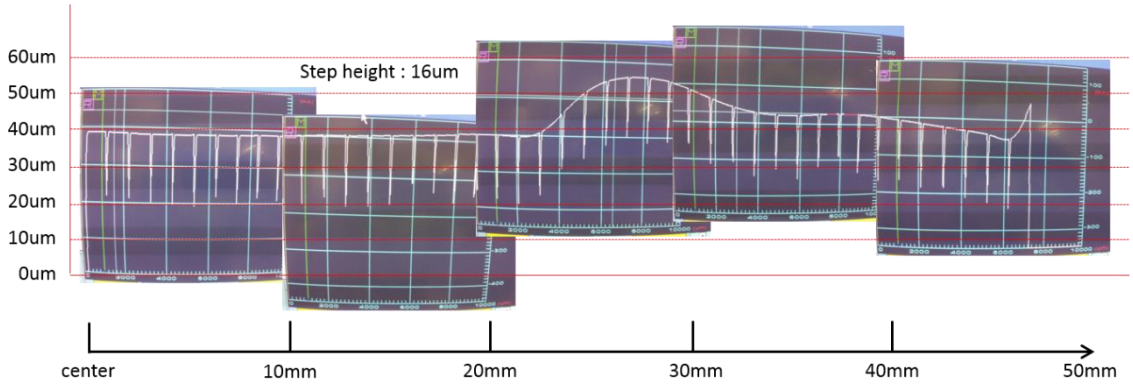

Figure 3-5　Step measurement results of the SU-8 coated using the general method

The thickness of the resist at center of the wafer was approximately 40 μm. The resist rose up nearly 16 μm at about 30 mm from the center of the wafer. The space between the patterns was narrow, so it was not possible to measure the thickness exactly. An array pattern of 500 μm × 500 μm squares with a pitch of 5 mm was subsequently made and measured. Figure 3-8 shows the test pattern with 500 μm × 500 μm squares.

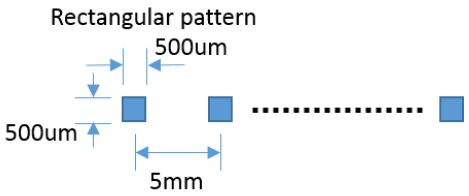

Figure 3-6 Square test pattern for evaluation of SU-8 thickness

Figure 3-9 shows the thickness distribution of the resist. The SU-8 thickness at the center of the wafer was approximately 40 μm. Similar to the previous result, the resist rose up nearly 15 μm at about 30 mm from the center of the wafer. When SU-8 was placed on the Si wafer, the periphery of SU-8 was approximately 30 mm from the center of the wafer, which matched the position where the resist rose up. Based on the variation in thickness, SU-8 on the Si wafer was not uniformly coated using the general method.

Distance of the wafer center (mm)	Thickness (μm)
0	37.65
5	38.00
10	38.10
15	38.56
20	39.41
25	50.73
30	53.13
35	46.56
40	41.62
45	56.35

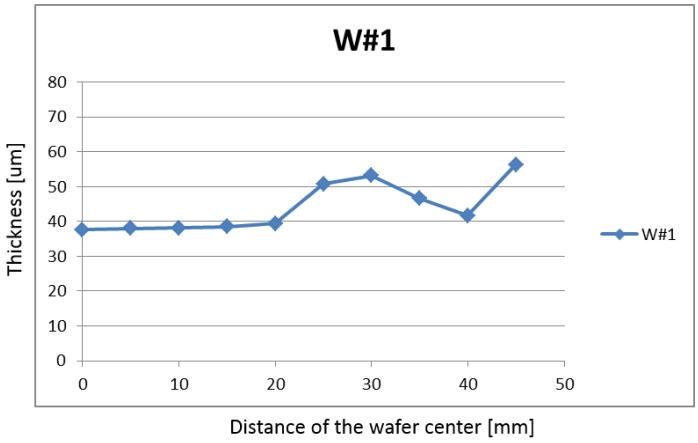

Figure 3-7 Thickness of the SU-8 test pattern shown in Figure 3-9 when coated using the general method

Consequently, various coating methods were attempted. The tested coating methods and the results are shown below. Firstly, as a simple test, the surface roughness of the resist was measured using DekTak after soft baking to predict the uniformity of the thickness. The test pattern shown in Figure 3-8 was made using the best method, and the thickness and the uniformity were measured. A summary of the results is shown in Table 3-2.

(1) Placing SU-8 in a spiral shape from the center toward the periphery on the Si wafer using a syringe.

I had expected that by placing the resist in a spiral shape towards the periphery before spin coating, it would spread over the entire wafer. Table 3-2 (1) shows an illustration of the resist in a spiral pattern on the wafer. However, it was difficult creating a spiral pattern with SU-8 due to its high viscosity. The volume of resist, the spiral shape, and its pitch could not be controlled easily when applied manually. Moreover, numerous tiny bubbles that proved difficult to get rid of were generated in the resist as it was pushed out of the syringe. The gaps produced by the spiral shape could not be filled with SU-8, and the surface of the spin-coated SU-8 was visibly rough. Therefore, the surface roughness was not measured.

(2) Manually spreading the resist using a spatula.

SU-8 was placed at the center of the Si wafer while the wafer holder was rotated, and SU-8 was manually spread to the periphery using a spatula. This was done to help spread SU-8 over the entire wafer. Table 3-2 (2) shows an illustration of spreading SU-8 using a spatula. SU-8 got over the spatula, it could not be spread to the periphery, and a lot of fine bubbles were generated. The roughness of SU-8 surface was ± 6 μm. Since the thickness of SU-8 could not be controlled when it was

manually spread with a spatula, there were substantial variations in its thickness. The applied SU-8 actually had a conical shape.

(3) Placing SU-8 from the center toward the periphery on the Si wafer while rotating the wafer holder.

I had expected that by placing SU-8 from the center of the wafer toward the periphery while rotating the wafer shown in Table 3-2 (3), the resist would spread over the entire surface. However, the highly viscous SU-8 rotated together with the wafer, and the resist did not spread to the periphery of the wafer. The roughness of SU-8 surface was ± 5 μm. Although the variation in the thickness was relatively narrow, this method did not have sufficient repeatability.

(4) Placing the resist on approximately 80% of the wafer.

SU-8 was placed on approximately 80% of the wafer, and the extra resist was spread out by rotating the wafer holder. The variation in the roughness was approximately ± 3 μm. According to the measurement of the step, SU-8 thickness could be controlled to 50 μm ± 1 μm in the area within φ80 mm. Bubbles were sometimes generated when SU-8 was placed at the center of the Si wafer. However, the bubbles rose to the surface during the soft baking, and could be removed by puncturing them with a needle. This was the best method for achieving a uniform thickness of SU-8.

Each coating method and the results are summarized in Table 3-2. Since method (4) was the best method for achieving a uniform thickness of SU-8, the relationship

between the maximum rotational speed and the resist thickness for this method was investigated.

Table 3-2 Methods of SU-8 coating and thickness uniformity

(1) A method of placing SU-8 in a spiral shape from the center toward the outer periphery on Si wafer using a syringe

result	Many small bubbles generated, SU-8 became like foam.
Thickness uniformity(φ90)	No data

(2) A method of spreading the resist using a spatula in manual operation

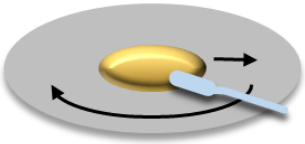

result	SU-8 got over the spatula and did not spread out. Also, many bubbles generated.
Thickness uniformity(φ90)	±6 μm

(3) A method of placing SU-8 from the center toward the outer periphery on Si wafer using a syringe while the wafer holder was rotated

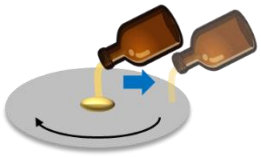

result	SU-8 rotated with the wafer and did not spread out because of high viscosity. Also, many bubbles generated.
Thickness uniformity(φ90)	±5 μm

(4) A method of placing the resist on about 80% area of the wafer

result	SU-8 spread out uniformly and no bubble generated.
Thickness uniformity(φ90)	±3 μm

Hexamethyldisilazane (HMDS) and SU-8 were spin-coated using the protocol shown in Table 3-1. The maximum rotational speeds were 3,000, 2,500, and 2,300 rpm. SU-8 was first coated on the Si wafer using method [4], and then the coated Si wafer was soft baked, exposed to the UV light, developed, and finally hard baked. Figure 3-10 shows the thickness distribution of SU-8 at each rotational speed. Table 3-3 shows the measurement data, average and standard deviation. Regardless of the maximum rotational speed, SU-8 thickness could be controlled to ±0.5 μm in the area within φ80 mm.

Figure 3-11 shows the average thickness of the resist (within φ80 mm) at each rotational speed. A thickness of 50 μm was achieved when the holder was rotated at 2,300 rpm.

Thus, to obtain an SU-8 thickness of 50 μm, the resist should be placed on approximately 80% of the wafer, and the wafer holder should be rotated at 2,300 rpm. Any extra resist will spin off the wafer.

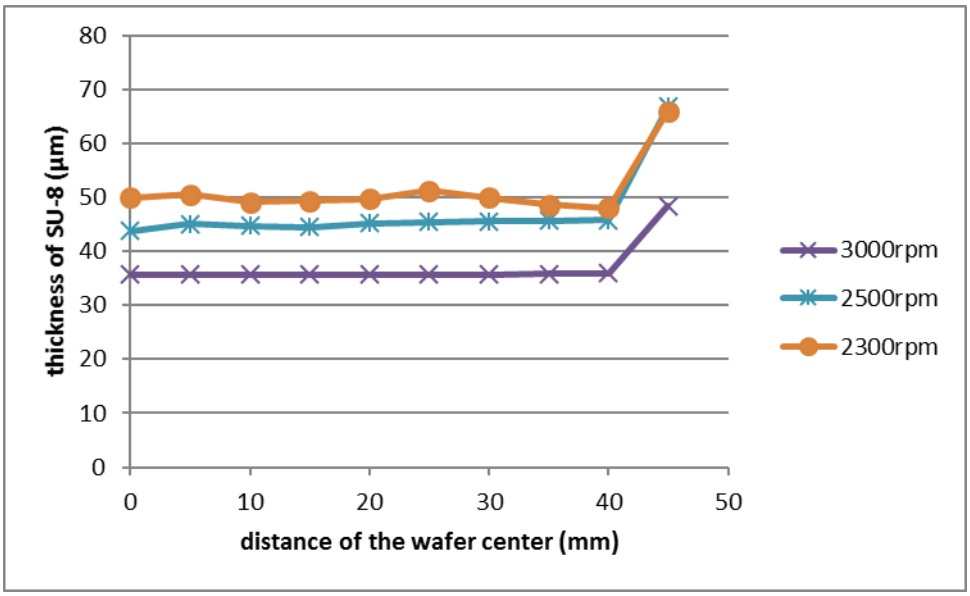

Figure 3-8 Uniformity of SU-8 thickness when coated using method [4]

Table 3-3 Thickness uniformity data of SU-8 when coated using method [4]

Distance of the wafer center (mm)	3000 rpm Thickness (μm)	2500 rpm Thickness (μm)	2300 rpm Thickness (μm)
0	35.73	43.72	49.98
5	35.70	45.03	50.59
10	35.65	44.78	49.12
15	35.75	44.47	49.39
20	35.75	45.14	49.72
25	35.65	45.48	51.23
30	35.75	45.58	49.95
35	35.84	45.69	48.68
40	35.92	45.81	48.09
45	48.43	66.87	66.04
Average (Center ~ 40 mm)	35.75	45.08	49.64
Standard Deviation(Center ~ 40 mm)	0.08	0.64	0.90

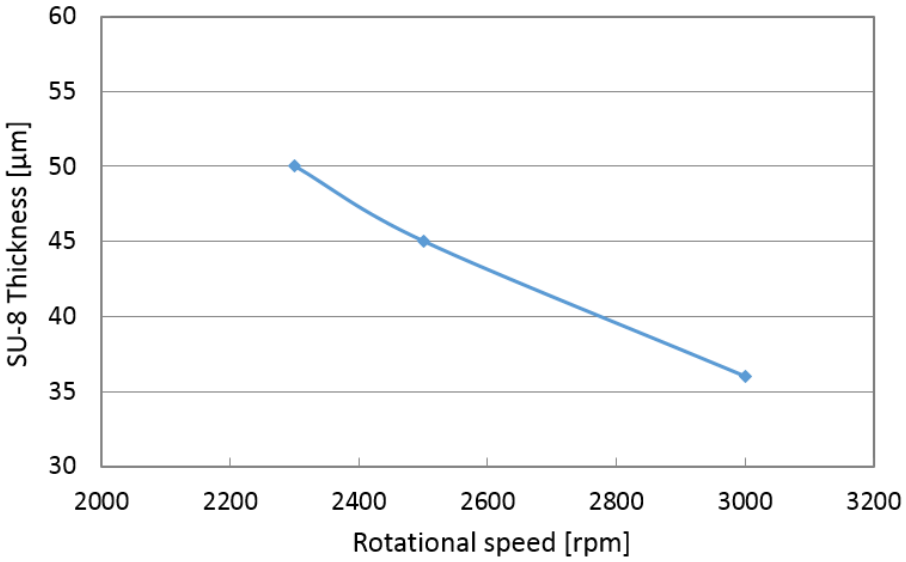

Figure 3-9 Thickness of SU-8 at different rotational speeds

3.2.3 Fabricated micro channel for testing

Based on the design shown in Figure 3-4, a prototype sheath flow cell was fabricated. Figure 3-12 shows a photograph of the fabricated sheath flow cell.

Figure 3-12 Prototype sheath flow cell

Spin coating of the resist was repeated to coat the resist at a final thickness of 150 μm. The final thickness of the coated resist was 120 μm, and the cross-sectional area of the sheath fluid channel of the mold was 120 μm × 100 μm. The sheath flow cell could be used to confirm the formation of sheath flow. Next, the flow in the channel was observed using a fluorescent fluid to assess the formation of sheath flow.

3.3 Observation of the flow in the twisted micro channel

The flow in the fabricated sheath flow cell was observed to check whether the twisted micro channel structure actually forms sheath flow [42], [43].

3.3.1 Observation setup

A setup using a microscope was constructed to observe the fluorescence in the micro channel. Figure 3-13 shows the observation setup with the twisted sheath flow cell. Both ends of the sheath flow cell were fixed to a special jig installed on the rotation stage. The sheath flow cell can be twisted at an arbitrary angle and the observation position can be changed using the jig. During the observation, the rotation stage was fixed so the micro channel was twisted by 90° between the first

junction and the second junction. The jig was designed so the rotational axis of twisting the sample fluid channel coincides with the rotational axis of the rotation stage. In other words, the center of the channel cross section coincides with the center of rotation. It was also confirmed using a microscope that no deformation of the sheath flow channel occurred except for twisting, and that the rotational axis of the sample fluid channel was linear. Two inlets for the sample fluid and the sheath fluid were made at the jig, and silicone tubes were attached to the inlets. Each fluid was injected using a syringe pump. A light illuminated the underside of the sheath flow cell, and transmitted light images were captured using a camera (EX-F1, Casio) attached to the microscope.

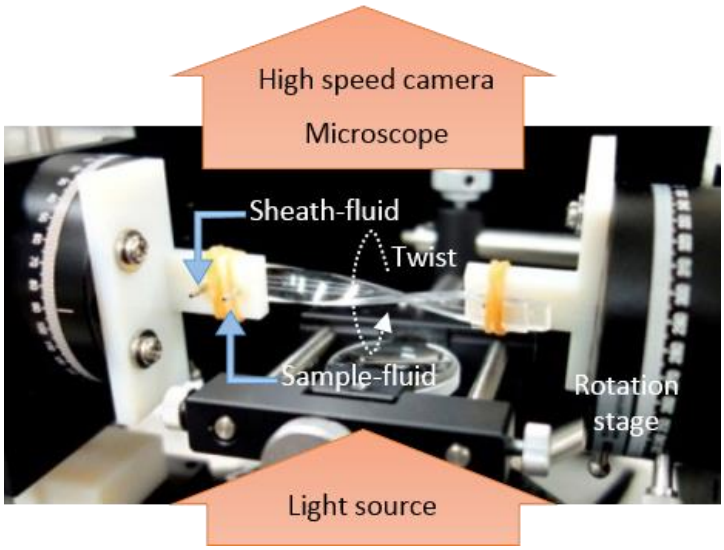

Figure 3-10 Photograph of the twisted sheath flow cell on the rotation stage

3.3.2 Fluorescent fluid flow

The flow was observed using a fluorescent fluid (uranine) as the sample fluid and pure water as the sheath fluid. The flow rates of the sample fluid and sheath fluid

were 0.083 µl/s and 0.56 µl/s, respectively. The flow was observed downstream of the first junction and downstream of the second junction. Figure 3-14 shows photographs of the flows at the first and second junctions. In both cases, the sample fluid was sandwiched between the sheath fluids and gathered in the width direction of the channel. However, it could not be confirmed whether the sample fluid was gathered in the depth direction of the channel. I attempted to observe the flow in the depth direction of the channel from the side of the sheath flow cell; however, it was impossible to clearly confirm that the sample fluid was gathered in the depth direction. It was considered that the main cause was the scattering of fluorescence due to the roughness of the cut surface on the side of the sheath flow cell. In this method, although 2D compression in the observation direction could be confirmed, compression of the fluid in the depth direction could not be confirmed. Therefore, to know the flow in the depth direction during observation from one direction, I proposed a method to predict the formation of sheath flow. This method is described in the next section.

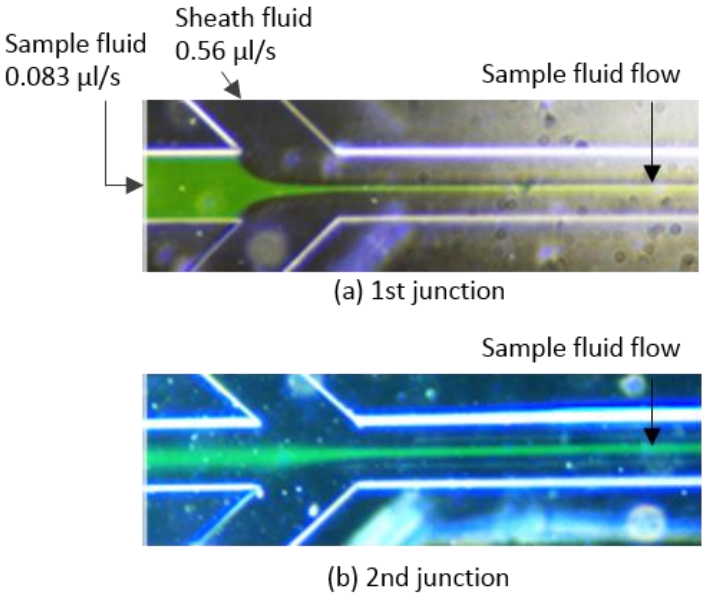

Figure 3-14 Photographs of the flows at each junction of the twisted sheath flow cell

3.4　Assessing sheath flow by tracking and counting particles

3.4.1　Novel method to predict sheath flow formation

During observation from one direction using a microscope, 3D formation of the sample fluid could not be confirmed. Therefore, I proposed a method to predict the 3D formation from the velocity of particles using water containing tracer particles as a sample fluid. Figure 3-15 (a) shows the velocity distribution of the particles and frequency without 3D formation of the sample fluid. Figure 3-15 (b) shows the velocity distribution of the particles and frequency with successful 3D formation of the sample fluid. It is assumed that the particles flow within the area formed by the dotted lines in the figure in each case.

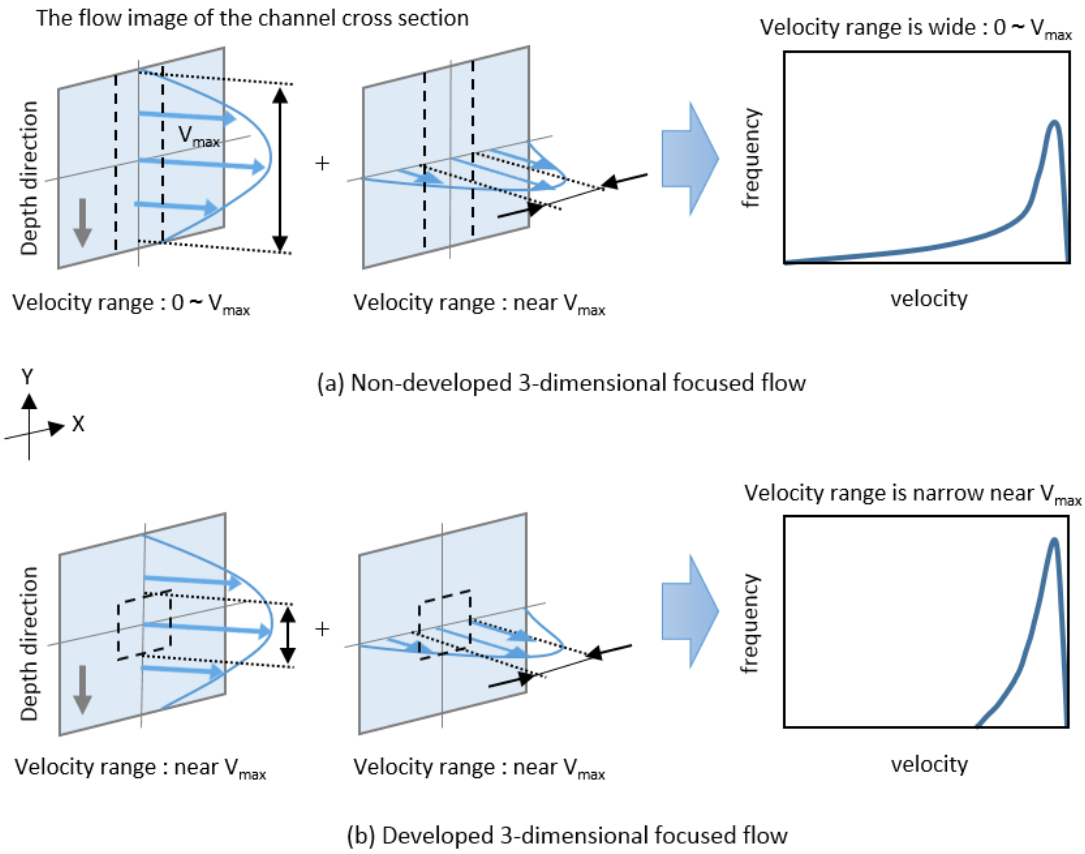

Figure 3-11 Proposed method to estimate 3D focusing flow

The number of particles in a certain velocity range can be estimated from the multiplication of the cross-sectional area of the velocity range and the typical flow velocity. The flow within the micro channel is assumed to be Poiseuille flow; therefore, the flow velocity has a parabolic distribution both in the width direction and the depth direction, and the center of the channel cross section is the area of the fastest flow (V_{max}). If the particles are gathered only in the width direction, as shown in the figure 3-15, and 3D formation of the sample fluid is not developed, as in case (a), the particles are widely distributed in the depth direction, so the velocities of the observed particles are also distributed widely in the range of 0 to V_{max} and the frequency distribution tends to increase toward the right of the graph. In contrast, if the particles are gathered in the center of the channel cross section and there is

3D formation of the sample fluid, as in case (b), the velocities of the particles are distributed only in the high velocity range around V_{max}, and the frequency distribution tends to be biased on the right side.

Therefore, I considered that it is possible to predict whether sheath flow is formed by obtaining the frequency distribution of the particle velocity. The measurement results are shown in the next section.

3.4.2 Measurement of particle velocity

The flow of particles downstream of the two junctions was measured using a sample fluid containing particles. In this experiment, the flow of the micro channel is laminar, where the Reynolds number is 4.35. The velocity distribution follows that of Poiseuille flow. The velocities of the sample fluid containing φ5 μm particles and the sheath fluid were 0.083 μl/s and 1.07 μl/s. Photographs of particles were captured at 1,200 frames/s using the setup shown in Figure 3-11. The velocity of the particles was calculated using the displacement over time, which was calculated from the number of frames (0.83 ms × the number of frames). The velocities of 150 particles were measured downstream of the first junction and downstream of the second junction of the twisted sheath flow cell, respectively. Figure 3-16 shows photographs of flowing particles. The particles are flowing from left to right in these photographs. The frame-by-frame motion of two particles is labeled using arrows. Figure 3-17 shows the frequency distribution that was obtained from the velocities of the particles measured in this way.

The velocity on the horizontal axis was normalized by the maximum velocity (V_{max}) of the second junction, and the frequency on the vertical axis was normalized by the number of measured particles (N = 150). For this reason, the maximum velocity downstream of the first junction was about half of the maximum velocity downstream of the second junction. Figure 3-15 (a) shows the frequency distribution

of the particle velocities downstream of the first junction, and Figure 3-15 (b) shows the frequency distribution of the particle velocities downstream of the second junction. Since the depth of focus of the lens was approximately 200 μm, all particles distributed in the depth direction of the channel were observed.

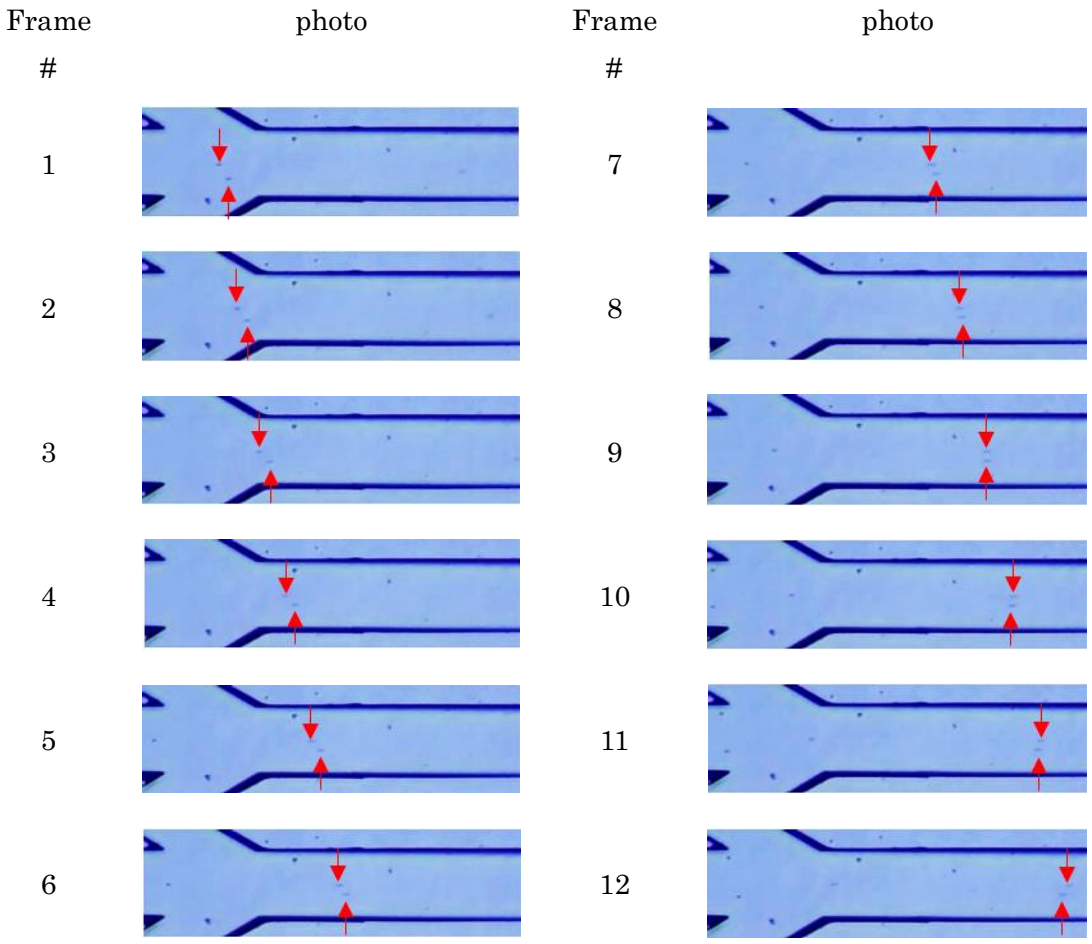

Figure 3-12 Photographs of flowing particles

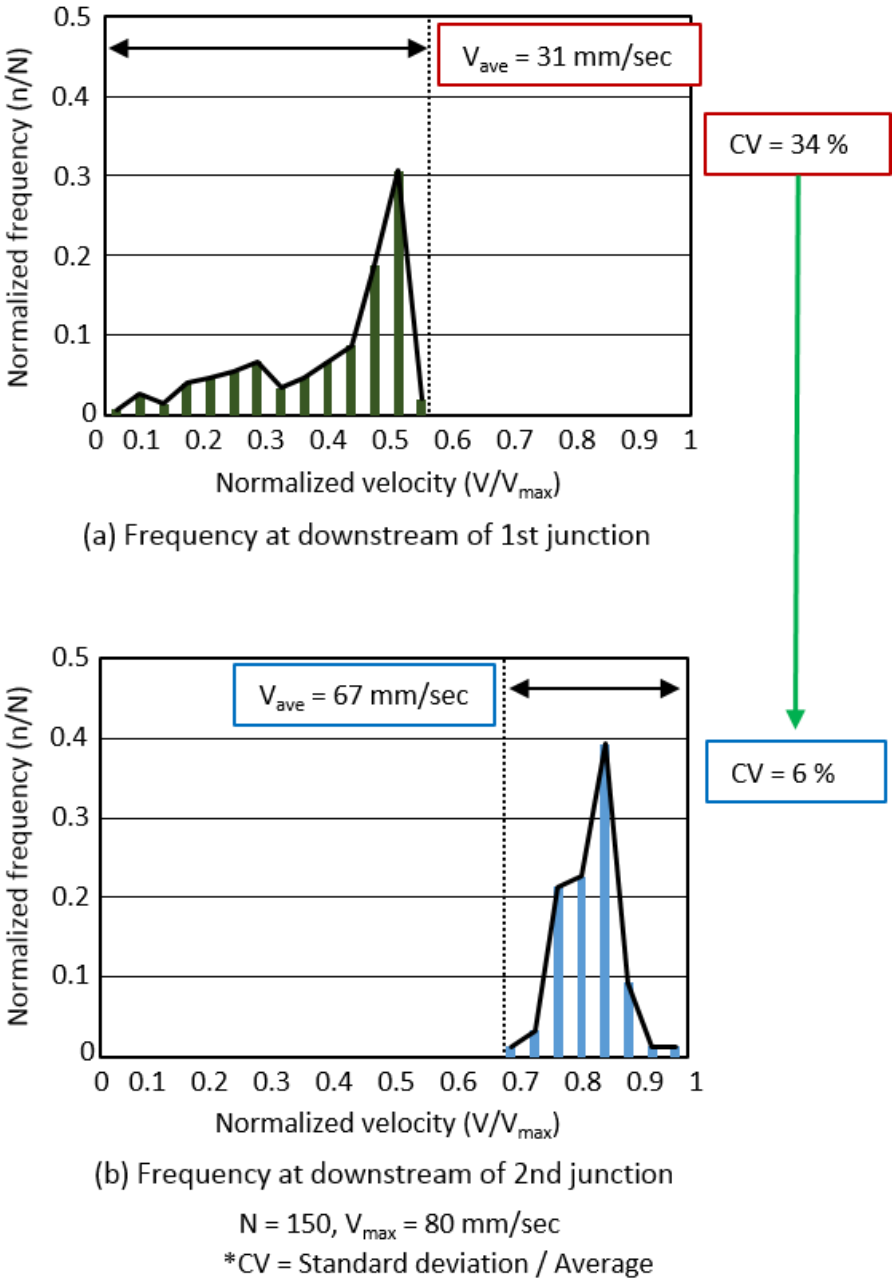

Figure 3-17 Frequency distribution of particle velocities

According to the data shown in Figure 3-17 (a), the particles with low velocities close to 0 mm/s were measured downstream of the first junction. It was predicted that the sample fluid was widely distributed in the depth direction, as shown in

Figure 3-15 (a). In contrast, according to the data shown in Figure 3-17 (b), the frequency was distributed in a narrow velocity range around the maximum velocity V_{max} downstream of the second junction, and particles with low velocities were not measured. Comparing the coefficient of variation (CV: the standard deviation / average value) of each frequency distribution, the CV in the case of the first junction was 34% and the CV in the case of the second junction was 6%. The variation in the case of the second junction was remarkably small.

These data suggested that the twisted sheath flow cell formed an isotropic sheath flow.

It was confirmed that the flow of particles could be measured from photographs captured using an optical microscope, however, the method is cumbersome and time-consuming. Therefore, I designed a setup to automate particle counting. The configuration of this setup and the measurement results are described in the next section. In the case of the non-twisted channel, the shape of the sample fluid flow at downstream of the second junction is expected to be the same as that at downstream of the first junction. The sample fluid flows in the case of the non-twisted channel and in the case of the twisted channel are explained by the measurements using the new setup in the next section.

3.4.3 Prototype particle counting setup

To create a compact, low-cost flow cytometer, particles will need to be counted automatically. Data processing with electronic signals is more suitable than photo processing of microscopy images captured by a high-speed camera. However, the light detected from particles must be converted into an electronic signal for data processing, so I designed a new setup that uses a photomultiplier tube (PMT) to detect a single particle.

First, to reliably detect the signal from the particle, the optical components were combined on the optical bench with reference to the configuration of an epifluorescence microscope typically used for fluorescence observation of a biological sample. Generally, the fluorescent light from one biological cell is weak, but the detection sensitivity can be enhanced by increasing the intensity of the excitation light. In a transmission-type fluorescence microscope, the eyepiece lens receives not only the fluorescence but also the excitation light, so there is a limit to how much the intensity of the excitation light can be increased. In an epi-illumination-type of microscope, the eyepiece lens does not receive the excitation light, so it is possible to increase the intensity of the excitation light. The configuration of an epi-illumination-type of microscope is preferable for detecting weak fluorescence. Figure 3-18 shows a schematic of the prototype setup for automated particle counting.

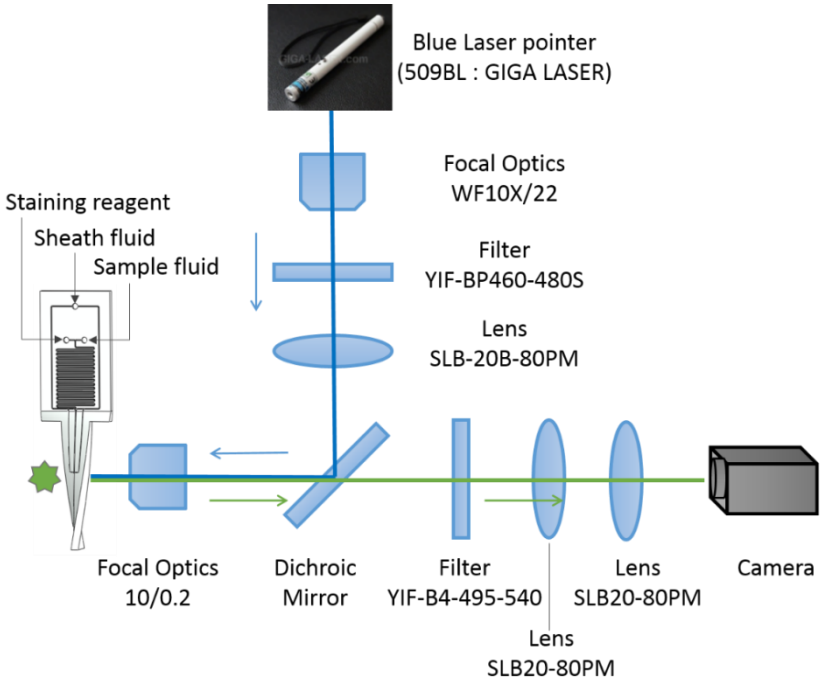

Figure 3-13 Schematic of the setup for automated particle counting

The excitation and emission wavelengths of different staining reagents and their specifications were surveyed to select the appropriate optical components. Common excitation and fluorescence emission wavelengths in studies of biological cells are 488 nm and 510 nm, respectively.

All of the optical components shown in Figure 3-16 were made by SIGMA KOKI Co., Ltd., and their respective model numbers are noted.

Figure 3-19 shows a photograph of the setup for automated particle counting assembled with the optical components on the optical bench. A camera was set for alignment of the optical axis, which is the most important aspect of the optical measurement system. The camera is a charge-coupled device (CCD) camera (Dino-Lite Premier M Fluorescence GFBW; Sanko Co., Ltd.) with a long-pass filter that transmits light at wavelengths of 510 nm or more. The channel of the sheath flow cell, which was filled with fluorescent fluid, was observed and the optical axis was

aligned. The PMT was placed at the position where the fluorescence intensity is the highest, as detected using the camera.

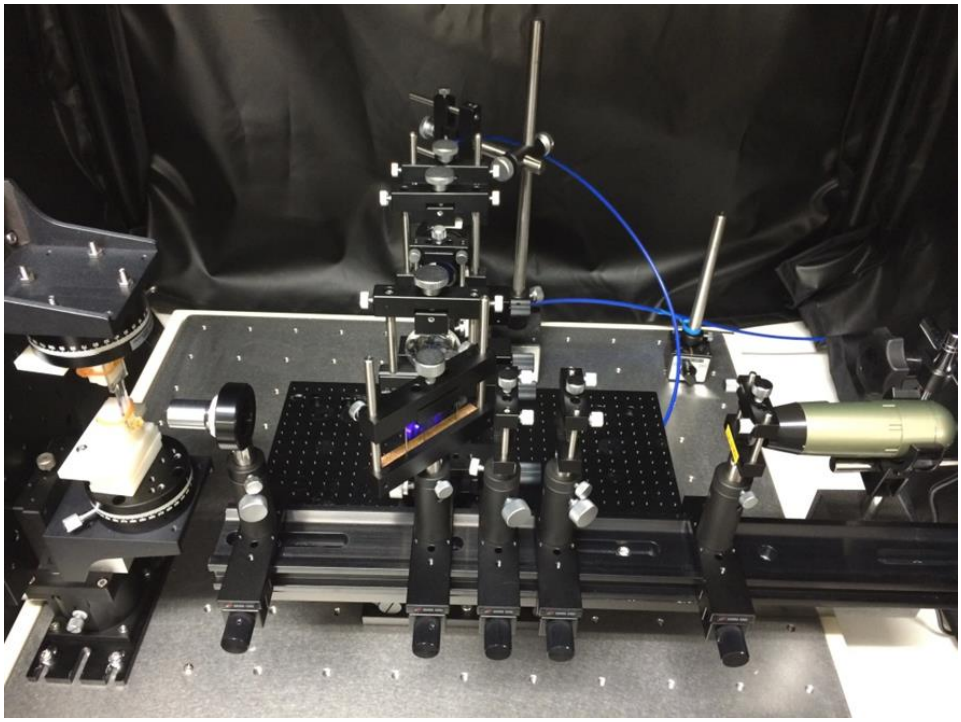

Figure 3-14　Photograph of the setup for automated particle counting assembled with the optical components on the optical bench

A blue 460 nm laser with an output of 1 mW was used as the excitation light source. To prevent any leakage of light, the entire system was covered with a black curtain.

The excitation light from 460 nm to 480 nm was band-pass filtered (YIF-BP 460-480S) and then reflected by the dichroic mirror and irradiated on the sheath flow cell. Fluorescence emitted from the sample passed through the dichroic mirror and another band-pass filter (YIF-B4 455-540) before reaching the detector.

I attempted to observe stained cells using this setup. The micro channel had a rectangular cross section measuring 250 μm wide and 400 μm deep. The channel of

the sheath flow cell was filled with yeast cells previously stained with SYTO® 9 (Life Technologies), and the fluorescence could be observed with the CCD camera. SYTO® 9 permeates a cell membrane and stains deoxyribonucleic acid (DNA) and ribonucleic acid (RNA) of both living and dead cells. The stained cells are excited by the 488 nm light and emit 510 nm fluorescent light. Figure 3-18 shows an image of the stained cells using the prototype setup. Figure 3-20 (a) shows a photograph of the stained yeast cells captured using the CCD camera. The stained yeast cells in the channel appeared green. For reference, an image of the same point using a fluorescence microscope is shown in Figure 3-20 (b). These results confirmed that the assembled setup was able to detect stained cells.

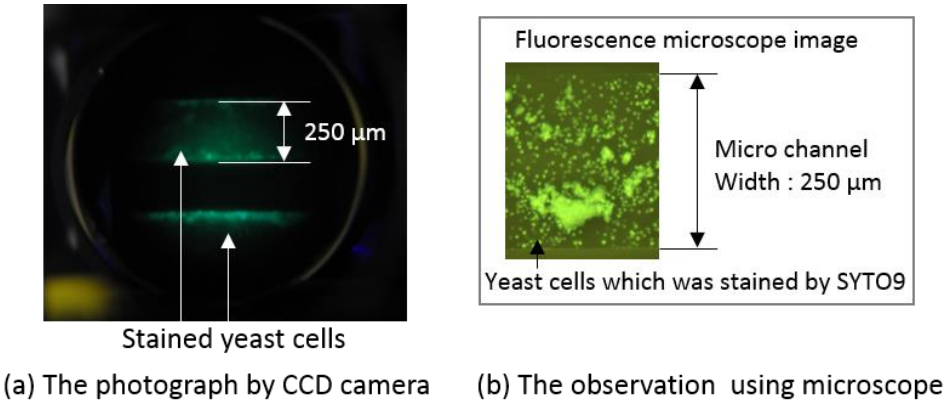

Figure 3-15 Photographs of stained yeast cells captured using a CCD camera and fluorescence microscope

Next, to detect the signal quantitatively, the camera was replaced with the PMT. The signal from the PMT was first detected with an oscilloscope to align the components. The position and the angle of each optical component was adjusted to maximize the signal intensity from the PMT.

The C7169 (Hamamatsu Photonics) is a power supply unit for driving PMT modules. The PMT H11901 (Hamamatsu Photonics) outputs current, and this signal was converted to voltage using the C6438 (Hamamatsu Photonics) amplifier. The sampling frequency and measurement voltage range were controlled using a NR 600 data logger (KEYENCE). The control voltage applied from the power supplier C7169 was fixed at 0.47 V based on the results of measuring fluorescent particles described later. The output data was statistically processed using MATLAB.

In the setup with the PMT, I changed the flow rate of each fluid and the measurement conditions, and investigated the variations in the signal. Figure 3-21 shows the flow of the signal processing.

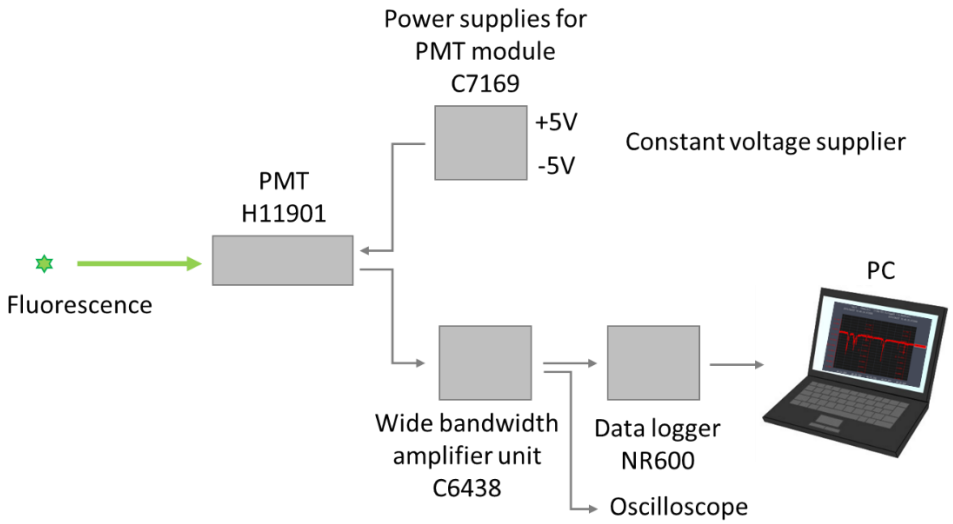

Figure 3-21 Flow of the fluorescence signal processing

3.4.4　Detection of fluorescent particles using the setup with PMT

First, standard fluorescent particles were measured under various conditions to obtain the optimal measurement conditions.

The standard fluorescent particles were φ6 μm Fluoresbrite Plain Microspheres (2.5% Solid-Latex, Polysciences, Inc.) with a maximum excitation wavelength of 458 nm and a maximum emission wavelength of 540 nm. A band-pass filter of 495 to 540 nm was set in front of the PMT. In this experiment, the sheath flow cell was not twisted.

(1) Flow rate

The flow of the particles was measured while the flow rate of the sample fluid was constant at 5 μl/m and that of the sheath fluid was changed to 12.5, 25, and 125 μl/m. The particle concentration in the sample fluid was 1×10^{6} particles/ml.

First, only the sheath fluid was flowed through the sheath flow cell, and the background signal was measured. The sampling frequency was 1 ms. The measured results are shown in Figure 3-22. The horizontal axis represents the time, and the vertical axis represents the output voltage corresponding to the fluorescence intensity. Figure 3-22 shows the background noise.

Sheath fluid: 25 µl/m

Sample fluid: 0 µl/m

(Background)

Figure 3-22 Background noise

In Figures 3-23, 3-24, and 3-25, the upper diagrams show the measurement results and the lower diagrams show the enlarged views of the signals. The half width of the peak indicated by the yellow arrow is related to the time required for particles to flow through the area of the light and is inversely proportional to the flow velocity. A faster flow velocity corresponds to a narrower full width at half maximum(FWHM) of the peak. FWHM is described in detail later. When the flow rate of the sheath fluid increased and the flow velocity became faster, the peak of the signal from the particle became sharper and was occasionally masked by noise. Therefore, at faster flow velocities, the sampling frequency will need to be increased.

Here, the optical filters were selected according to the stain regent. Since the maximum emission of the particles used for measurement is 540 nm, it might be cut off. Therefore, the band-pass filter was changed to a long-pass filter that transmits light at wavelengths higher than 500 nm. The results are shown in the next section.

Sheath fluid: 12.5 µl/m

Sample fluid: 5 µl/m

Flow velocity: 2.9 mm/s

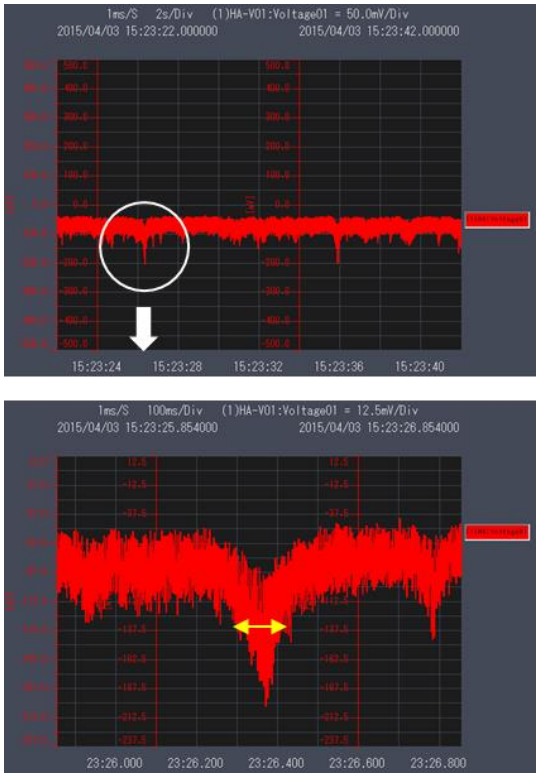

Figure 3-23 Signal depending on flow rate (1)

Sheath fluid: 25 µl/m

Sample fluid: 5 µl/m

Flow velocity: 5 mm/s

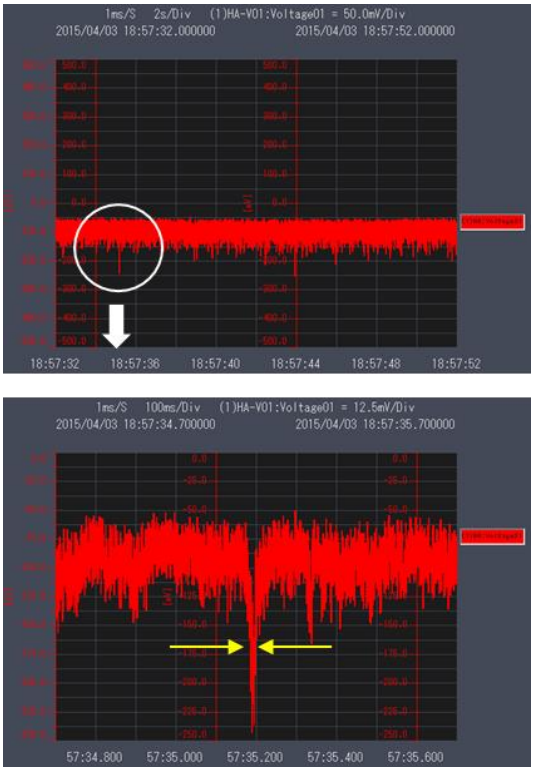

Figure 3-24 Signal depending on flow rate (2)

Sheath fluid: 125 µl/m

Sample fluid: 5 µl/m

Flow velocity: 21.7 mm/s

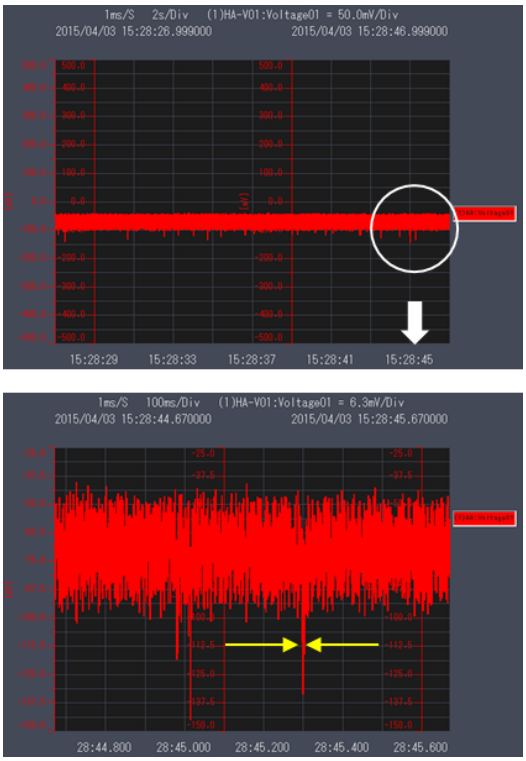

Figure 3-25 Signal depending on flow rate (3)

(2) Long-pass filter

Figure 3-26 shows the background noise when using the different filters. There is little difference in noise between the band-pass and long-pass filters. Figures 3-27 and 3-28 show the signals of the particles when the different filters are used. The noise when using the long-pass filter is higher than when using the band-pass filter. When particles are flowing, peaks in the fluorescence signal are more visible when using the long-pass filter because there are less fluctuations in the background noise. However, the overall noise level seems to increase, so there is a possibility that the peak signal from the particle will be masked. Even when fluorescent particles are not flowing, the output ranges from 70 to 150 mV, and it is still necessary to reduce

the background noise.

Long pass filter

Sheath fluid: 25 μl/m

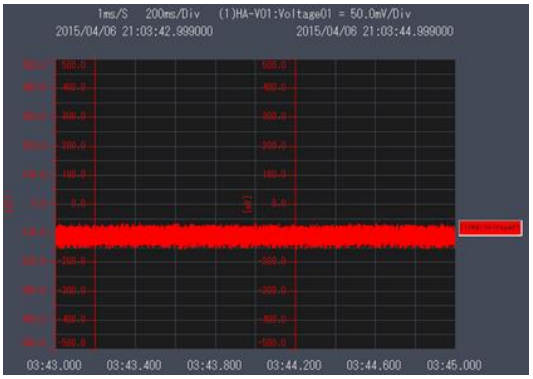

Ref: Band pass filter

Sheath fluid: 25 μl/m

(Ref. : Figure 3-22)

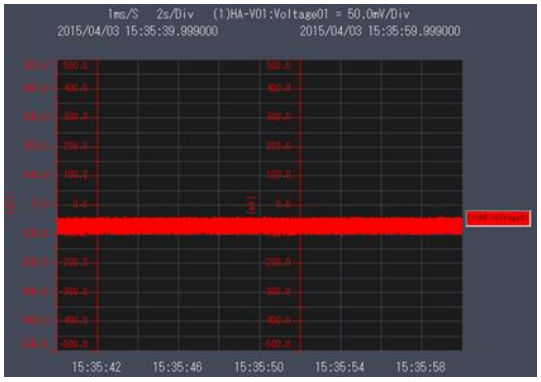

Figure 3-26 Background noise when using long-pass and band-pass filters

Long pass filter

Sheath fluid: 25 µl/m

Sample fluid: 5 µl/m

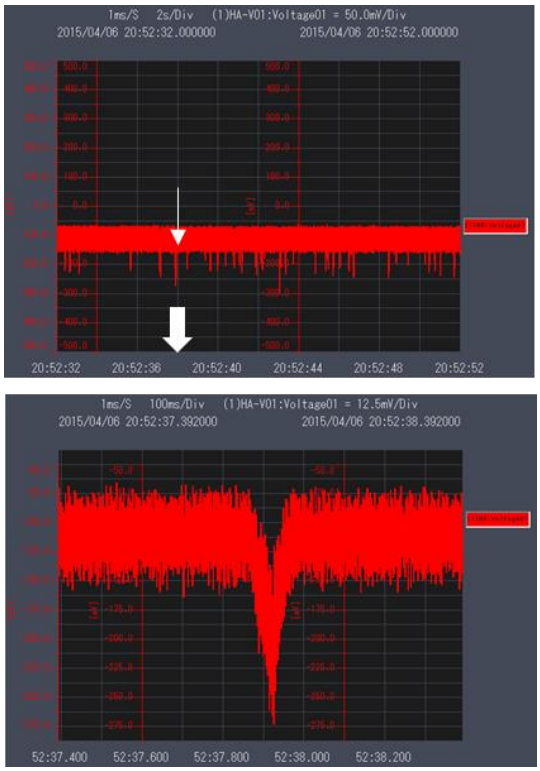

Figure 3-27 Signal when using a long-pass filter

Ref: Band pass filter

Sheath fluid: 25 µl/m

Sample fluid: 5 µl/m

(Ref. : Figure 3-22)

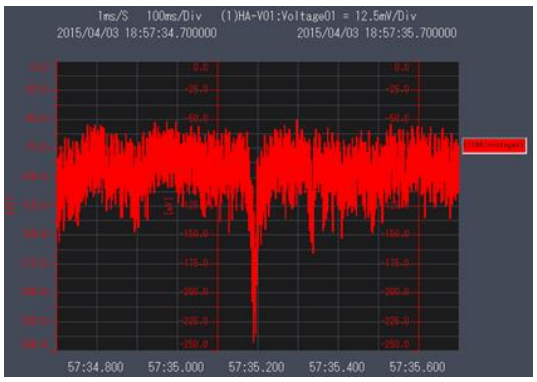

Figure 3-28 Signal when using a band-pass filter

(3) Optical slit

In the optical system used up to this point, none of the light returned from the objective lens travels toward the detector, and unnecessary light was blocked. Such as a confocal microscope, it is desirable that only in-focus light reaches the detector and any unnecessary light is blocked. A confocal microscope blocks light that is out of focus using pinholes at the focal point between the two plano-convex lenses. To achieve the same effect, I placed a slit-shaped light shielding plate (slit board) between the two lenses. The slit board is a black acrylic plate with a slit width of 1 mm. The location of the slit board in the optical setup is shown in Figure 3-29.

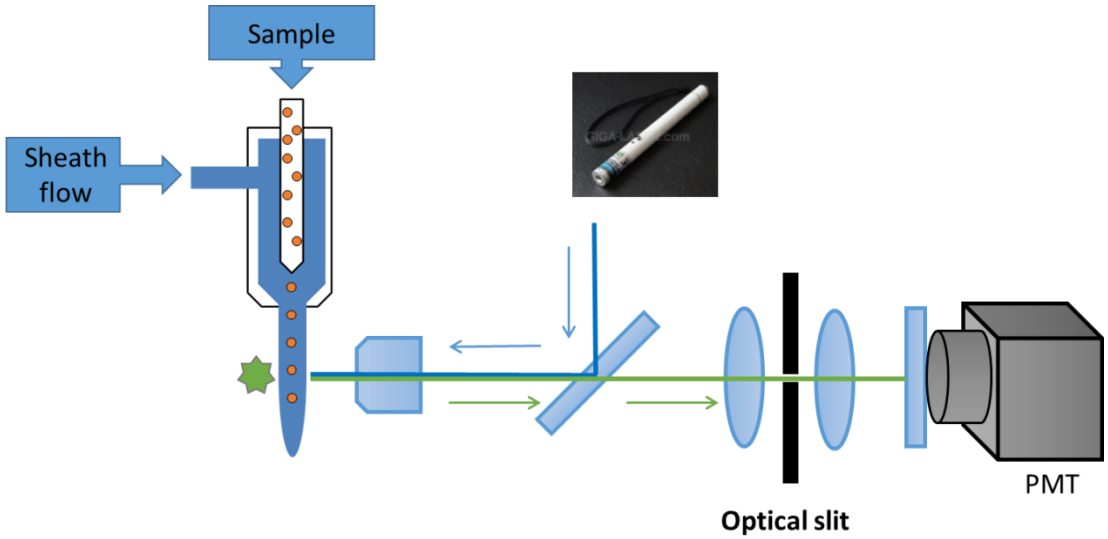

Figure 3-29 Placement of an optical slit to block noise

The results of measuring the flow of fluorescent particles with this optical system are shown in Figure 3-30 and Figure 3-31. They show the effect of using the slit board on background noise and the signal from particles. When only the sheath fluid was flowed, the output was in the range of 25–72 mV, and the overall noise level was low. Fluorescent particles were subsequently measured. The sheath fluid rate was

25 µl/m and the sample fluid rate was 5 µl/m. The enlarged photograph shows that the signal peak and the noise were more clearly distinguishable. These results indicate the effectiveness of using the slit board.

Sheath fluid: 125 µl/m only

Figure 3-30 Background noise when using the optical slit

Sheath fluid : 125 µl/m

Sample fluid : 5 µl/m

Figure 3-31 Effect of the optical slit on the signal

3.4.5 Formation of sheath flow

I assessed the formation of sheath flow using standard fluorescent particles (Polysciences, Fluoresbrite® YG Microspheres 6 μm; excitation 441 nm, emission 486 nm) in the sample fluid [54]. To evaluate whether sheath flow is formed, the PMT signals from particles in the twisted and non-twisted channels were compared. Successful formation of the sheath flow should result in a more consistent PMT signal. Ethanol was used as the sheath fluid to prevent particles and bubbles from adhering to the channel wall, and water including the fluorescent particles (5×10^5 particles/ml) was used as the sample fluid. The flow rates of the sheath fluid and the sample fluid were set to 2.1 μl/s and 0.017 μl/s, respectively. The mean flow velocity at the detection point was calculated as 21 mm/s, since the cross section of the channel was 250 μm × 400 μm.

Figure 3-32 shows the signals from particles during 30 s, and Figure 3-33 shows the histogram of the signals. For the non-twisted sheath flow channel, the counts of the signal are distributed over a wide range. For the twisted sheath flow channel, most of the signals are within a narrow range around 0.15 V.

Fewer particles were detected in the non-twisted channel. Our system was likely unable to detect the particles that flow near the channel wall in the non-twisted channel due to the low intensity of the signals.

Next, I examined the FWHM at each intensity peak. The FWHM is defined as the width that is 50% of the peak value, and here the FWHM is the time required for particles to transit through the laser illumination area. The FWHM is proportional to the particle velocity; that is, a narrower FWHM indicates a faster particle velocity.

Figure 3-34 shows the frequency of the FWHM. The FWHM distribution of the peak for the twisted sheath flow channel is narrower than that for the non-twisted sheath flow channel. The transit time is shorter when a particle flows closer to the

center of the channel. The CV of the FWHM was 82% in the non-twisted sheath flow channel and 13% in the twisted sheath flow channel. This means that the particles in the twisted sheath flow channel are gathered in the central area of the cross section. According to the above results, the twisted sheath flow channel achieved sheath flow.

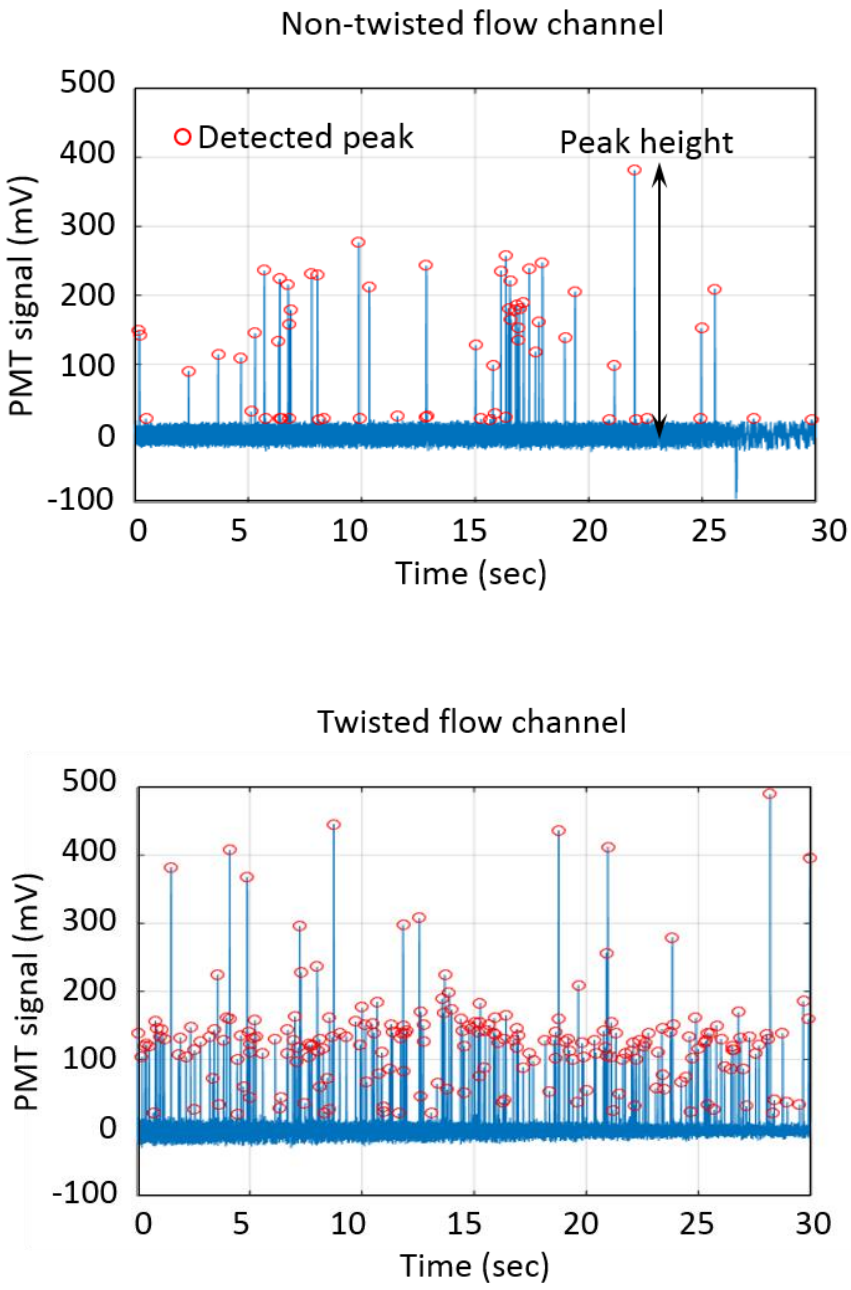

Figure 3-16 Signals detected from the fluorescent particles

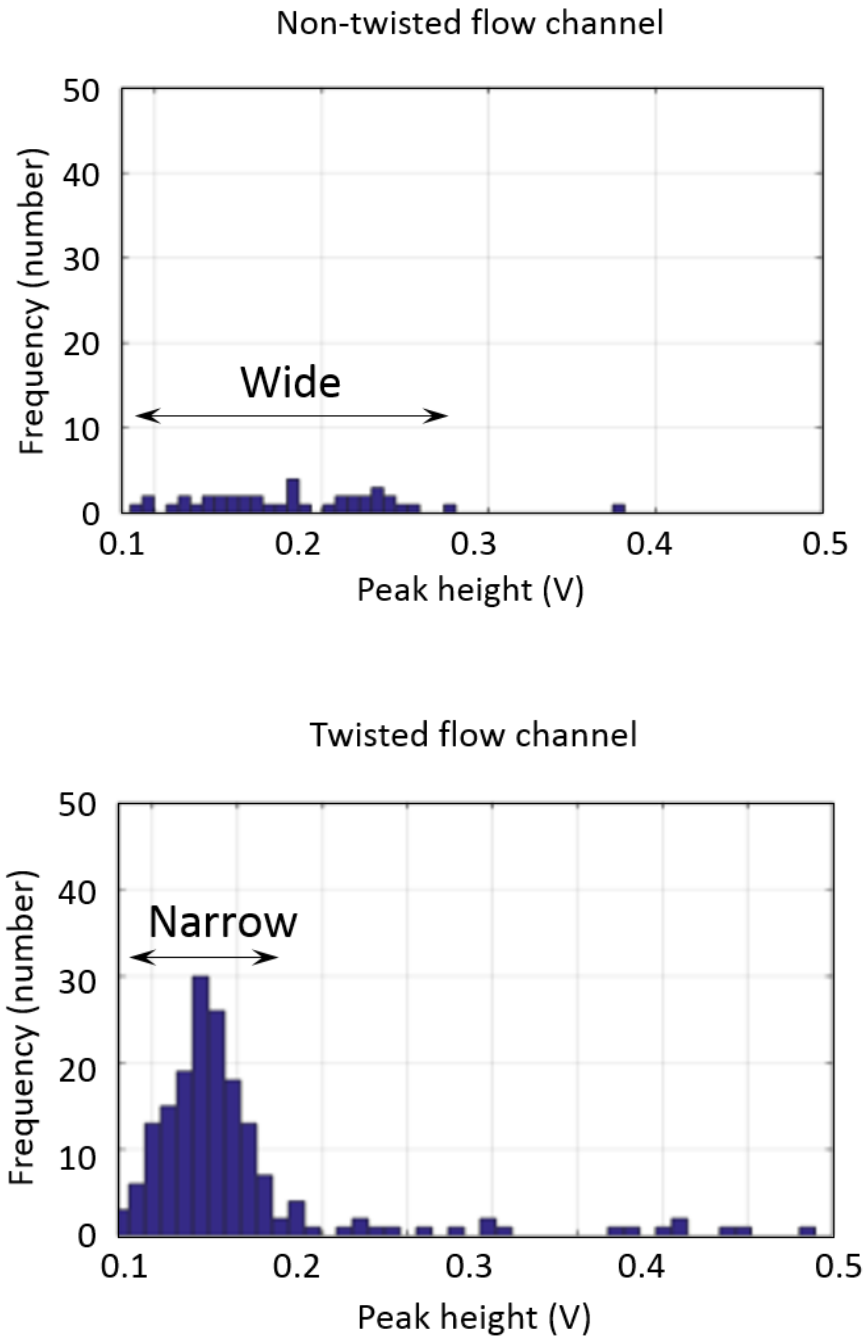

Figure 3-33 Frequency of the signals detected from fluorescent particles

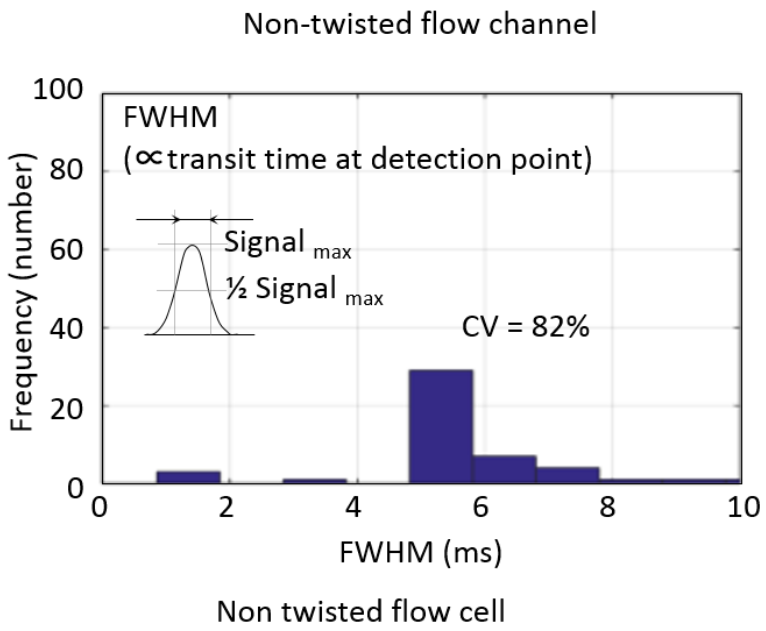

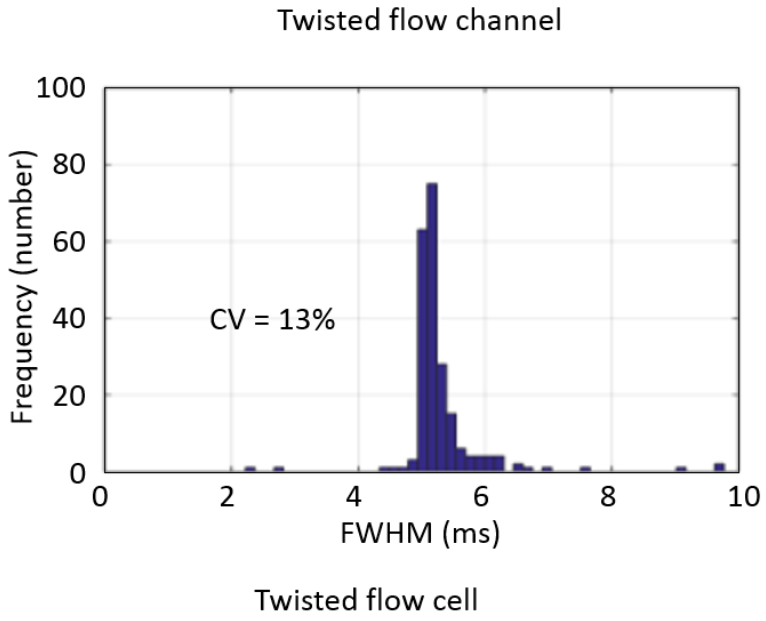

Figure 3-34 Frequency of the FWHM

3.5　Results and discussion

3.5.1　Histogram of the velocity

The frequency of the particle velocity shown in Figure 3-17 (b) was compared with the calculated value from statistical processing.

Assuming that particles are uniformly present in the channel and the particles continue to be supplied, the number of particles with a certain velocity is proportional to the volume [flow velocity × area of the channel cross section]. As shown in Figure 3-35, the area S_n containing particles with the same velocity v_n was calculated using equations (4) and (5), and the frequency of the particle velocity was obtained.

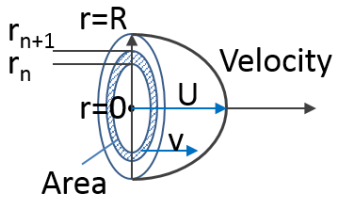

Figure 3-17 Calculation of the number of the particles

$$v_n = U\left\{\left(1-\left(\frac{r_n}{R}\right)^2\right)\right\} \tag{4}$$

$$S_n = \pi {r_{n+1}}^2 - \pi {r_n}^2 \tag{5}$$

v_n : Flow velocity at diameter r

U : Maximum velocity

r: Distance of the center

R: Radius of the channel

The frequency of the velocity was calculated for the region where the sample solution was constricted from the central 5% to the central 25%. Figure 3-36 shows a graph of the calculated values superimposed on the measured data shown in Figure 3-17 (b). Here, the maximum value of the measured data and the overlapping theoretical values are excluded. The frequency of the measured data agrees well with the frequency of the particle velocity calculated assuming that the particles are present within 15% from the center. In this experimental condition, it was expected that the sample fluid was constricted within 15% from the center.

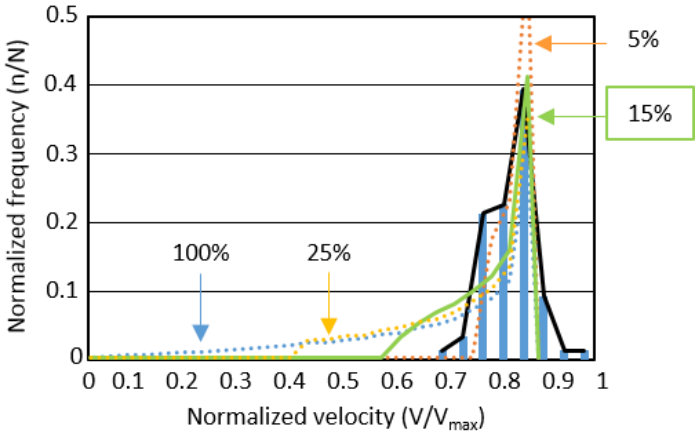

Figure 3-36 Graph of calculated values superimposed on data measured using the sheath flow cell

3.5.2　Rotational flow in the channel cross section

According to our original idea, a twisted cylindrical tube is an ideal structure, as shown in Figure 2-8. However, since the cross section of the sheath flow channel is

rectangular, this shape may induce a rotational flow near the channel wall. Therefore, the flow depending on the twist angle was analyzed using numerical simulation. If the cross section of the micro channel is circular and the channel is twisted by 90°, the flow in the channel maintains a stable laminar flow. However, when the cross section of the micro channel is rectangular, a rotational flow in the channel cross section may be generated depending on the twist angle. Since the flow near the wall is complex, the flow in the micro channel was predicted using numerical simulation. Figure 3-37 shows the flow in the channel depending on the twist angle. The rotational flow near the wall by twisting the rectangular channel is smaller than the main flow in the X direction, and when the twist angle is in the range of 90° to 120°, the particles are mostly gathered in the center. As a result of considering the control of the twist angle and the assembly with the detection setup, the twist angle of the micro channel was set to 90°.

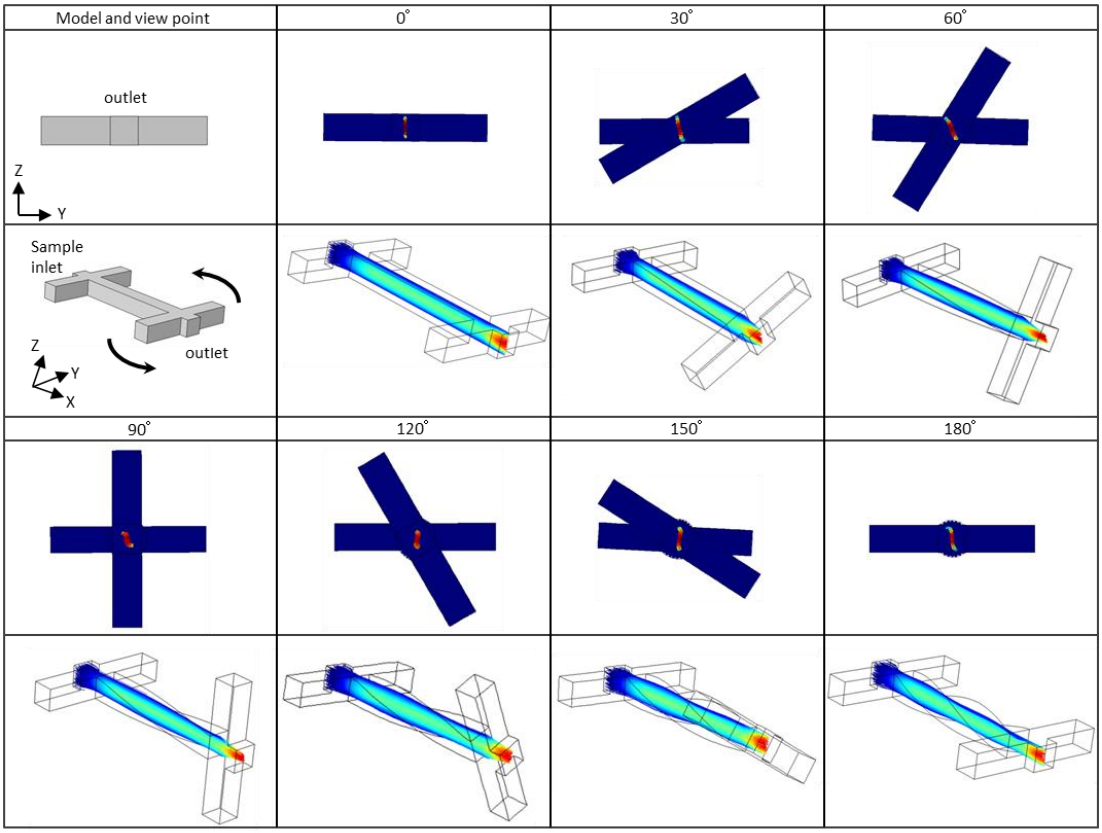

Figure 3-18　Particle trajectory depending on the twist angle

3.6　Summary

The method for determining the specifications of the sheath flow cell constructed using the simple formation method was described. By analyzing the flow rate distribution using a basic model of the sheath flow cell, the channel dimensions that achieved an isotropic focusing flow were determined.

Next, based on the design specifications, a sheath flow cell was fabricated, and the flow in the micro channel was observed to verify whether sheath flow was formed. Uranine (fluorescein sodium salt) solution as a sample fluid and water as a sheath fluid were flowed in the twisted sheath flow cell, and observed at a point downstream of the second junction using a microscope. However, although 2D compressed flow

in the observation direction could be confirmed, compressed flow in the depth direction could not be confirmed. Therefore, to confirm the flow in the depth direction even when observing the flow from one direction, I proposed a method to predict the formation of sheath flow from the velocity of particles using water containing tracer particles as a sample fluid. The velocity of particles was calculated from the number of frames per second and the displacement of the particles by high-speed camera, and the frequency distribution of the particle velocity was obtained. To improve the verification accuracy, a fluorescent particle observation setup using a laser as the light source was assembled. Fluorescent particles (φ6 μm) as the observation target were used to obtain the frequency distribution of the signal intensity and the full width at half maximum (FWHM) of the signal. When the particle velocity is high, the signal peak is sharp and the FWHM is narrow, so the FWHM is inversely proportional to the particle velocity. The position of the particles within the channel cross section can be estimated from the frequency distribution of the particle velocity. Results of this experiment show that the frequency distribution was within a narrow range, and it was predicted that sheath flow was formed using the twisted sheath flow cell.

Chapter 4　Integrated flow cytometry chip

In chapter 4, a flow cytometry chip, which uses a continuous micro channel to connect the pre-treatment part and the twisted sheath flow cell, is proposed. When the micro channels with different performance are integrated, their matching and design method concerning operational conditions such as flow rate and others are described. In the pre-treatment part, a certain amount of incubation time is required to stain biological cells sufficiently. This time depends on both the channel volume of the pre-treatment part and the flow rate of the sample solution, whereas the flow rate of the sample solution depends on the specifications of the entire system, such as the measurement time and the amount of sample solution. Therefore, it is necessary to determine the structure and flow rate of the pre-treatment part to satisfy both conditions.

In this chapter, the design method concerning the operating conditions of the flow cytometry chip is described, and the results of a demonstration using the fabricated chip based on this method are presented [54], [55].

4.1　Concept of flow cytometry chip

A flow cytometer is a device that analyzes particles and biological cells one by one using flow cytometry technology. In a conventional flow cytometer, pre-treatment such as dispensing and mixing of sample fluid and staining reagent is handled

manually. A flow cytometry chip can be used as a compact, low-cost analyzer without manual processing, and as a result, flow cytometry chips are expected to be useful in a wide variety of fields. The following issues, however, need to be addressed:

(1) Volume of reagent and sample fluid: In manual operations, it is difficult to handle fluid less than 1 μl accurately, and more than 10 μl of staining reagent is often used. The volume of the staining reagent is approximately 1/10 the volume of the sample fluid, but the volume used is directly related to the cost of the procedure. Reducing the volume of the reagent therefore reduces the costs. Not only would it be easy to control less than 1 μl of fluid using a flow cytometry chip with a micro channel, but the volume of reagent could also be reduced.

(2) Time from pre-treatment to measurement: In common staining procedures, cells must be incubated with the sample fluid and staining reagent for approximately 20 min. The mixture is subsequently centrifuged and purified with buffer fluid, and the contaminants and unreacted reagent are removed. The stained cells can then be detected with high accuracy. All of these steps take more than 30 min, and involve cumbersome manual tasks, such as centrifugal separation and the dispensing operation.

(3) Dead volume: Residual volumes of the staining reagent and sample fluid are wasted each time the dispensing operation is repeated.

I considered that the above problems can be solved by consistent processing using the flow cytometry chip with the pre-treatment part for cell staining and the sheath flow-forming part for forming sheath flow. Figure 4-1 shows the conventional method for flow cytometry analysis.

I propose an integrated flow cytometry chip in which the micro channel of the pre-treatment part and that of the sheath flow cell are combined in series using a micro channel.

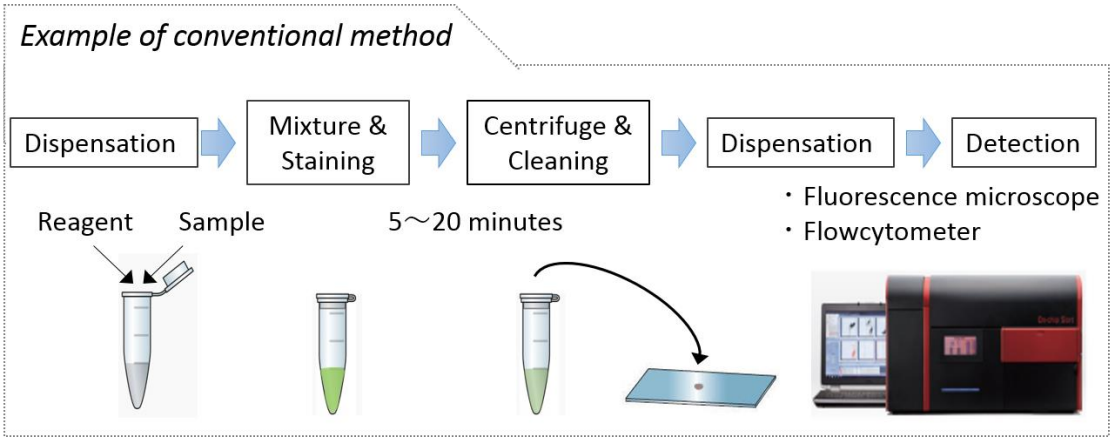

Figure 4-1 Conventional flow cytometry analysis

The pre-treatment part combines diffusion, mixing and reaction functions for staining cells. Substantially by using a micro channel, less staining reagent and sample fluid can be used compared to the conventional method thanks to less dead volume and manual steps. After mixing, cells must be incubated with the staining reagent for a certain amount of time. I propose a meandering channel for this purpose. While the sample fluid and the staining reagent flow through the meandering channel, they are mixed via diffusion and the secondary flow in the curved channel [56], [57]. However, sheath flow must be formed and the cells must be detected in the sheath flow cell. Therefore, both the design of the micro channel and the flow rate are important for the staining reaction and formation of the sheath flow. Figure 4-2 shows an image of the flow cytometry chip and the protocol.

The method for designing the flow cytometry chip is described in the next section [58].

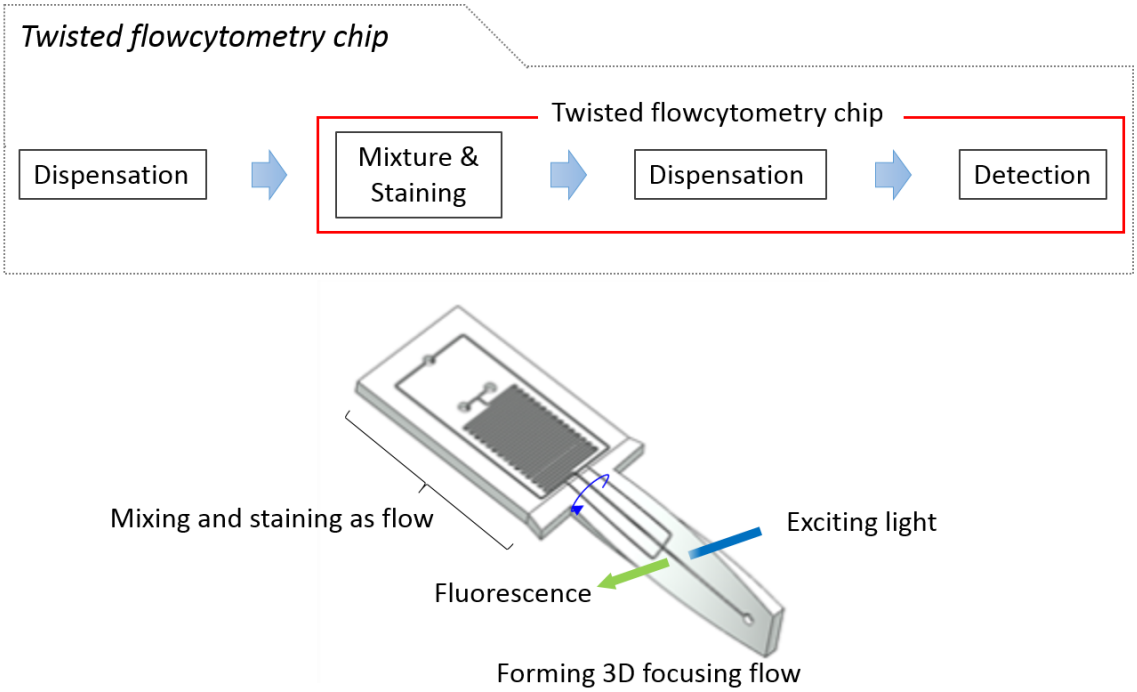

Figure 4-2 Image of the flow cytometry chip and its various functions

4.2　Flow matching design between flow cell and pre-treatment part

First, the design of the pre-treatment part is described. Since the mixing time of the sample and the staining reagent depends on the diffusion distance, a shorter time can be achieved using a smaller channel cross section. However, as the cross section of the channel becomes smaller, either the length of the meandering channel must be increased or the flow rate must be decreased, to keep the cells flowing in the pre-treatment part during incubation. Generally, since the flow rate of the sample is determined based on the required treatment speed, the incubation time is adjusted by shortening or lengthening the meandering channel. Keeping the flow rate constant, the length of the channel was calculated for three different cross-sectional areas. The pressure difference under each case was also calculated. Figures 4-3 and 4-4 show the calculated results.

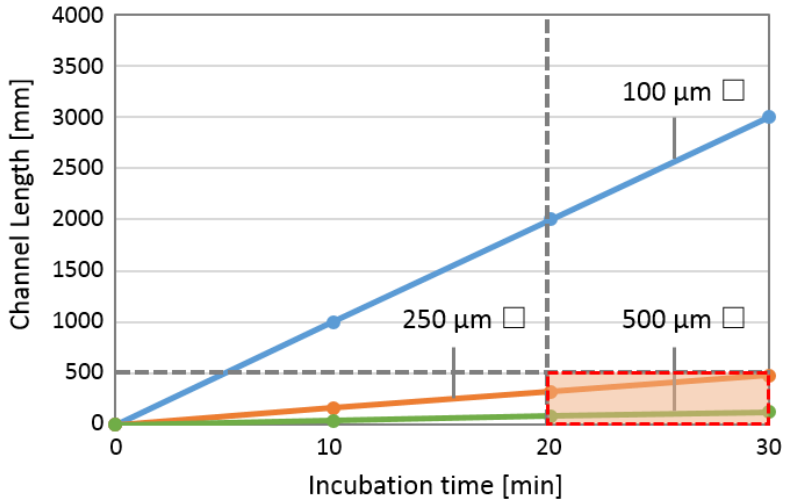

Figure 4-3 Required channel length depending on the cross-sectional area of the channel

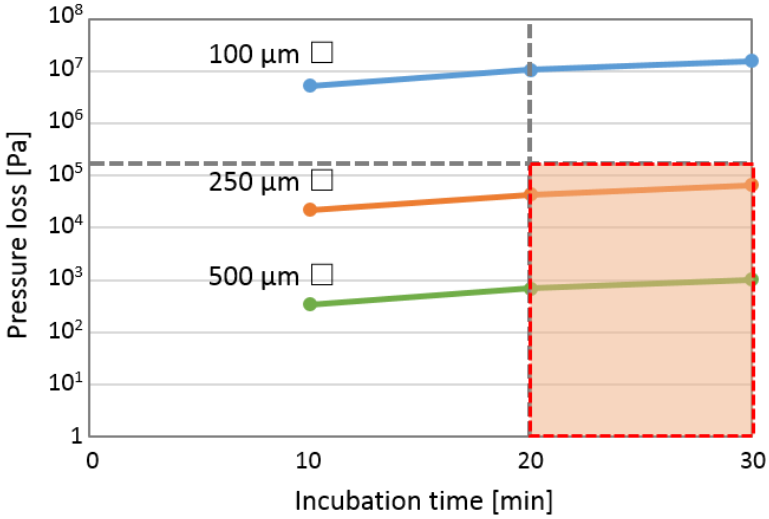

Figure 4-4 Pressure loss depending on the cross-sectional area of the channel

For the same incubation time, a smaller cross section required a longer channel, and the pressure difference increased remarkably. The dimensions of the channel were selected for an incubation time of 20 min or more. The design range of the

pressure difference was determined as follows. If the force to dispense the fluids is too low, the fluids will not flow. Since a syringe pump able to produce high force is large and expensive, this makes the flow cytometer large and expensive. I considered that the same force produced when flowing water from a tap is necessary to develop a useful flow cytometer. Therefore, the pressure difference of the flow cytometry chip was determined to be 0.2 MPa or less. When the size of the flow cytometry chip is assumed to be that of a glass slide, the meandering channel in the pre-treatment part can be made within half of the slide. Therefore, the length of the meandering channel was determined to be 500 mm or less. Here, the cross section and the length of the channel are assumed to be 250 μm × 250 μm and 300 mm, respectively. When the cross section of the channel is 100 μm × 100 μm, the pressure difference is too large. In contrast, making a structure with a height of 500 μm for a 500 μm × 500 μm cross section is difficult. Therefore, I selected a cross section of 250 μm × 250 μm. The length of the channel is determined to be 300 mm based on the data shown in Figure 4-4.

Next, the sheath flow-forming part was designed to achieve isotropic sheath flow using model-based simulation. The method for the numerical simulation was described in section 3.1. Since the flow rate ratio Q_1/Q_2 depends on the cross-sectional area rather than the channel length, the channel length was fixed at 15 mm and the distance between the second junction and the outlet was fixed at 15 mm. If these distances are equal and the channel is twisted by 180° at the outlet, the channel is twisted 90° at the second junction. Figure 4-5 shows the flow rate ratio as a function of the channel width W_2.

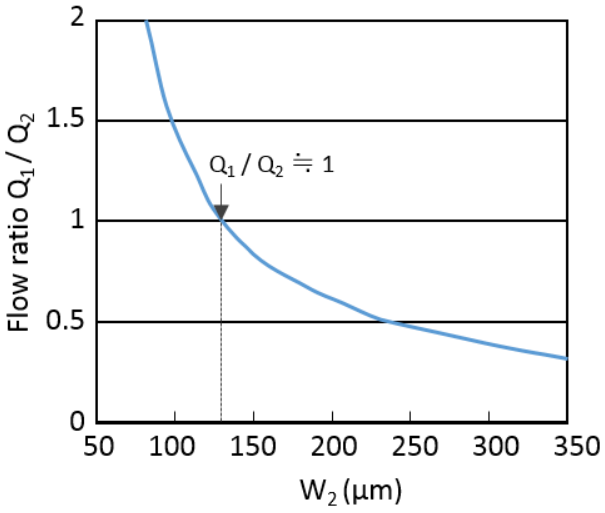

Figure 4-5 Flow rate ratio as a function of the channel width W2

From these results, a W_2 of 125 μm, where $Q_1/Q_2 = 1$, was selected. Figure 4-6 shows the design of the flow cytometry chip, and Figure 4-7 shows the flow in the sheath flow-forming part. The cross section of the central channel is designed to be 250 μm × 250 μm. The micro channel is twisted by 90° between the two junctions, as shown in Figure 4-8, by utilizing the elasticity of the PDMS.

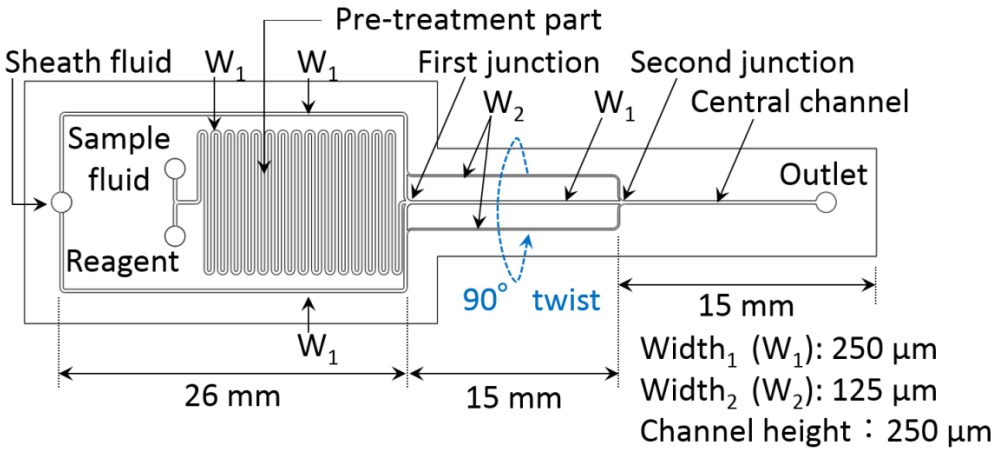

Figure 4-6 Design of the flow cytometry chip

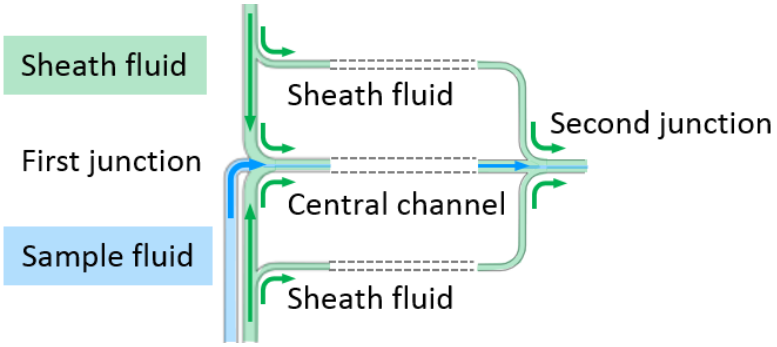

Figure 4-7 Flow in the sheath flow-forming part

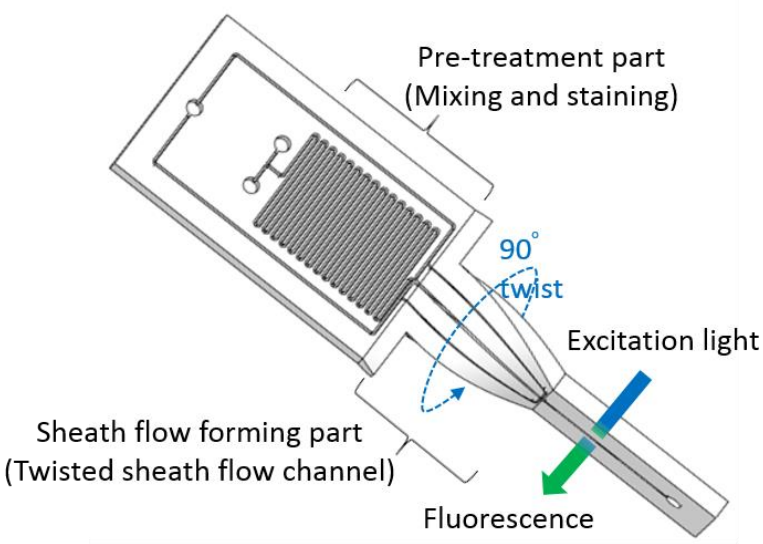

Figure 4-8 Flow cytometry chip with a 90° twist

A sample fluid is introduced from the upper inlet, and a reagent is introduced from the lower inlet. The sheath fluid introduced from the inlet located on the left side flows into both of the branched channels. The sample fluid mixes and reacts with the reagent in the meandering channel (pre-treatment part). The sample fluid then flows into the sheath flow-forming part.

Table 4-1 lists the prospective advantages of the integrated flow cytometry chip compared with a conventional system.

Table 4-1 Prospective advantages of the integrated chip

	Conventional system	Integrated flow cytometry chip
Sample volume	More than 100 μl	50 μl
Reagent volume	More than 10 μl	5 μl
Dead volume	More than 50 μl	0 μl
Transfer time	More than 10 min	Less than 1minute

Usually, the sample is stained manually, which consumes extra sample and reagent. With the integrated chip, however, it is possible to reduce the volumes of sample and reagent used because the dead volume of the connection between the pre-treatment part and the sheath flow-forming part is zero. Moreover, this connection drastically reduces the transfer time between the two parts.

Next, the flow cytometry chip was fabricated using the fabrication process described in section 3.2. Figure 4-9 (a) shows a photograph of the fabricated flow cytometry chip. The channel was twisted easily as shown in Figure 4-9 (b).

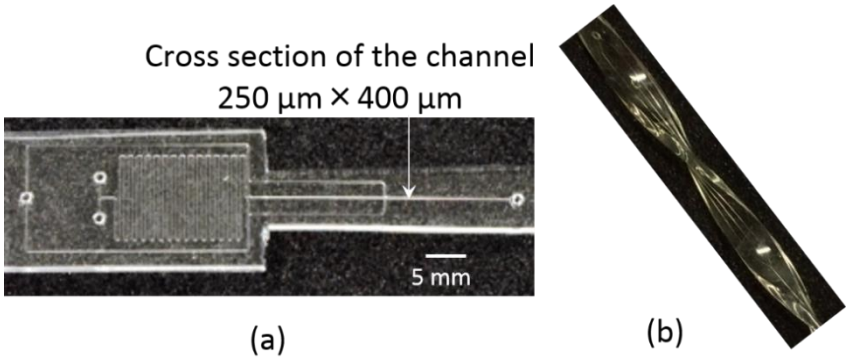

Figure 4-9 Photographs of the fabricated flow cytometry chip

It was confirmed that the complex 3D flow channel network including the pre-treatment part and the sheath flow cell can be fabricated quickly and easily by soft lithography and twisting the channel. The resulting flow cytometry chip was very compact, just 60 mm in length.

The cross section of the central channel was a rectangle measuring 250 μm × 400 μm, and not the proposed 250 μm × 250 μm. This larger cross section is an adjustment error introduced to control the thickness of the SU-8. However, I considered that a preliminary evaluation of the formation of sheath flow was possible using this fabricated chip.

4.3　Staining yeast cells in the micro channel

I attempted to stain yeast cells in the pre-treatment part of the flow cytometry chip. First, the biological cells and the staining reagent were adjusted to suitable

concentrations.

The suspension of dry yeast with water as the sample fluid and SYTO® 9 as a staining reagent were flowed in the channel. A yeast cell is elliptical, having a shorter length of 3 to 7 μm and a longer length of 4 to 14 μm. The concentration of yeast cells was adjusted to 1 to 3 × 10^{6} cells/μl, and the concentration of SYTO® 9 was adjusted based on experimentation. Because excess SYTO® 9 that does not react with the cells becomes noise, and the flow cytometry chip does not have a purifying function to remove contamination, it was necessary to determine a sufficient concentration of SYTO® 9 for the staining reaction. Yeast cells were stained using different concentrations of SYTO® 9 and then observed using both a fluorescence microscope and the optical setup. A SYTO® 9 concentration of 500 nM was found to adequately stain the cells and produce low noise. However, the fluorescence intensity using the light in the setup was weaker than that using the light from the microscope. Therefore, the SYTO® 9 concentration was adjusted to 5 μM and was found to adequately stain the cells and produce sufficient fluorescence for detection using the light in the setup.

Next, I attempted to stain yeast cells with SYTO® 9 in the pre-treatment part. Each fluid was dispensed using a syringe pump. Specifically, a suspension of yeast cells at 10 μl/min and SYTO® 9 at 1 μl/min were introduced into the pre-treatment part and observed. Figure 4-10 shows a schematic of the flow cytometry chip and a photograph of the stained yeast cells in the micro channel. The observation position was 100 mm downstream from the junction of the yeast cell suspension and SYTO® 9. Yeast cells reached that position after 1 min from the start of the staining reaction. It was confirmed that the yeast cells could be stained by flowing them with SYTO® 9 in the channel of the pre-treatment part. Although the flow rate is nearly 10 times greater than the proposed flow rate, the fluorescence was captured with the camera, so the intensity is considered to be a level detectable by the PMT.

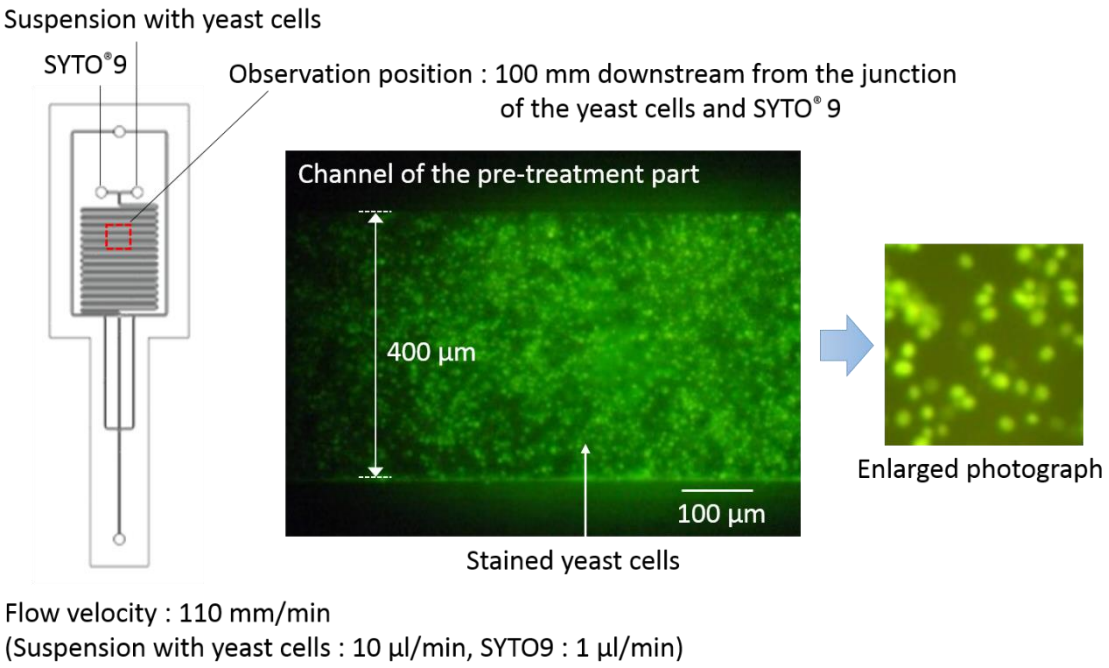

Figure 4-10 Schematic of the flow cytometry chip and a photograph of the stained yeast cells in the micro channel

Next, I attempted to detect biological cells that were treated within the sheath flow cell of the flow cytometry chip.

4.4　Counting biological cells

Up to this point, to confirm the performance of the proposed chip, the setup had the same configuration as an epifluorescence microscope, so the excitation light was not detected as noise. However, as shown in Figure 3-16, the configuration takes up a lot of space, and it is difficult to downsize. Therefore, I investigated a method for detecting fluorescence from a direction 90° to the excitation light. Figure 4-11 shows a schematic of the setup with the new configuration. The excitation light was changed to a BioRay (488 nm, 20 mW, Coherent) to match the excitation wavelength of the staining reagent. The excitation light illuminated the flat surface of the

twisted flow cytometry chip and the fluorescence from the cells was detected from the side using the PMT. The camera was installed on the opposite side of the PMT, and the fluorescence signal was measured while the flow of the cells was captured using the camera. Here, the side surface of the chip is the cut surface of the PDMS, and it is rough and opaque. Coating the side of the chip with a little PDMS improved the transparency of the side surface. The flow of cells in the channel was captured by the camera.

To confirm the alignment of the setup, I attempted to measure stained yeast cells using the improved setup. Yeast cells and SYTO® 9 were mixed and incubated for 20 min. The fluorescence of the yeast cells was confirmed using an optical microscope and then the cells were introduced into the flow cytometry chip. Figure 4-12 shows a screenshot of a stained yeast cell and its associated signal. The left side of the screen is the PMT signal, and the right side is the image captured by the camera. The horizontal axis of the PMT signal is time and the vertical axis is the signal intensity (voltage). It was confirmed that the PMT could reliably detect the fluorescence of the stained yeast cell. Next, using this system, while the biological cells and staining reagent were separately introduced in the pre-treatment part, I attempted to detect the fluorescence at the sheath flow cell of the flow cytometry chip. The results of treating and counting two kinds of cells with the flow cytometry chip are shown in the next section.

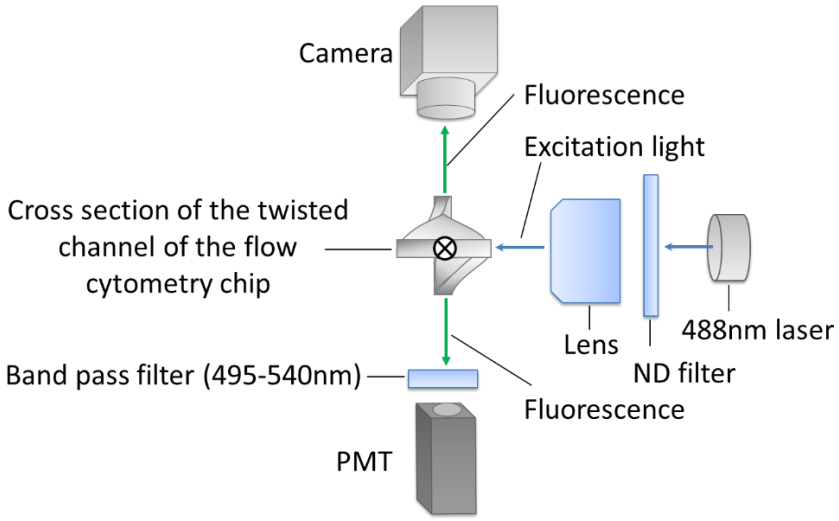

Figure 4-11 Schematic of the setup with the new configuration for counting biological cells

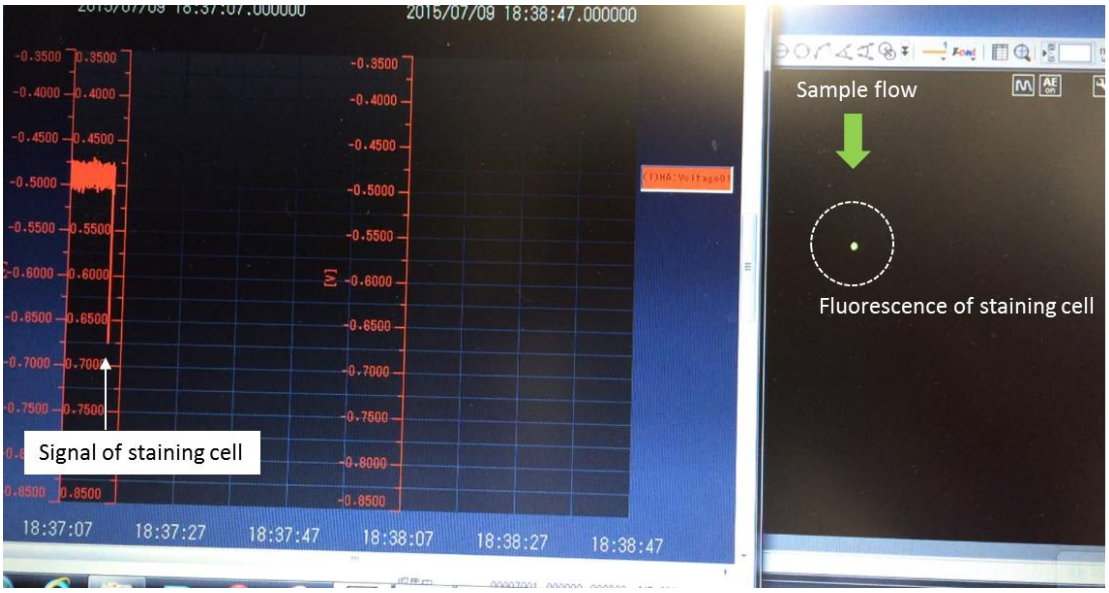

Figure 4-12 Screenshot showing a stained yeast cell and its associated signal

4.5　Results and discussion

I measured two kinds of cells to evaluate the integration of staining and counting biological cells, and assessed the feasibility of achieving the prospective advantages listed in Table 4-1.

4.5.1 Counting yeast cells

The flow rates of the sample fluid with yeast cells (~5×10^5 cells/ml), SYTO® 9 as the staining reagent and deionized water with 50% ethanol as the sheath fluids were 0.17, 0.04 and 0.83 μl/s, respectively. Deionized water containing 50% ethanol was used as the sheath fluid to prevent the cells from adhering to the channel wall. Figure 4-13 shows the signals from the stained yeast cells (red circles). The yeast cells could be detected approximately 150 s after introduction of the sample. The volume of the sample fluid was 24 μl, and the volume of the reagent was approximately 6 μl. Yeast cells flowing with SYTO® 9 were stained and could be detected in the flow cytometry chip using the improved setup. Moreover, the volume of each fluid was substantially decreased. However, the measurement data was noisy. One of the causes of the high level of noise is contamination. Since the yeast cells used as a sample were a commercial food product, it was inferred that the sample had contaminants in addition to the yeast cells. In the conventional protocol (Figure 4-1), the cells are mixed with the staining reagent, and the mixture is stirred and kept in an incubator to ensure complete staining. After centrifugation, the remaining cells are purified with buffer. Repetition of this purifying operation removes the contaminants. However, in the new protocol using the flow cytometry chip, since the cells cannot be purified, contaminants likely remained in the sample fluid. Therefore, since biological cells cultured from cell lines have few contaminants, these types of cells were subsequently measured using the flow cytometry chip. The

details of this experiment are described in the next section.

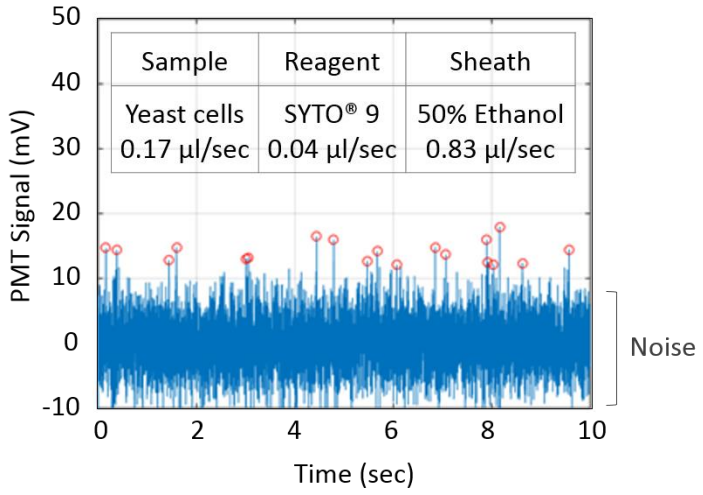

Figure 4-13 Signals from stained yeast cells

4.5.2 Counting PC-9 cells

PC-9 cells are derived from a human lung cancer cell line and are approximately 15 µm in diameter. SYBR® GREEN (Life Technologies) was selected as the staining reagent. SYBR® GREEN does not require purification of cells after staining, so SYBR® GREEN is more suitable for the protocol of the flow cytometry chip than SYTO® 9. SYBR® GREEN permeates a cell membrane and stains deoxyribonucleic acid (DNA) and ribonucleic acid (RNA) regardless of whether the cells are living or dead. The stained cells are excited by the 494 nm light and emit 521 nm fluorescent light. The flow rates of the sample fluid (~1 × 10^{5} cells/ml), the reagent and the sheath fluids were 0.08, 0.02 and 0.42 µl/s, respectively.

Figure 4-14 shows the signals from the stained PC-9 cells (red circles). The PC-9 cells could be detected approximately 300 s after introduction of the sample.

Fluorescent PC-9 cells were successfully detected using the flow cytometry chip.

In these experiments, I confirmed that the transfer time was nearly zero, the dead volume was zero, only 24 μl of sample fluid was needed, and only about 6 μl of reagent was needed.

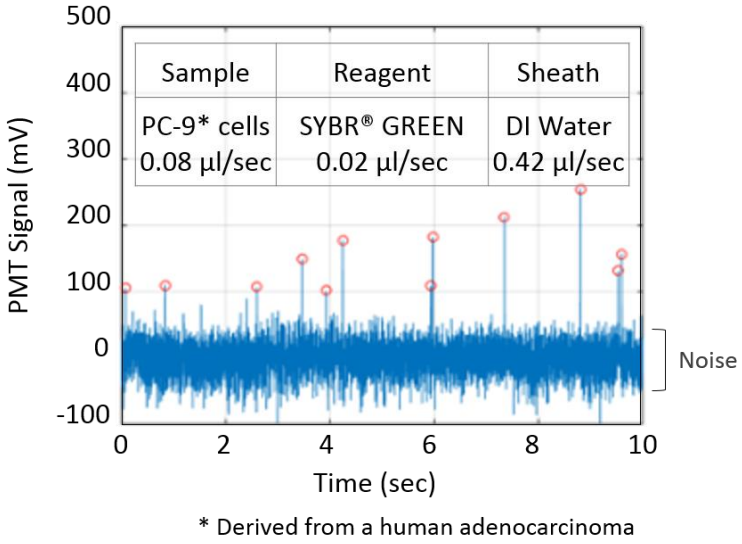

Figure 4-14 Signals from stained PC-9 cells

4.5.3　Discussion

The signal intensity of each cell varied during the experiment. The reason for this variation in the signal intensity is discussed based on the viscous flow analysis using FEM described in chapter 2.

The flow was analyzed under experimental conditions using numerical simulation. Figure 4-15 (a) shows a model of the twisted sheath flow-forming part and the trajectories of the particles. The central channel has two junctions. The central

channel has a width of 250 μm and a height 400 μm, identical to the dimensions of the actual channel, and the length between the first junction and the second junction is 15 mm. The model is identical to the sheath flow part of the fabricated flow cytometry chip. The flow rate of the sample fluid was set to 0.083 μl/s, and the flow rates of the sheath fluids from inlets 1, 2, 3 and 4 were set to 0.52 μl/s. A total of 2000 particles with the sample fluid were released at the sample inlet. Figure 4-15 (b) shows the distribution of the particles at positions (1), (2), (3) and (4), which were selected to examine the influence of the rotational flow. As shown in Figure 4-15 (b), the particles near the wall of the channel were slightly offset counterclockwise. It was predicted that this offset is likely due to the counterclockwise rotational flow that occurs in the rectangular cross section.

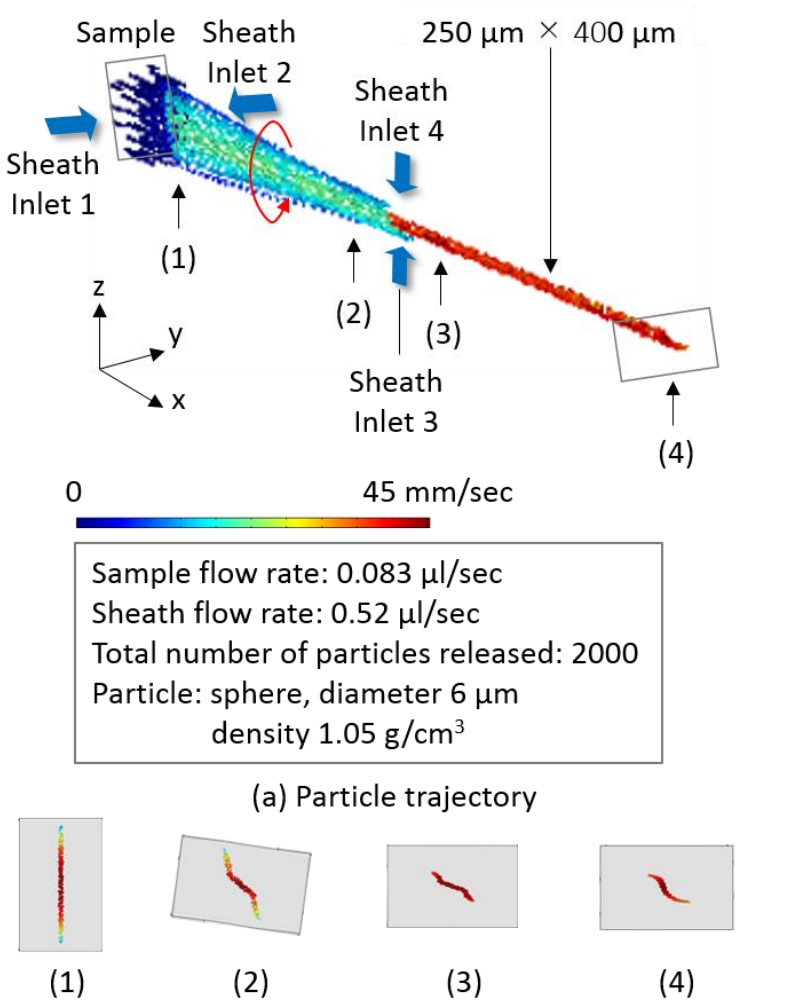

Figure 4-15 Model of the twisted sheath flow-forming part of the fabricated chip and the particle trajectory

Figure 4-16 shows the frequency of the FWHM. The CV of the FWHM was 10%, which is close to that of the experimental results (Figure 3-32, (c) twisted sheath flow cell, CV = 13%).

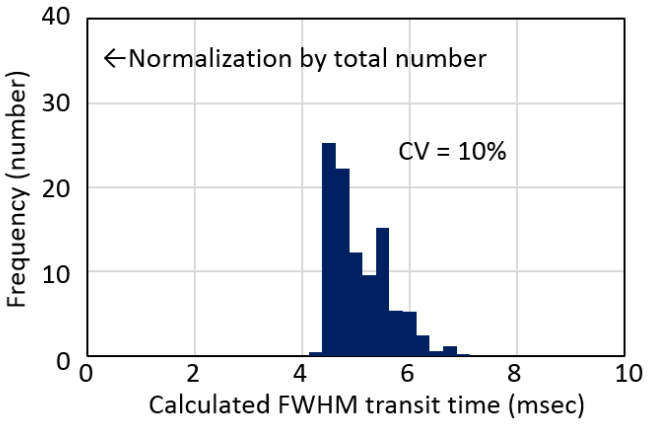

Figure 4-16 Frequency of the FWHM (channel cross section is rectangular)

For comparison, the particle flow in a channel with a square cross section was calculated. Figure 4-17 shows the model and the results, and Figure 4-18 shows the histogram of the FWHM. It was confirmed that most particles flow in a small area around the central axis. Similarly, the FWHM of the particle transit time in the square channel was also calculated. The range of the histogram becomes narrow, with an expected CV of 7%.

Here, I considered that the pass time of each particle differed because the area of the laser light changed depending on the position in the channel through which the particle flowed. It is predicted that the laser light spreads as shown in Figure 4-19. As the particle flows away from the focal position, the area of the light spreads out, so the particle velocity may be estimated later than the actual velocity. The spot size of the laser light at the focal position is assumed from experimental results.

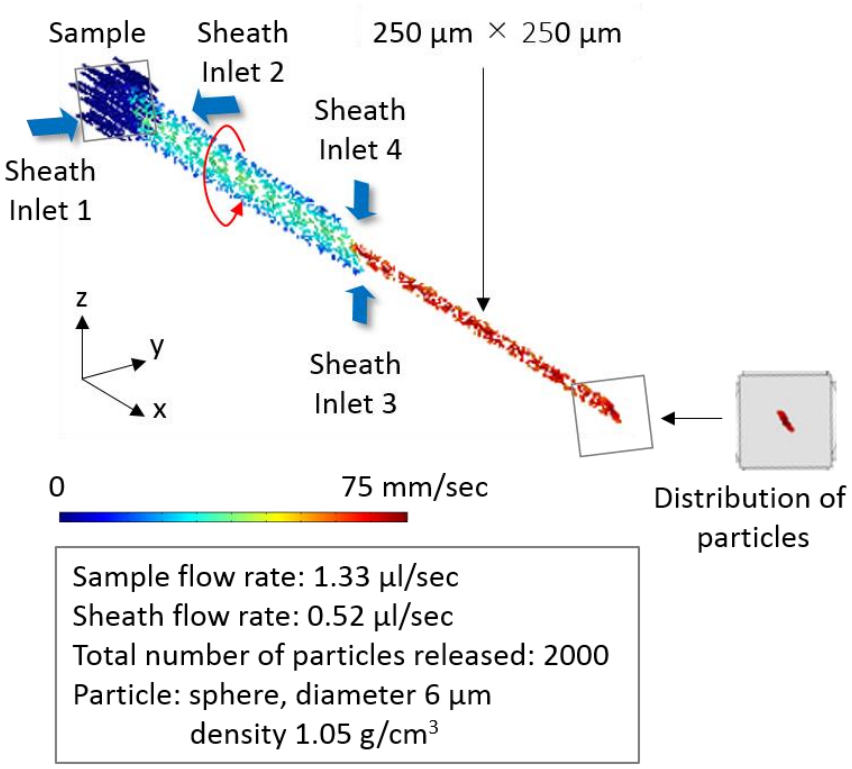

Figure 4-17 Twisted channel model with a square cross section and the particle trajectory

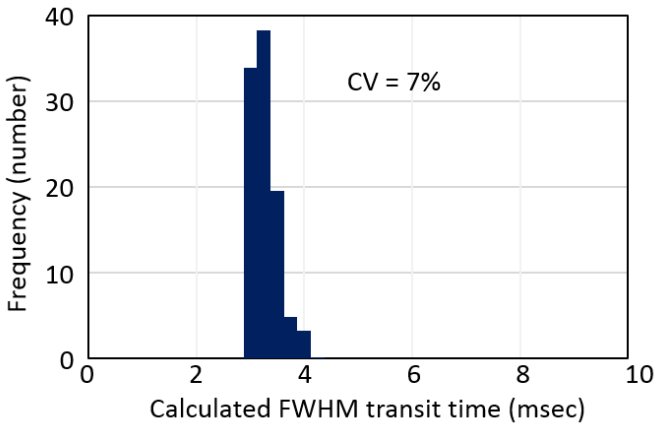

Figure 4-18 Frequency of the FWHM (channel cross section is square)

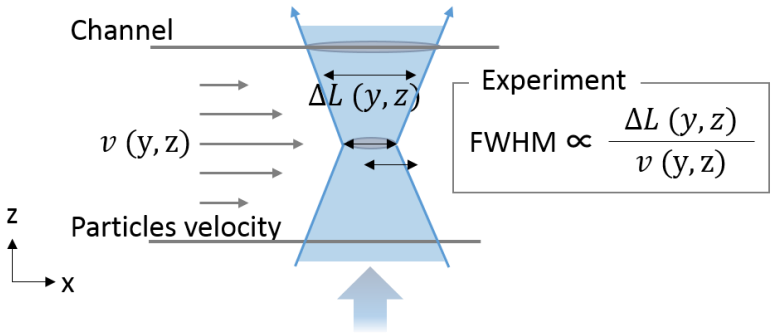

Laser beam through a convex lens

(a) Schematic of laser beam focusing

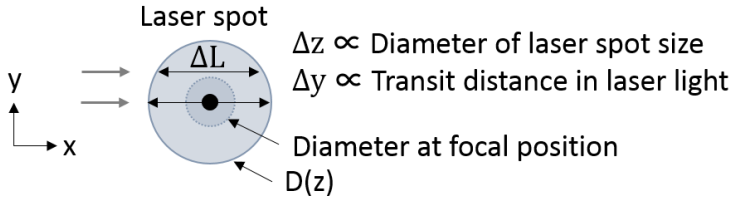

(b) Position dependence of particle transit distance in laser light

Figure 4-19 Laser spot size

Based on the experimental results shown in section 3.4.5, the diameter of the laser spot at the focal position was assumed to be 210 μm from the maximum flow velocity and the FWHM. The light spread angle was calculated from the numerical aperture of the lens. The transit distance of each particle can be calculated from ⊿z, ⊿y. The laser spot size at position (y, z) is calculated from ⊿z, and the transit distance is calculated from ⊿y in the spot. FWHM of each particle was calculated from the transit distance and the velocity. There were no slow particles at the outlet. The variation in the particle velocity (CV) is 10%, which is very close to the experimental result (CV = 13%), and it is indicated that the distribution of actual particles matches the simulation results (Figure 3-32).

Based on the numerical analysis, a channel with a square cross section would reduce the swirling flow around the central axis. Thus, to improve the accuracy of

the measurement, a channel with a square cross section is recommended.

Table 4-2 shows the performance of the flow cytometry chip estimated from the experimental results. The performance of the flow cytometry chip is almost equivalent to the expected performance.

Table 4-2 Performance of the integrated flow cytometry chip.

Issues	Conventional system	Expected performance	Actual performance
Sample volume	More than 100 μl	50 μl	Less than 30 μl
Reagent volume	More than 10 μl	5 μl	7 μl
Dead volume	More than 50 μl	0 μl	0 μl
Measurement time	More than 10min	Less than 1min	Less than 1min

4.6 Summary

A flow cytometry chip, which uses a continuous micro channel to connect the pre-treatment part and the twisted sheath flow cell, was proposed. When the micro channels with different performance were integrated, their matching and design method concerning operational conditions such as flow rate and others were described. In the pre-treatment part, a certain amount of incubation time is required to stain biological cells sufficiently. This time depends on both the channel volume of the pre-treatment part and the flow rate of the sample fluid, whereas the flow rate of the sample fluid depends on the specifications of the entire system, such as

the measurement time and the amount of sample fluid. Therefore, it is necessary to determine the structure and flow rate of the pre-treatment part to satisfy both conditions. According to the above design guidelines, a prototype of the flow cytometry chip was created. Fabrication of the prototype confirmed that the complex 3D flow micro channel network including the pre-treatment part can be made quickly and easily by soft lithography and twist deformation. The resulting flow cytometry chip was very compact, just 60 mm in length.

Next, biological cells were measured using the prototype chip. First, it was confirmed whether biological cells were stained under designed conditions in the pre-treatment part. For the experiments, cells with different sizes, yeast cells and PC-9 cells (human lung adenocarcinoma cell line), were used. The signals from stained cells can be detected with a photomultiplier tube (PMT), although there is a lot of noise due to contaminants. Presently, it is difficult to measure bacteria with a diameter of approximately 1 μm, but cells with a diameter of a few micrometers can be measured. I also verified the (1) reduction of dead volume, (2) reduction of sample and reagent volumes, and (3) shortening of the time from pre-treatment to detection due to direct connection of the pre-treatment part and the sheath flow cell. In summary, the performance ability of the current flow cytometry chip was summarized as specifications. The signal intensity of each cell varied during the experiment. The reason for this variation in the signal intensity was discussed based on the viscous flow analysis using FEM described in chapter 2. It was predicted that a sheath flow cell channel with a squarer cross section would gather the particles more toward the center of the channel. The range of variation in the signal intensity narrowed as the channel became squarer, which indicated that even finer particles could likely be measured.

Chapter 5 Feasibility of optical system using light-emitting diode and phototransistor

In chapter 5, the feasibility of applying compact and simple optical systems to flow cytometry chips to achieve an ultra-compact flow cytometer is examined [59]. The optical system currently used hinders miniaturization of the entire flow cytometer system. Therefore, to develop a simple, compact system, a prototype of an optical setup using a light-emitting diode (LED) and optical sensor was created and combined with a flow cytometry chip. The feasibility of the ultra-compact and low-cost flow cytometer is described [60]-[63].

5.1 Setup using LED

It is difficult to reduce the cost and size of the optical setup when it uses laser light. Therefore, I attempted to develop a compact, low-cost setup using an LED [64]. The laser and the PMT of the conventional optical setup were changed to an LED and an optical sensor in the new optical setup. The flow cytometry chip and the new optical setup with the LED and optical sensor were assembled into a 60 mm cube. The flow cytometry chip was designed and fabricated using the same method described in chapter 3, 4. The dimensions and a photograph of the fabricated flow cytometry chip are shown in Figure 5-1.

The channel height of the flow cytometry chip is 300 μm, the width is 300 μm, and the channel length of the pre-treatment part is 60 mm. The channel width of the sheath fluid at the sheath flow part is 170 μm. The sheath flow part was twisted by 180°. The second junction was at the center of the twist in the channel length, so the channel of the sheath flow part was twisted by 90° at the second junction. An OSUB3131P LED (wavelength: 470 nm, luminous intensity: 12000 mcd, OptoSupply) and NJL7502L optical sensor (max wavelength sensitivity: 560 nm) were selected for the optical setup. Figure 5-2 shows the prototype of the flow cytometer with the flow cytometry chip. The LED is set downstream of the second junction. The optical sensor is set inside the package, the window is open at the position for detecting fluorescence in the package, and a long-pass filter (500 nm) is installed in the window. The fluorescence from the side of the chip is detected. Next, I assessed the ability to measure particles using the LED-based setup with the flow cytometry chip.

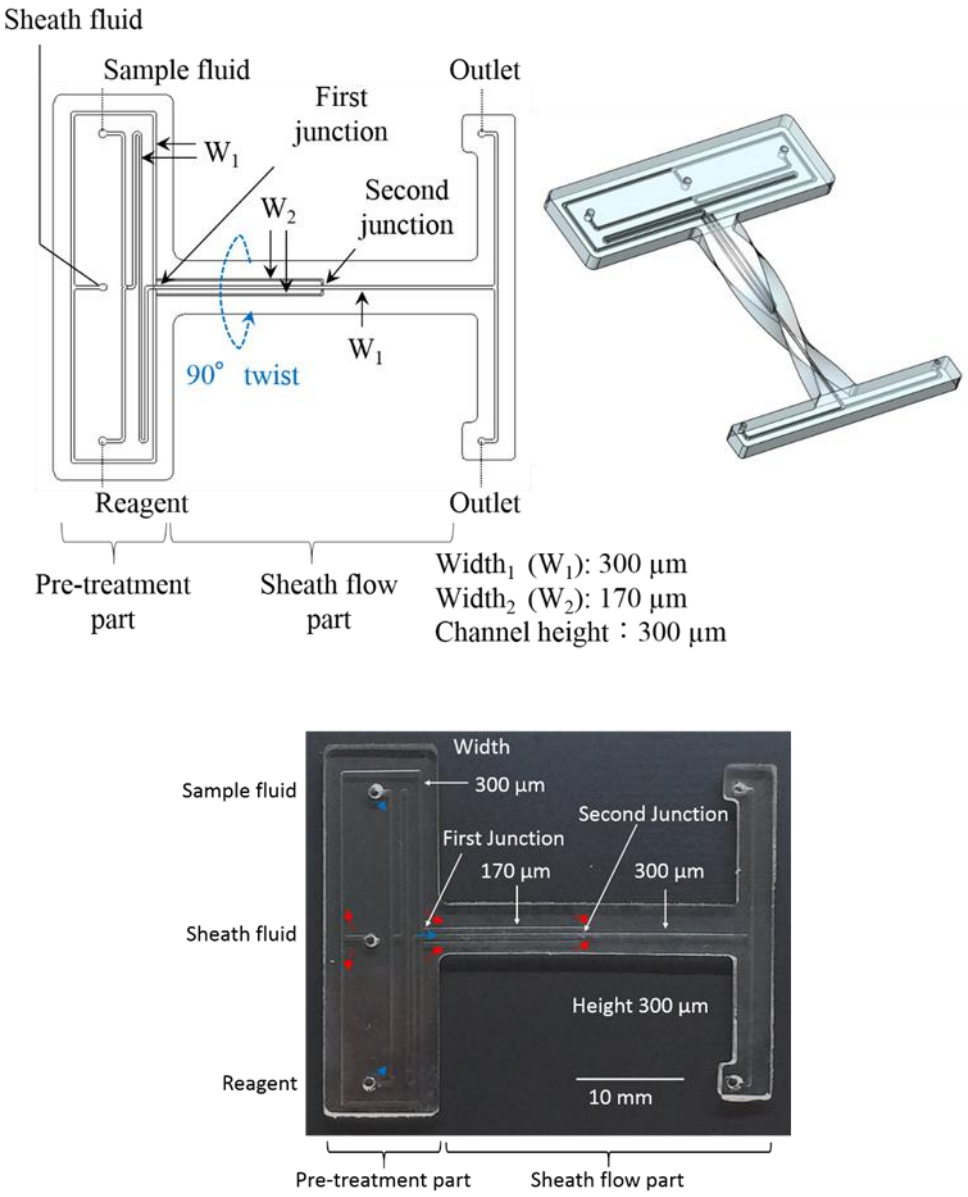

Figure 5-1 Design of the flow cytometry chip and a photograph of the flow cytometry chip fabricated for use as an ultra-compact, low-cost flow cytometer

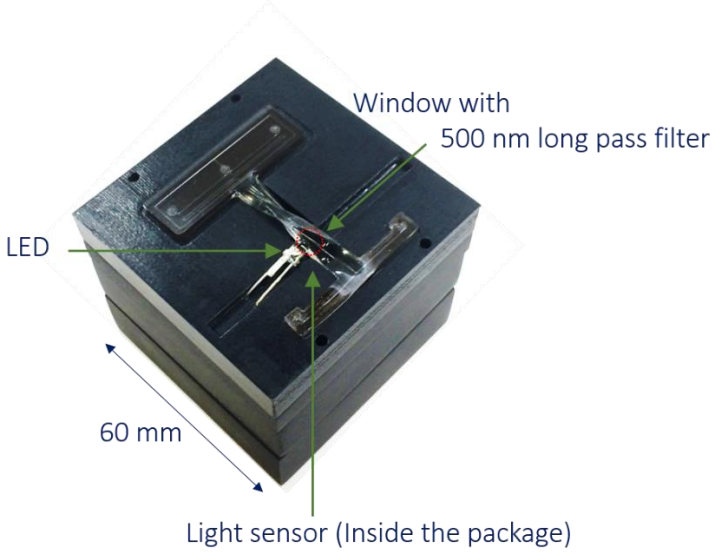

Figure 5-2 The ultra-compact, low-cost flow cytometer

5.2 Detection of fluorescent particles

To assess the detection ability of the new optical setup using an LED, I measured fluorescent particles in the flow cytometry chip. The sample fluid was deionized water containing φ50 μm fluorescent particles, and the sheath fluid and the reagent fluid were deionized water. The flow rates of the sheath fluid, the sample fluid and the reagent fluid were set to 0.104, 0.084 and 0.010 μl/s, respectively. The mean flow velocity at the observation point was 2.2 mm/s. Figure 5-3 shows a schematic of the LED-based setup. The light from the LED illuminated the sheath flow-forming part of the flow cytometry chip, and the fluorescence of the particles was detected from the side of the flow cytometry chip with the optical sensor. A camera was installed on the opposite side of the sensor to confirm whether the detected signal was due to the flow of particles. Figure 5-4 shows a photograph of the setup for the measurement. The current of the optical sensor was converted to the voltage value and amplified. The sampling period was 200 ms.

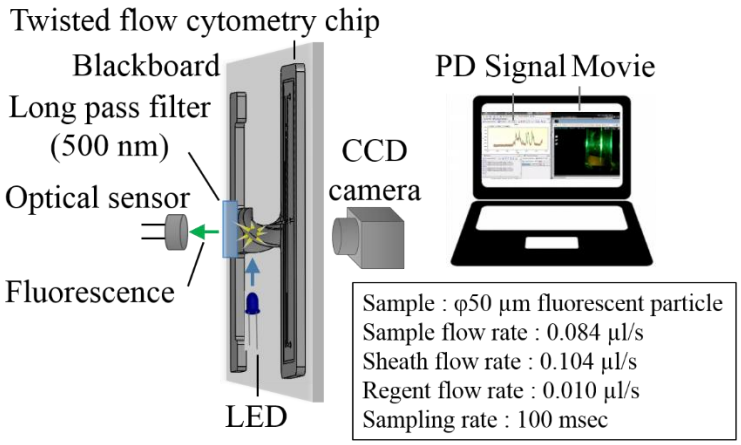

Figure 5-3 Schematic of the LED-based setup

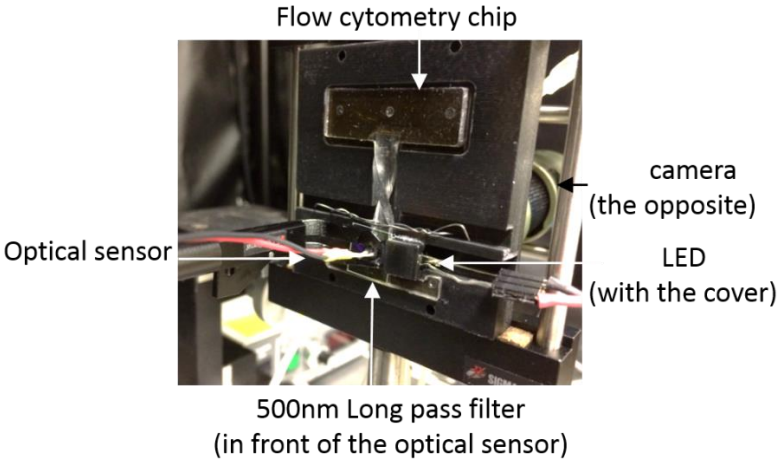

Figure 5-4 Photograph of the LED-based setup

5.3　Results and discussion

Figure 5-5 shows a photograph of the signal and the flow of the particles using the camera.

The measured signal intensity is a dimensionless value. The flow of particles was observed using the camera, and it was confirmed that the signals were detected when the particles flowed through the illuminated area. As shown in Figure 5-6, signals from the particles were successfully detected using the LED-based optical setup.

The signal intensity of the particles has variation. Figure 5-7 shows the photographs of the particles used in this measurement. (a) shows florescence image of (b). The variation of the particles size and the simultaneous transit of two particles are considered as the cause.

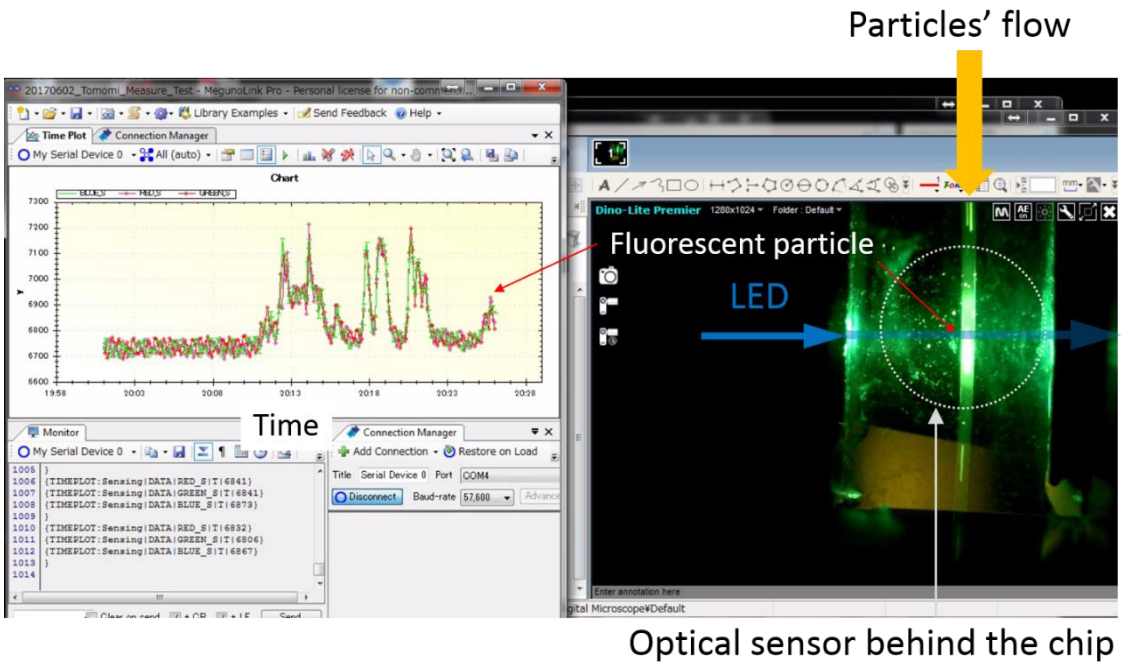

Figure 5-5 Photograph of signal measurement during observation of the flow of the particles using the camera

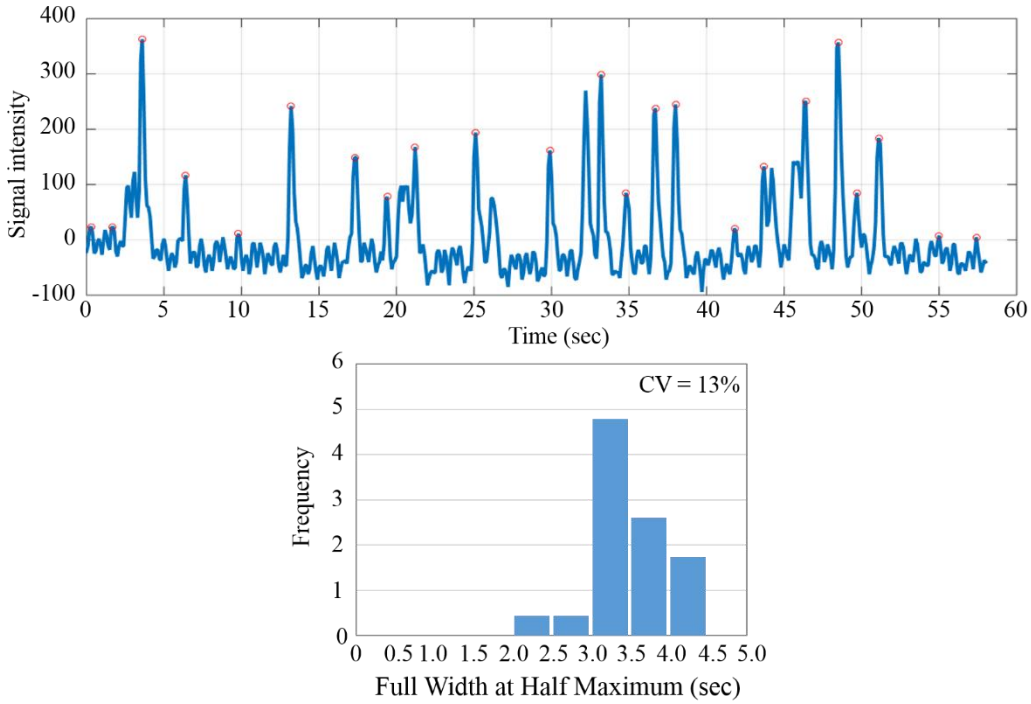

Figure 5-6 Signals from particles using the LED-based setup

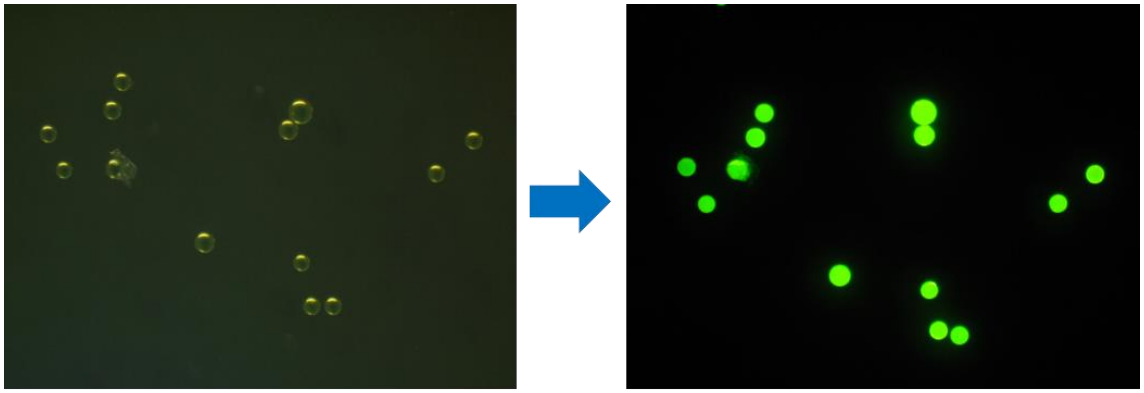

Figure 5-7 Photographs of particles used in this measurement

I attempted to measure φ6 μm fluorescent particles, but the signal could not be detected due to weak fluorescence. Generally, the light intensity of fluorescent particles varies depending on the square of their radius. However, in assays using

biological cells, the fluorescent intensity depends on not only the size of the cell but also several other factors, including the strength of the bond between the cells and fluorescent marker. Therefore, successful detection of φ50 μm fluorescent particles indicates that biological cells could be detected using the LED-based setup.

5.4 Summary

In chapter 5, the feasibility of applying compact and simple optical systems to flow cytometry chips to achieve an ultra-compact flow cytometer was examined. The optical system currently used hinders miniaturization of the entire flow cytometer system. Therefore, to develop a simple, compact system, a prototype of an optical setup using a LED and optical sensor was created and combined with a flow cytometry chip. The performance of the combined optical setup and flow cytometry chip was evaluated using φ50 μm fluorescent particles. Signals from the particles could be detected using specific arrangements of the LED and PT, demonstrating the feasibility of using this setup as an ultra-compact, low-cost flow cytometer.

Chapter 6 Conclusion

In chapter 6, the most important aspects of the research involving the novel, simplified method for fabrication of the 3D micro channel network are reviewed, and the feasibility of using this method for fabrication of general microfluidic systems is discussed. The findings and conclusions obtained throughout this research were summarized.

6.1 Summary of this study

Flow cytometry is a technique in which microscopic particles or cells are arranged linearly in fluid flow for high-speed analysis of their characteristics. To expand the availability of this technique, it is necessary to integrate the components, thereby providing a more compact, low-cost system that includes a pre-treatment system for the particle staining reaction. The most important technique of a flow cytometer is the formation of sheath flow to analyze particles accurately. The conventional sheath flow cell has a double glass tube structure, with a total length of a few centimeters. Fabricating such a complex glass structure on a small scale is extremely difficult. To reduce the size and cost of the entire system, it is ideal to fabricate an integrated pre-treatment part and sheath flow cell using a microfabrication technique, such as lithography. I proposed a 3D structure to form sheath flow by taking advantage of the unique material property of PDMS, its elasticity, and studied the method of design corresponding to requirement of the performance. Furthermore,

design technology for aligning and integrating a pre-treatment part and a flow cell was constructed and the specifications of flow cytometry chip were determined. The particles were detected using the optical setup based on LED with the fabricated flow cytometry. This design technology can be helpful design of other microfluidic devices and control of flow in the micro channel.

(1) The reported techniques related to microfluidic devices for forming sheath flow and the associated problems were surveyed.

(2) A method to form 3D micro channel network and a simple method for fabrication of the network using polydimethylsiloxane (PDMS) were proposed. The structure is 3D structure to form sheath flow by taking advantage of the unique material property of PDMS, its elasticity.

(3) A method for determining the specifications of a flow cell fabricated using simple fabrication method was established. By modeling of the complex structure and analysis of pressure fluctuations, it was possible to determine the specifications of the micro channel network and control the flow.

(4) A design technology for aligning and integrating a pre-treatment part and a sheath flow cell was established. It was possible to design integrated flow cytometry chip corresponding to the requirements of the performance.

(5) The flow cytometry chip was fabricated by using micro fabrication technique in a single step and the performance was evaluated.

(6) Versatility and potential of the method for fabrication of the 3D micro channel network were discussed. Particles were detected by using the optical setup based LED with flow cytometry chip. Furthermore, as shown in Table 6-1, the performance of the highly compact flow cytometry chip exceeded the target values, and the ultra-

compact and low-cost flow cytometer is expected to be applied to new field.

Table 6-1 Target values and results of this study.

Issues	Target	This study
Sample volume	Less than 100 μl	Less than 30 μl
Reagent volume	Less than 10 μl	7 μl
Dead volume	Less than 50 μl	0 μl
Transfer time	Less than 10 min	Less than 1 minute

6.2 Potential of flow cytometry chip

Flow cytometers analyze particles and biological cells, and can measure multiple items simultaneously. However, their size and cost are prohibitive. If the cost and size of the flow cytometer could be reduced using a flow cytometry chip, this technology could be used for more common inspections and bedside diagnoses [65]-[67].

Ultra-compact, low-cost flow cytometers can also be applied to systems that monitor water quality. A flow analyzer, like the one created in this study, is suitable for this type of continuous monitoring. For instance, a compact, low-cost water quality analyzer installed on local households or on a mountainside near a water source could provide instantaneous updates on water quality. A conventional water quality monitor has width 300 × height 400 × depth 20, and due to its dimension,

the installation location and number are limited [68]. We have been developing technology for a smart water quality monitoring network for water circulation systems using a model-based development method. The network comprises a control system, various analysis systems, and data transfer systems. Each function of the network is handled by a single modular unit, which can be combined easily with other units. Figure 6-1 shows a schematic of the modular unit. By standardizing the size of the units, they can be added and replaced easily, and the system can be built quickly. The development costs can be reduced, the application can be expanded, and safer and more reliable water can be supplied. The flow cytometer with a flow cytometry chip is expected to detect bacteria [69], [70]. According to the Drinking Water Quality Standards established based on Article 4 of the Waterworks Act, inspection for bacterial contamination requires a 24 h cultivation of samples for detection of only proliferative bacteria. However, a 24 h wait for results could be too long in cases that could become major health hazards. Since bacteria can be stained using the flow cytometry chip and monitored in real time, it is possible to respond as soon as a count variation is detected. It is expected that a prototype of the palm-top flow cytometer using an LED assembled with the flow cytometry chip will be applied for detection of bacteria. Figure 6-2 shows an image of the bacteria monitoring unit using the flow cytometry chip.

In the future, I aim to realize counting bacteria using flow cytometry chip.

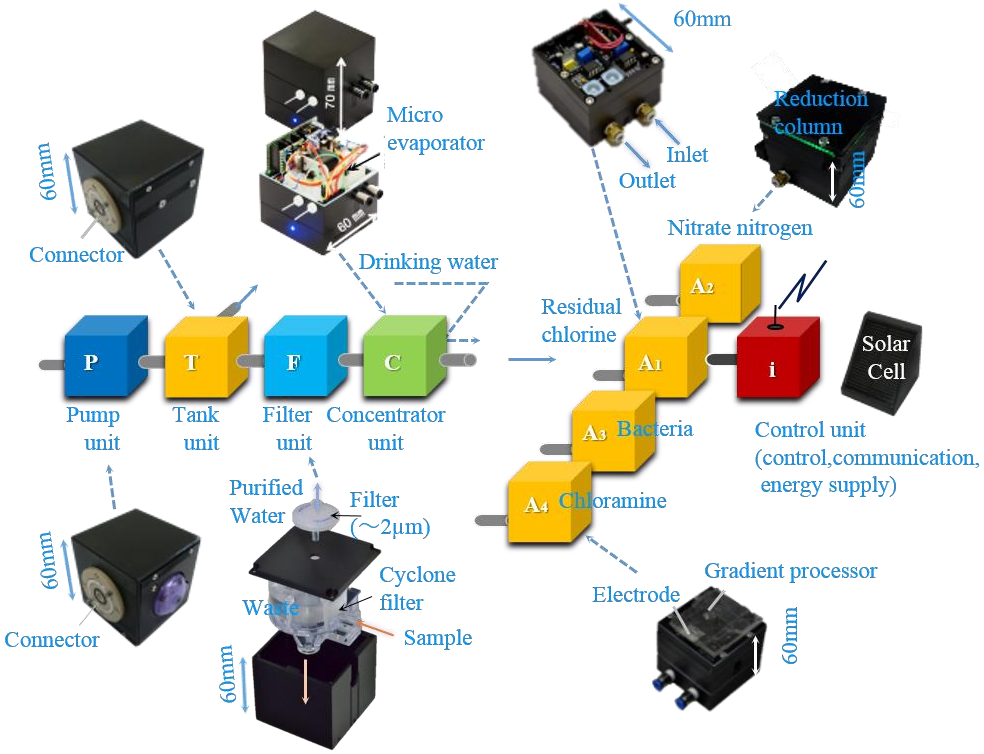

Figure 6-1 Schematic of the modular unit for the water quality monitoring system

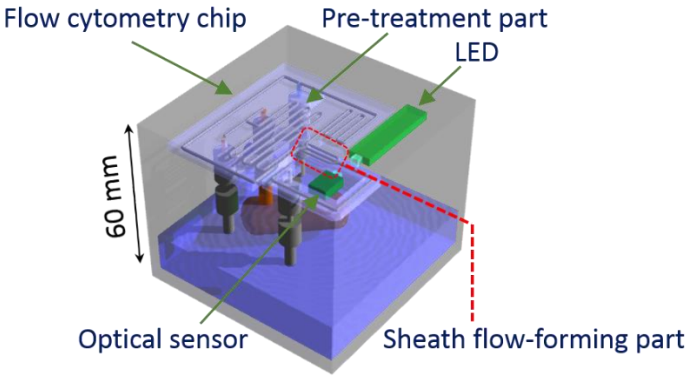

Figure 6-2 Bacteria monitoring unit using the flow cytometry chip

References

[1] Michael G. Ormerod, Flow cytometry, A basic introduction, DeNovo Software, (2008).

[2] H. Nakauchi and J. Seita, Flow cytometry, Yodosha, (2013).

[3] Japan Committee for Certified Cytometrist, Standard Flowcytometry, Ishiyaku publishers, (2009).

[4] B. Greve, R. Kelsch, K. Spaniol, H. T. Eich and M. Gotte, Flow Cytometry in Cancer Stem Cell Analysis and Separation, Cytometry Part A, **81**A, pp. 284-293, (2012).

[5] G-B. Lee, C-I. Hung, B-J. Ke, G-R. Huang, B-H. Hwei and H-F. Lai, Hydrodynamic Focusing for a Micromachined Flow Cytometer, Transactions of the ASME, **123**, pp. 672-679, (2001).

[6] R. Miyake, H. Ohki, I. Yamazaki, and R. Yabe, A development of micro sheath flow chamber, MEMS '91 proceedings, pp. 265-270, (1991).

[7] R. Miyake, H. Ohki, and I. Yamazaki, Investigation of sheath flow chambers for flow cytometers : 1st Report, Stabilization of sheath flow, Transactions of the Japan Society of Mechanical Engineers, Series B, **61 (591),** pp. 4039-4045, (1995).

[8] R. Miyake, H. Ohki, I. Yamazaki, and T. Takagi, Investigation of Sheath Flow Chambers for Flow Cytometers : Micro machined Flow Chamber with Low Pressure Loss, JSME International Journal Series B Fluids and Thermal Engineering, **40 (1)**, pp. 106-113, (1997).

[9] R. Miyake, H. Ohki, I. Yamazaki, and T. Takagi, Flow cytometric analysis by using micro-machined flow chamber, JSME International Journal Series B Fluids and Thermal Engineering, **43 (2)**, pp. 219–224, (2000).

[10] M. J. Kennedy, S. J. Stelick, S. L. Perkins, L. Cao, And C. A. Batt, Hydrodynamic focusing with a microlithographic manifold: controlling the vertical position of a focused sample, Microfluidics and Nanofluidics, **7**, pp. 569-578, (2009). 3D

[11] G. Hairer, and M. J. Vellekoop, An integrated flow-cell for full sample stream control, Microfluidics and Nanofluidics, **7**, pp. 647-658, (2009).

[12] N. Sundararajan, M. S. Pio, L. P. Lee, and A. A. Berlin, Three-dimensional hydrodynamic focusing in Polydimetylsiloxane (PDMS) microchannels, J. MEMS, **13** (4), pp. 559-567, (2004).

[13] C-H. Tsai, H-H. Hou, and L-M. Fu, An optimal three-dimensional focusing technique for micro-flow cytometers, Microfluidics and Nanofluidics, **5**, pp. 827-836, (2008).

[14] C. Simonnet, and A Groisman, Two-dimensional hydrodynamic focusing in a simple microfluidic device, Applied Physics Letters, **87** (11), pp. 114104-1-114104-3, (2005).

[15] X. Mao, S-C. S. Lin, C. Dong and T. J. Huang, Single-layer planar on-chip flow cytometer using microfluidic drifting based three-dimensional (3D) hydrodynamic focusing, Lab Chip, **9**, pp. 1583-1589, (2009).

[16] M. G. Lee, S. Choi, and J-K. Park, Three-dimensional hydrodynamic focusing with a single sheath flow in a single-layer microfluidic device, Lab on a Chip, **9**, pp. 3155-3160, (2009).

[17] https://ls.beckmancoulter.co.jp/products/flow-cytometers/gallios

[18] J. Skommera, J. Akagi, K. Takeda, Y. Fujimura, K. Khoshmaneshc and D. Wlodkowica, Multiparameter Lab-on-a-Chip flow cytometry of the cell cycle, Biosensors and Bioelectronics, **42**, pp. 586-591, (2013).

[19] J. Balsam, H. A. Bruck and A. Rasooly, Webcam-based flow cytometer using wide-field imaging for low cell number detection at high throughput, Analyst, **139**, pp. 4322-4329, (2014).

[20] N. Watkins, B. M. Venkatesan, M. Toner, W. Rodriguez and R. Bashir, A robust electrical microcytometer with 3-dimensional hydrofocusing, Lab on a chip, **9**, pp. 3177-3184, (2009).

[21] R. Sekine, T. Sakurai, D. H. Yoon, R. Iizuka, T. Sekiguchi, T. Funatsu and S. Shoji, Controllable three-dimensional sheath flow with wide range Reynolds number and its application for efficient, The 15th International Conference on Miniaturized Systems for Chemistry and Life Sciences, pp. 1903-1905, (2011).

[22] R. Yang, D. L. Feeback and W. Wang, Microfabrication and test of a three-dimensional polymer hydro-focusing unit for flow cytometry applications, Sensors and Actuators A, **118**, pp. 259-267, (2005).

[23] J. P. Golden, J. S. Kim, J. S. Erickson, L. R. Hilliard, P. B. Howell, G. P. Anderson, M. Nasir and F. S. Ligler, Multi-wavelength microflow cytometer using groove-generated sheath flow, Lab on a chip, **9**, pp. 1942-1950, (2009).

[24] A. Wolff, I. R. Perch-Nielsen U. D. Larsen, P. Friis, G. Goranovic, C. R. Poulsen, J. P. Kuttera and P. Telleman, Integrating advanced functionality in a microfabricated high-throughput fluorescent-activated cell sorter, Lab on a chip, **3**, pp. 22-27, (2003).

[26] 60R. Scott, P. Sethu, and C. K. Harnett, Three-dimensional hydrodynamic focusing in a microfluidic Coulter counter, Review of Scientific instruments, **79**, pp. 046104.1-046104.3, (2008).

[27] G. Eluru, L. A. N. Julius and S. S. Gorthi, Single-layer microfluidic device to realize hydrodynamic 3D flow focusing, Lab on a Chip, **16,** pp. 4133-4141, (2016).

[28] J. Shi, X. Mao, D. Ahmed, A. Colletti, and T. J. Huang, Focusing microparticles in a microfluidic channel with standing surface acoustic waves (SSAW), Lab on a Chip, **8**, pp. 221-223, (2008).

[29] J. Shi, S. Yazdi, S-C. S. Lin, X. Ding, I-K. Chiang, K. Sharp and T. J. Huang, Three-dimensional continuous particle focusing in a microfluidic channel via standing surface acoustic waves (SSAW), Lab on a chip, **11**, pp. 2319-2324, (2011).

[30] A. Lenshof, A. Ahmad-Tajudin, K. Jaras, A-M. Sward-Nilsson, L. Aberg, G. Marko-Varga, J. Malm, H. Lilja, and T. Laurell, Acoustic Whole Blood Plasmapheresis Chip for Prostate Specific Antigen Microarray Diagnostics, Analytical chemistry, **81**, pp. 6030-6037, (2009).

[31] C. Grenvall, C. Antfolk, C. Z. Bisgaard and T. Laurell, Two-dimensional acoustic particle focusing enables sheathless chip Coulter counter with planar electrode configuration, Lab on a Chip, **14**, pp. 4629-4637, (2014).

[32] D. Holmes, H. Morgan and N. G. Green, High throughput particle analysis: Combining dielectrophoretic particle focusing with confocal optical detection, Biosensors and Bioelectronics, **21** (8), pp. 1621-1630, (2006).

[33] P. B. Howell Jr, J. P. Golden, L. R. Hilliard, J. S. Erickson, D. R. Mott and F. S. Ligler, Two simple and rugged designs for creating microfluidic sheath flow, Lab on a Chip, **8**, pp. 1097-1103, (2008).

[34] S-C. Lin, P-W. Yen, C-C Peng and Y-C Tung, Single channel layer, single sheath-flow inlet microfluidic flow cytometer with three-dimensional hydrodynamic focusing, Lab on a chip, **12**, pp. 3135-3141, (2012).

[35] A. A. S. Bhagat, S. S. Kuntaegowdanahalli and I. Papautsky, Continuous particle separation in spiral microchannels using dean flows and differential migration, Lab on a chip, **8**, pp. 1906-1914, (2008).

[36] A. Russom, A. K. Gupta, S. Nagrath, D. D. Carlo, J. F. Edd and M. Toner, Differential inertial focusing of particles in curved low-aspect-ratio microchannels, New Journal of Physics, **11**, pp. 075025.1-075025.9, (2009).

[37] C. Xu, M. Wang, and X. Yin, Three-dimensional (3D) hydrodynamic focusing for continuous sampling and analysis of adherent cells, Analyst, **136 (19)**, pp. 3877-3883, (2011).

[38] D. D. Carlo, D. Irimia, R. G. Tompkins and M. Toner, Continuous inertial focusing, ordering, and separation of particles in microchannels, PNAS Applied Physical Sciences, **104** (48), pp. 18892-18897, (2007).

[39] Y. Gambin, C. Simonnet, V. VanDelinder, A. Deniz and A. Groisman, Ultrafast microfluidic mixer with three-dimensional flow focusing for studies of biochemical kinetics, Lab on a Chip, **10**, pp. 598-609, (2010).

[40] Y. W. Kim and J. Y. Yoo, Axisymmetric flow focusing of particles in a single microchannel, Lab on a Chip, **9**, pp. 1043-1045, (2009).

[41] N. Watkins, B. M. Venkatesan, M. Toner, W. Rodriguez and R. Bashir, A robust electrical microcytometer with 3-dimensional hydrofocusing, Lab on a Chip, **9**, pp.

3177-3184, (2009).

[42] T. Fujii, PDMS-based microfluidic devices for biomedical applications, Microelectronic Engineering **60-61**, pp. 907-914, (2002).

[43] D. Qin, Y. Xia and G. M. whitesides. Soft lithography for micro- and nanoscale patterning, nature protocols, **5** (3), pp. 491-502, (2010).

[44] T. Sato and R. Miyake, Sheath flow forming by using twisted micro-channel, Transaction of the JSME, **80** (813), (2014). DOI:10.1299/transjsme.2014 mn0132 (in Japanese).

[45] T. Sato and R. Miyake, Sheath-flow forming by using twisted micro-channel, The 26th IEEE International Conference on Micro Electro Mechanical Systems, pp. 1175-1178, (2013).

[46] T. Sato and R. Miyake, Particle measurement by using twisted micro sheath flow cell, The 19th International Conference on Miniaturized Systems for Chemistry and Life Sciences, pp. 458-460, (2015).

[47] B. J. Kirby, Micro- and Nanoscale Fluid Mechanics Transport in Microfluidic devices, Chapter 3 Hydraulic Circuit Analysis, pp. 60-78, Cambridge, (2010).

[48] H. Bruus, Theoretical Microfluidics, Chapter 3 Basic flow solutions, pp. 47-70, Oxford, (2007).

[49] Journal of the Japan Society of Mechanical Engineers ed., Fluid Mechanics (2005), pp. 89-92, MARUZEN (in Japanese).

[50] H. Lorenz, M. Despont, N. Fahrni, N. LaBianca, P. Renaud and P. Vettiger, SU-8 : a low-cost negative resist for MEMS, J. Micromech. Microeng., **7**, pp. 121-124, (1997).

[51] A. Mata, A. J. Fleischman and S. Roy, Fabrication of multi-layer SU-8 microstructures, J. Micromech. Microeng., **16**, pp. 276-284, (2006).

[52] M. A. Eddings, M. A. Johnson and B. K. Gale, Determining the optimal PDMS–PDMS bonding technique for microfluidic devices, J. Micromech. Microeng., **18**, pp. 067001.1-067001.4, (2008).

[53] D. Fuard, T. Tzvetkova-Chevolleau, S. Decossas, P. Tracqui and P. Schiavone, Optimization of poly-di-methyl-siloxane (PDMS) substrates for studying cellular

adhesion and motility, Microelectronic Engineering, **85**, pp. 1289–1293, (2008)

[54] T. Sato and R. Miyake, Cell Measurement by Flow Cytometry Chip with Twisted Micro Sheath Flow Channel, Analytical Methods, **9**, pp. 3992-3997, (2017).

[55] S-Y. Yang, K-Y Lien, K-J Huang, H-Y. Lei and G-B. Lee, Micro flow cytometry utilizing a magnetic bead-based immunoassay for rapid virus detection, Biosensors and Bioelectronics, **24**, pp. 855-862, (2008).

[56] A. D. Stroock, S. K. W. Dertinger, A. Ajdari, I. Mezic, H. A. Stone, G. M. Whitesides, Chaotic Mixer for Microchannels, **295**, pp. 647-651, (2002).

[57] F. Schönfeld, V. Hessel and C. Hofmann, An optimised split-and-recombine micro-mixer with uniform 'chaotic' mixing, Lab on a chip, **4**, pp. 65-69, (2004).

[58] CHEMINAS, Technology and application of Micro Chemical chip, Section 2.6 Overview of micro process system, Maruzen, pp. 163-177, (2006).

[59] T. Sato and R. Miyake, Compact and Low-cost Flow Cytometry Unit for Monitoring Particles in Water, The 7th International Multidisciplinary Conference on Optofluidics 2017, (2017).

[60] R. C. Habbersett, and J. H. Jett, An analytical system based on a compact flow cytometer for DNA fragment sizing and single-molecule detection, Cytometry Part A, **60A**, pp. 125-134, (2004).

[61] Y-C. Tung, M. Zhang, C-T. Lin, K. Kurabayashi and S. J. Skerlos, PDMS-based opto-fluidic micro flow cytometer with two-color, multi-angle fluorescence detection capability using PIN photodiodes, Sensors and Actuators B, **98**, pp. 356–367, (2004).

[62] C-H. Lin and G-B. Lee, Micromachined flow cytometers with embedded etched optic fibers for optical detection, J. Micromech. Microeng., **13**, pp. 447-453, (2003).

[63] L-M. Fu, R-J. Yang, C-H Lin, Y-J. Pan, G-B. Lee, Electrokinetically driven micro flow cytometers with integrated fiber optics for on-line cell/particle detection, Analytica Chimica Acta, **507**, pp. 163-169, (2004).

[64] The Spectroscopical Society of Japan, Fundamentals of optical experiments and improvement tips, Chapter 3, How to select and use light source and detector, Kodansha scientific, pp. 113-138, (2009).

[65] W. Jung, J. Han, J-W. Choi, C. H. Ahn, Point-of-care testing (POCT) diagnostic

systems using microfluidic lab-on-a-chip technologies, J. Microelec. Microeng., **132** (25), pp. 45-57, (2015).

[66] F. A. Gomez, The future of microfluidic point-of-care diagnostic devices, Bioanalysis, **5** (1), pp. 1-3, pp. 3-21, (2013).

[67] C. D. Chin, S. Y. Chin, T. Laksanasopin, and S.K. Sia, Low-Cost Microdevices for Point-of-Care Testing, Point-of -Care Diagnostics, Chapter 1~3, Springer, pp. 3-66, (2013).

[68] https://www.hitachi-hightech.com/file/hsl/pdf/products/instruments/brcr_water_an770a_03.pdf

[69] http://www.mhlw.go.jp/stf/seisakunitsuite/bunya/topics/bukyoku/kenkou/suido/suishitsu/07.html

[70] http://www.mhlw.go.jp/file/06-Seisakujouhou-10900000-Kenkoukyoku/0000045881. pdf

Publications

Journals

(1) Sheath flow forming by using twisted micro-channel,

T. Sato and R. Miyake

Transaction of the JSME, **80** (813), (2014). DOI:10.1299/transjsme.2014 mn0132 (in Japanese) (11 pages)

(2) Cell Measurement by Flow Cytometry Chip with Twisted Micro Sheath Flow Channel

T. Sato and R. Miyake

Analytical Methods, **9**, pp. 3992-3997, (2017). DOI:10.1039/C7AY00886D

(3) Sheath-flow forming by using twisted micro-channel

T. Sato and R. Miyake

The 26th IEEE International Conference on Micro Electro Mechanical Systems, pp. 1175-1178, (2013). DOI:10.1109/MEMSYS.2013.6474461

(4) Particle measurement by using twisted micro sheath flow cell

T. Sato and R. Miyake

The 19th International Conference on Miniaturized Systems for Chemistry and Life Sciences, pp. 458-460, (2015).

(5) Compact and Low-cost Flow Cytometry Unit for Monitoring Particles in Water

T. Sato and R. Miyake

The 7th International Multidisciplinary Conference on Optofluidics 2017, (2017).

DOI:10.3390/optofluidics2017-04233

(6) Computer Simulation of Stress Induced Dislocation Multiplication in Large-Diameter Silicon Wafer in High-Temperature Device Processing

H. Shimizu, D. Sudou, T. Satoh, and S. Saitou

Materials Transactions, JIM, **38** (1), pp. 69-77, (1997).

DOI:10.2320/matertrans1989.38.69

(7) Computer Simulation for estimation of dislocation multiplication due to gravitational stress : challenges and opportunities toward slip-free 300mm-silicon wafers for ultra-large-scale-integration

H. Shimizu, S. Isomae, K. Minowa, and T. Satoh

The Society of Photo-Optical Instrumentation Engineers, **3215**, pp. 167-179, (1997).

DOI:10.1117/12.284678

(8) Gravitational Stress-Induced Dislocations in Large-Diameter Silicon Wafers Studied by X-Ray Topography and Computer Simulation

H. Shimizu, S. Isomae, K. Minowa, T. Satoh, and T. Suzuki

J. Electrochem. Soc., **145** (7), pp. 2523-2529, (1998).

DOI:10.1149/1.1838672

(9) Low-Cost P^-/P^- Epitaxial Silicon Wafers for Densely Packed Metal-Oxide-Semiconductor Devices

H. Shimizu, T. Satoh, M. Muranaka, K. Makabe, and M. Miura

J. Electrochem. Soc., **147** (5), pp. 1930-1935 (2000).

DOI:10.1149/1.1393460

Presentations at conferences

(1) Sheath-flow forming by using twisted micro-channel

T. Sato and R. Miyake

The 26th IEEE International Conference on Micro Electro Mechanical Systems, (2013).

(2) Particle measurement by using twisted micro sheath flow cell

T. Sato and R. Miyake

The 19th International Conference on Miniaturized Systems for Chemistry and Life Sciences, (2015).

(3) Compact and Low-cost Flow Cytometry Unit for Monitoring Particles in Water

T. Sato and R. Miyake

The 7th International Multidisciplinary Conference on Optofluidics 2017, (2017).

(4) Visualization of behavior of relatively large particles in microchannel

T. Sato and R. Miyake

The 24th CHEMINAS, (2011)

(5) Sheath flow forming by using twisted micro channel

T. Sato and R. Miyake

JSME The 4th Micro Nano engineering symposium, **4**, OS3-2-3, pp. 1-2, (2012)

DOI:10.1299/jsmemnm.2012.4.79

(6) Measurement of biological cells using twisted flow cytometry chip

T. Sato and R. Miyake

JSME The 6th Micro Nano engineering symposium, **6**, 21pm3, PM012, pp. 1-2, (2014)

DOI:10.1299/jsmemnm.2014.6._21pm3-PM0_12

(7) Development of compact analysis system with twisted flow cytometry chip

T. Sato and R. Miyake

JSME The 7th Micro Nano engineering symposium, **7**, 30am, PM012, pp. 1-2, (2015)

DOI:10.1299/jsmemnm.2015.7._30am2-PN-_8

(8) Study of P^-/P^- Epitaxial wafer・behavior of oxygen precipitation

T. Sato, N. Suzuki, H. Shimizu, S. Saitoh, Y. Sugino, T. Tanaka, S. Isomae and K. Takeda

The JSAP Autumn Meeting, (1996)

(9) Gettering evaluation by resistance measurement of Al gate electrode

T. Sato, N. Suzuki, H. Shimizu, Y. Matsuda, T. Sugino and T. Tanaka

The JSAP Autumn Meeting, (1997)

Acknowledgements

I would like to express my gratitude to all those who supported me and cooperated with me during my doctoral research. I would also like to express my sincerest thanks to Professor Ryo Miyake, my study supervisor at The University of Tokyo and Hiroshima University. He gave me the opportunity for this study. Without his guidance and encouragement, none of this would have been possible.

I would like to express my gratitude to Professor Takamaro Kikkawa and Professor Shin Yokoyama at Hiroshima University who supported me and guided me during my doctoral research.

I would like to express my gratitude to Professor Michihiro Hide, Professor Seiichiro Higashi and Professor Masakazu Iwasaka at Hiroshima University for useful comments and suggestions.

I thank the members of Miyake laboratory in The University of Tokyo and the members of Research Institute for Nanodevice and Bio Systems in Hiroshima University.

I would like to acknowledge Dr. Kazuo Takeda and Dr. Yuu Fujimura at On-chip Biotechnologies, who supplied me PC-9 cells and taught me the knowledge of flow cytometer.

A part of this study was supported by Japan Science and Technology Agency, Strategic Basic Research Programs CREST.

Finally, I thank Dr. Seong-Hun Choe who supported me and cooperated with my study.

公表論文

(1) Sheath flow forming by using twisted micro-channel
T. Sato and R. Miyake
Transaction of the JSME, 80(813), (2014).
DOI:10.1299/transjsme.2014 mn0132 (in Japanese) (11 頁)

(2) Cell Measurement by Flow Cytometry Chip with Twisted Micro Sheath Flow Channel
T. Sato and R. Miyake
Analytical Methods, 9, pp.3992-3997, (2017). DOI:10.1039/C7AY00886D

参考論文

(1) Sheath-flow forming by using twisted micro-channel

T. Sato and R. Miyake

The 26th IEEE International Conference on Micro Electro Mechanical Systems, pp.1175-1178, (2013). DOI:10.1109/MEMSYS.2013.6474461

(2) Particle measurement by using twisted micro sheath flow cell

T. Sato and R. Miyake

The 19th International Conference on Miniaturized Systems for Chemistry and Life Sciences, pp.458-460, (2015).

(3) Compact and Low-cost Flow Cytometry Unit for Monitoring Particles in Water

T. Sato and R. Miyake

The 7th International Multidisciplinary Conference on Optofluidics 2017, (2017). DOI:10.3390/optofluidics2017-04233